Universidad de Concepción
Dirección de Postgrado
Facultad de Ingeniería Agrícola
Programa de Doctorado en Recursos Hídricos y Energía para la Agricultura

Caracterización Hidroquímica de Cuencas Andinas con Énfasis en la Zona Semiárida de Chile

Tesis para optar al grado de Doctora en Recursos Hídricos y Energía para la Agricultura

DENISSE JAVIERA DUHALDE SÁEZ

CHILLÁN-CHILE

2025

Profesor Guía: José Luis Arumí Ribera
Depto. de Recursos Hídricos
Facultad de Ingeniería Agrícola
Universidad de Concepción
Profesor Co-Guía: Ricardo Oyarzún Lucero
Depto. Ingeniería de Minas
Facultad de Ingeniería
Universidad de La Serena

Esta tesis ha sido realizada en el Departamento de Recursos Hídricos de la Facultad de Ingeniería Agrícola, Universidad de Concepción.

Profesor Guía

Dr. José Luis Arumí Ribera
Facultad de Ingeniería Agrícola
Universidad de Concepción

Profesor Co-Guía

Dr. Ricardo Oyarzún Lucero
Facultad de Ingeniería
Universidad de La Serena

Comisión Evaluadora

Dr. Sebastián Krogh Navarro
Facultad de Ingeniería Agrícola
Universidad de Concepción

Dr. Mario Lillo Saavedra
Facultad de Ingeniería Agrícola
Universidad de Concepción

Dr. Jan Boll
Civil and Environmental Engineering
Washington State University, USA

Director del Programa

Dr. Sebastián Krogh Navarro
Facultad de Ingeniería Agrícola
Universidad de Concepción

Agradecimientos

A la Agencia Nacional de Investigación y Desarrollo (ANID) a través de la Beca Doctoral y al Centro de Recursos Hídricos para la Agricultura y Minería (CRHIAM) a través del proyecto ANID/FONDAP/15130015 y ANID/FONDAP/1523A0001. Finalmente, al proyecto Fondecyt Proyect ANID/FONDECYT/1210177

RESUMEN

Dada la importancia hidrológica de las cuencas de cabecera para los ecosistemas y las actividades humanas, comprender la dinámica hidroquímica de las cuencas de cabecera de montañas y la influencia de las características de las cuencas en la calidad del agua es esencial para diseñar estrategias de gestión eficaces. Especialmente relevante es la zona semiárida en Chile donde el abastecimiento hídrico proviene principalmente de las cuencas andinas. El objetivo principal de la presente tesis fue caracterizar la hidroquímica de cuencas andinas con énfasis en la zona semiárida de Chile. Como primer enfoque (Capitulo II) se abordó un análisis hidroquímico de largo plazo y baja frecuencia para un transecto de treinta cuencas, mediante la determinación de la relación caudal concentración (c-Q) de los ríos caracterizando los regímenes de exportación (enriquecimiento, dilución y constate) con la ley de potencia y los patrones de histéresis (sentido horario, sentido antihorario y no-histéresis). El patrón predominante para los iones mayores resultó ser dilución- antihorario y para Fe enriquecimiento-horario Además, para determinar la composición iónica del agua, se aplicó el diagrama de Stiff, y se identificó fuentes relevantes de aporte de solutos. Con estadísticos no paramétricos U de Mann-Whitney y δ de Cliff se analizó la relación entre características climáticas y de terreno con la relación c-Q. Para el segundo enfoque (Capítulo III), considerando el rol relevante de los humedales en la hidroquímica, se analizó, durante 37 años (verano), la relación entre la cobertura vegetal, la precipitación y la concentración de solutos en una cadena de doce humedales altoandinos del Santuario de la Naturaleza Estero Derecho, mediante los índices NDVI y NDMI obtenidos de los satélites Landsat-5 y Landsat-8. Se determinó correlación significativa entre ambos índices, la precipitación y parámetros de calidad del agua (CE, Cl, Mg, Na y Fe). El análisis de la cobertura vegetal de cada humedal mostró diferentes comportamientos, atribuibles a la altitud, la pendiente del terreno y los aportes hídricos adicionales de los arroyos. Finalmente, de manera integrada la investigación ha logrado resultados que ofrecen una caracterización de la dinámica hidroquímica de las cuencas andinas estudiadas y como factores naturales y antropogénicos influyen en el comportamiento de los parámetros de la calidad del agua. La relación identificada entre el comportamiento de los solutos, el índice de aridez y la cobertura vegetal permite, en un escenario de cambio climático, proyectar cambios en la hidroquímica de los ríos que sirvan de insumo para tomas de decisión en la gestión de cuencas. Considerando la amplitud del transecto (29°-35°S), la diversidad de condiciones de las diferentes cuencas, incluido el humedal de altura, esta investigación puede ser útil para estudios similares, en especial para cuencas montañas donde es habitual la escasez de datos. Se plantea proyecciones de estudios sobre la caracterización de fuentes específicas de los solutos, dinámica nival, aporte de aguas subterráneas y caracterización física y química de los sedimentos. El estudio de la cadena de humedales tuvo una aplicación directa a la comunidad ya que la información generada será considerada para actualizaciones del plan de manejo y educación ambiental del Santuario.

ABSTRACT

Understanding the hydrochemical dynamics of mountain headwater basins—and the influence of catchment attributes on water quality, is essential for designing effective water-resource management strategies, given their hydrological importance for both ecosystems and human activities. This is particularly relevant in the semi-arid zone of Chile, where water supply depends largely on Andean headwaters. The main objective of this thesis was to characterize the hydrochemistry of Andean catchments, with an emphasis on semi-arid Chile.

In the first component (Chapter II), a long-term, low-frequency hydrochemical analysis was conducted for a transect of thirty basins. Concentration–discharge (c–Q) relationships were evaluated to characterize export regimes (enrichment, dilution, constancy) using power-law scaling, alongside hysteresis patterns (clockwise, anticlockwise, no hysteresis). Major ions predominantly exhibited dilution–anticlockwise behavior, whereas Fe showed enrichment–clockwise patterns. Water ionic composition was examined using Stiff diagrams, enabling identification of key solute sources. Non-parametric Mann–Whitney U tests and Cliff's delta were applied to assess links between climatic and terrain characteristics and c–Q behavior.

In the second component (Chapter III), recognizing the hydrological relevance of high-Andean wetlands, the relationship between vegetation cover, precipitation, and solute concentrations was analyzed over 37 summers for a chain of twelve wetlands within the Estero Derecho Nature Sanctuary. Vegetation indices (NDVI and NDMI) derived from Landsat-5 and Landsat-8 revealed significant correlations with precipitation and with water-quality parameters (EC, Cl, Mg, Na, Fe). Vegetation-cover dynamics differed among wetlands, influenced by altitude, terrain slope, and additional inflows from tributary streams.

Overall, this research provides an integrated characterization of hydrochemical dynamics in Andean basins and demonstrates how natural and anthropogenic factors shape water-quality behavior. The identified links between solute dynamics, aridity index, and vegetation cover offer a basis for projecting hydrochemical responses under climate-change scenarios, supporting informed decision-making in catchment management.

Given the geographic breadth of the transect (29°–35°S) and the heterogeneity among basins—including high-altitude wetlands—the results of this study may inform similar research, particularly in mountain regions where data scarcity is common. Future work should include the characterization of specific solute sources, snow-regime dynamics, groundwater contributions, and the physical and chemical properties of sediments. The wetland-chain analysis also had direct application for the local community, as the information generated will contribute to updating the management plan and environmental-education initiatives of the Sanctuary.

INDICE

Lista de Figuras

Lista de Tablas

CAPÍTULO I: INTRODUCCIÓN

1. Introducción

En los últimos años, a las montañas se les ha asociado con el concepto de “torres de agua”, ya que, al compararlas con las áreas ubicadas aguas abajo de éstas, favorecen diferentes procesos hidrológicos como son la precipitación por el efecto orográfico (y, por consiguiente, la escorrentía); además de potenciar el almacenamiento hídrico mediante la nieve, los glaciares, humedales y cuerpos lacustres; e influir en la infiltración hacia aguas subterráneas (Immerzeel et al., 2019). Es por esto, que las montañas y, por ende, las cuencas de cabecera tienen un rol trascendental en el almacenamiento y distribución del recurso hídrico, que sustenta los ecosistemas y actividades vinculadas a los asentamientos humanos (industria y agua potable) existentes en ellas y aguas abajo (Viviroli et al., 2007; Nauditt et al., 2017; Markovich et al., 2019; Immerzeel et al., 2019).

En este contexto, y dado que se estima que más del 20% de la población mundial (aproximadamente 1900 millones) depende de los procesos hidrológicos que ocurren en las montañas (Nauditt et al., 2017, Immerzeel et al., 2019), es de gran importancia conocer estos procesos, ya que así es posible desarrollar estrategias de gestión sostenible del agua y evaluar las consecuencias de los cambios naturales y/o antropogénicos a escala de cuenca (Bogena et al., 2018).

Lo anterior cobra especial relevancia en un contexto de Cambio Climático, dado que estas áreas, dependientes de la acumulación nival y del deshielo, son altamente vulnerables a los efectos del calentamiento Global sobre la nieve, los glaciares y los ecosistemas, como los humedales de altura (Markovich et al., 2019). De hecho, la creciente evidencia apunta hacia la ocurrencia actual de procesos de calentamiento que son amplificados por la elevación, conocidos como "calentamiento dependiente de la elevación (EDW, por sus siglas en inglés)". Este EDW puede tener consecuencias importantes para la hidrología de las áreas montaña y, por lo tanto, también para sus ecosistemas y zonas aguas abajo (Pepin et al., 2015). Además, la ocurrencia de sequías meteorológicas (ej., debido al Cambio Climático) puede afectar no solo la disponibilidad de agua, sino también la calidad del agua en tales entornos (Peña-Guerrero et al., 2020).

Bajo el contexto descrito, la cordillera de los Andes en Chile constituye la principal fuente de agua para los ríos más importantes del país. En el transecto comprendido entre 29° y 35°S se concentra

más del 75% de la actividad agrícola nacional y una fracción significativa de la población urbana (Vicuña et al., 2013; Garreaud et al., 2019; Peña-Guerrero et al., 2020). Esta región, al ser un ecosistema montañoso, presenta una vulnerabilidad climática característica para áreas afectadas por el derretimiento de glaciares y a cambios en los patrones de precipitación, como lo evidencian una megasequía prolongada, el retroceso acelerado de nieve y glaciares y la creciente demanda de agua potable e industrial, todo lo cual ha contribuido a reducciones sistemáticas de caudales en los últimos 15 a 20 años (Garreaud et al., 2019; Muñoz et al., 2020; Peña-Guerrero, 2020; Shaw et al., 2021; Cordero et al., 2024; Ugalde & Sepúlveda, 2025). Se espera que estos impactos se intensifiquen en los próximos años (Vicuña et al., 2011; Pörtner et al., 2022).

El escenario descrito evidencia una gran presión sobre el recurso hídrico que, sumado a la variabilidad espacial y temporal de la calidad de agua de los ríos (Pohle et al., 2021; Guo et al., 2019; Lintern et al., 2018) refleja la necesidad de generar conocimiento detallado sobre el estado y la dinámica hidroquímica de los cursos superficiales de las cuencas de cabecera andinas. Esto, a fin de identificar los impactos sobre el comportamiento de los solutos, y, así, permitir diseñar medidas efectivas de mitigación a los posibles efectos sobre la calidad de agua y de protección a los ríos en las cuencas de montaña (Bieroza et al., 2018; Bol et al., 2018; Liu et al 2022).

Dada la complejidad temporal y espacial de la relación entre los procesos hidrológicos y biogeoquímicos fluviales, que varía entre cuencas e incluso a escala regional (Ali et al., 2017; Zhou et al., 2017; Diamantini et al., 2018; Liu 2019). El estudio de la relación entre el caudal y la concentración y la identificación de factores que inciden en el comportamiento de los solutos en los cursos de agua de cuencas de cabecera como usos de suelo, presencia/estado de la vegetación, magmatismo, litología, características del terreno y factores climáticos, proporcionan antecedentes clave para caracterizar la hidroquímica de los ríos (Bende-Michl, et al., 2018; Liu et al., 2018; Nainggolan et al 2019; Liu et al 2022).

El análisis de las relaciones concentración–caudal (relaciones c–Q) cuantifica cómo varían las concentraciones de solutos y partículas con el caudal. Estas relaciones permiten identificar cuencas y procesos de flujo que gobiernan los patrones de exportación de solutos (Moatar et al., 2020; Pohle et al., 2021; Liu et al., 2022; Goldrich-Middough et al., 2022).

Por la complejidad descrita, no resulta sencillo determinar las causas subyacentes de una relación c–Q, y los mecanismos que explican estos comportamientos aún no se comprenden completamente. De hecho, es bastante común observar relaciones c–Q contrastantes para distintos solutos dentro de una misma cuenca, o para un mismo soluto en diferentes cuencas (Zhi et al., 2019). Por lo que, análisis a una escala territorial amplia y a largo plazo contribuyen a comprender mejor el comportamiento de los solutos con una perspectiva amplia"…

1.1 Relación Caudal Concentración

Existen numerosos métodos c–Q, cada uno de los cuales documenta los cambios en la concentración de solutos con respecto a los caudales. Knapp y Mussolf (2024) identificaron que diferentes procesos de cuenca pueden conducir a relaciones c-Q similares, y que estas relaciones se aplican a diferentes escalas de tiempo pueden transmitir información diferente por dependiendo de la zonas que estén aportando solutos. Dentro de las relaciones más aplicadas se identifican: a) la pendiente c–Q; y b) la histéresis (Speir et al., 2023):

a. La pendiente c–Q**.** Godsey et al. (2009) analizaron relaciones c–Q para cationes mayoritarios en 59 cuencas de Estados Unidos, con áreas de cuenca entre 1,5 y 2.500 km². Sus resultados revelaron relaciones log-lineales entre caudal (Q) y concentraciones (c), lo que sugiere una relación de tipo ley de potencia de la forma $C = aQ^b$. Los autores propusieron una interpretación física de la pendiente "b": valores cercanos a cero se asocian a comportamiento quimoestático, esto es, sin variación de la concentración con cambios en el caudal, mientras que una pendiente próxima a 1 refleja procesos de dilución. Más recientemente, Hunsaker & Johnson (2017), con un enfoque similar al de Godsey et al. (2009), estudiaron relaciones c–Q en ocho arroyos perennes de primer y segundo orden en la Sierra Nevada (California, EE. UU.) para solutos como Ca^{2+}, Mg^{2+}, K^+, Na^+, SO_4^{2-}, NO_3^-, Cl^-, NH_4^+ y PO_4^{3-}. Observaron comportamiento cercano a la quimoestasis para los cationes básicos, así como para SO_4^{2-} y Cl^-, pero señalaron que diferencias en características de cuenca, profundidad del suelo, geología del basamento, cobertura vegetal, vías de flujo, hidrología y clima— pueden producir relaciones c–Q distintas incluso dentro de una misma región.

Otros trabajos recientes incluyen Kaltenecker et al. (2024), quienes estudiaron tendencias de largo plazo en relaciones c–Q para ocho variables de calidad de agua en Ontario identificando principalmente patrones de enriquecimiento para Cl, NO_3 y fosforo total.

b. Histéresis. Se establece como un enfoque complementario a la relación c–Q que revela desfases temporales entre las variaciones de caudal y concentración entregando información adicional para identificar diferentes orígenes de las fuentes de agua en las cuencas (Pohle et al., 2021). Las trayectorias cíclicas c–Q reflejan diferencias en disponibilidad y accesibilidad de fuentes y en tiempos de respuesta (Klein, 1984; Evans & Davies, 1998; Lloyd et al., 2015; Vaughan et al., 2017; Speir et al., 2023). El análisis de histéresis a escala de eventos con leyes de potencia es el enfoque más común (House & Warwick, 1998; Krueger et al., 2009; Minaudo et al., 2017; Winter et al., 2020; Knapp et al., 2020), mientras que algunos estudios han extendido este enfoque a datos de largo plazo y baja frecuencia, en particular Pohle et al. (2021) y Cairoli et al. (2024).

En Chile, algunos estudios han investigado la relación c-Q en cuencas seleccionadas. Salmon et al. (2001) realizaron investigación en una microcuenca forestal remota (1,2 ha) en la Cordillera de Piuchue en Chiloé, sur de Chile, encontrando comportamiento de dilución para Ca^{2+} y Si y comportamiento quimoestático para K^{+}. Sin embargo, se llevó a cabo lejos del área de estudio de la presente tesis (transecto de 30 cuencas andinas desde la región de atacama a Ñuble) y bajo un clima húmedo (Perez et al., 1998).

Flores et al. (2016) analizaron relaciones c-Q de agua superficial en la cuenca del río Elqui (norte-centro de Chile; latitud 29.96°) usando datos de baja frecuencia (trimestral) durante 30 años, mediante diferentes modelos (lineal, logarítmico, polinómico, potencial, exponencial). Reportaron relaciones c-Q inversas para SO_4^{2-}, directas para Fe y patrones erráticos para As y Cu. Peña-Guerrero et al. (2020) evaluaron correlaciones entre caudales diarios y constituyentes de aguas superficiales en la cuenca del Maipo (Chile central), aunque solo proporcionaron correlaciones c-Q descriptivas, sin análisis quimoestáticos ni matemáticos detallados. Hernández et al. (2023) estudiaron relaciones c–Q en cuencas de cabecera del río Choapa, enfocándose en la influencia potencial del cambio climático. Finalmente, Macchioli-Grande et al. (2025) analizaron relaciones concentración–caudal en dos subcuencas contrastantes de Chile central (Maipo Alto y Mapocho Alto). En Maipo Alto, la mayoría de los solutos exhibieron dilución con el aumento del caudal, salvo en el estero Melosas (enriquecimiento) y el río Yeso (quimoestasis). En Mapocho Alto, los solutos fueron principalmente quimoestáticos o levemente de dilución, mientras que el nitrato mostró enriquecimiento; patrones atribuidos a la litología, el uso de suelo y la hidrología local.

1.2 Humedales de altura y su relación con la calidad del agua

Una de las áreas relevante en las cuencas de montaña son los humedales tipo bofedales por su capacidad de almacenamiento de agua y el soporte ecológico (Barducci et al., 2009; RAMSAR, 2013; Mitsch et al., 2015; Yager et al., 2021; EPA, 2024; USGS; 2024).
En este sentido, la sostenibilidad de estos humedales está estrechamente ligada a la disponibilidad hídrica y se ve significativamente influida por la variabilidad de la precipitación, factor climático clave que afecta tanto a los ecosistemas aguas abajo asociados como a las actividades humanas que dependen de ellos (Squeo et al.,2006; RAMSAR, 2013; Hribljan et al., 2015; Aponte-Saravia et al., 2016; De La Fuente et al., 2020; Anderson et al., 2021; Ashok et al., 2021; Uribe-Álvarez et al., 2021; Chávez et al., 2022; Luo et al., 2024).

Los estudios sobre el comportamiento de la cobertura vegetal y la calidad del agua bajo la influencia de distintos factores climáticos (como la variación de la precipitación, incluyendo períodos de sequía) se han realizado con mayor frecuencia en el hemisferio norte (Valois et al., 2020).

Por otra parte, dado que los humedales de altura se encuentran en zonas montañosas de difícil acceso, la teledetección y los índices normalizados como el NDVI (índice de vegetación de diferencia normalizada) han demostrado ser especialmente útiles para obtener datos espacio-temporales que de otra manera habrían sido imposibles o complejos de conseguir (Guo et al., 2017, De La Fuente et al., 2020; Ashok et al., 2021; Chávez et al., 2022; Ju et al., 2022; Jombo et al., 2023; Mashala et al., 2023; Rapinel et al., 2023; Zhang et al., 2023). Además, el NDMI (índice de humedad de diferencia normalizada), empleado específicamente para analizar el estrés hídrico de la cobertura vegetal, es pertinente para la gestión de los recursos hídricos y de la vegetación (Guo et al., 2017; Monteiro et al., 2024), lo que hace que el NDMI sea particularmente útil para comprender el comportamiento de los humedales en áreas con escasez de agua.

Los análisis de series temporales precipitación–vegetación han identificado diversos comportamientos de la cobertura vegetal relacionados con la ocurrencia de precipitaciones y eventos de sequía en ecosistemas de montaña, incluidos los humedales de altura. Con base en el NDVI, se detectaron incrementos generales del enverdecimiento en los Alpes Occidentales y en Suiza (incluidos sistemas montañosos) por efecto de variables climáticas (entre ellas la precipitación) y se observó que la precipitación rara vez resultó estadísticamente significativa (Filippa et al., 2019; Obuchowicz et al., 2023). El estudio realizado por Zhang et al. (2013) en la

cuenca del río Koshi (Himalaya) sobre el cambio en la vegetación demostró que la productividad vegetal aumentó entre 1982 y 1994, en concordancia con estudios previos en Eurasia, sin embargo, a una escala temporal menor, los autores detectaron una disminución abrupta de la productividad entre 1994 y 2000, seguida de un aumento entre 2000 y 2011. Además, se comprobó que la precipitación influye en el comportamiento de la cobertura vegetal. Por otra parte, se identificó una rápida expansión de los humedales en la meseta tibetana entre 1990 y 2019, asociada a un aumento de la precipitación en el contexto del cambio climático (Zhang et al., 2013). Asimismo, en un estudio realizado en una zona montañosa de la Reserva Nacional de la Naturaleza de Yangguan se observó que la presencia y acumulación de precipitación son factores importantes en los altos valores de NDVI asociados con la vegetación de estos humedales (Pan, 2018).

El uso de técnicas de teledetección para comprender las complejas interacciones entre los cambios en la reflectancia de la cobertura vegetal y las concentraciones de calidad de agua es relativamente reciente (Mashala et al., 2023). En el Parque Nacional Everglades (Florida, EE. UU.) se identificó que, a largo plazo, la calidad del agua en manglares (iones mayoritarios, nitrato y fosfato) se correlacionó con los índices biofísicos de reflectancia (como NDVI y EVI) de la cobertura vegetal (Lagomasino et al., 2014). En Xinjiang y el Tíbet, en el oeste de China, se determinó que existe una correlación significativa entre las concentraciones de iones mayoritarios y el NDVI (Liu et al., 2021). Mediante un enfoque que predice la calidad del agua del río Araçuaí, ubicado en la zona semiárida del estado de minas Gerais en Brasil, a partir del NDVI de la cobertura vegetal de la cuenca, se demostró el potencial de este índice para predecir la calidad del agua (Vieira et al., 2024).

En Chile existen aproximadamente 17 000 humedales, que representan un área de cerca de 14 604 km² (Vivanco, 2024). Los humedales de alta altitud y los conjuntos de humedales andinos (denominados en Chile "altoandinos") son principalmente praderas inundables [Valois, 2020; Vivanco, 2024, RAMSAR, 2024]. Al igual que otros ecosistemas terrestres y acuáticos, se ven impactados por el cambio climático (Pörtner et al., 2022; Salimi et al. 2021). En el valle del río Maipo (Chile), utilizando teledetección complementada con datos del área de estudio, se identificaron y cartografiaron los humedales andinos de este valle (Araya-López et al., 2018). Esta investigación reveló que el enfoque de teledetección es particularmente valioso para el monitoreo de humedales de alta montaña con acceso limitado, como ocurre en los Andes.

Los estudios sobre la dinámica de humedales altoandinos y la influencia del clima en Chile se han concentrado en el extremo norte del país (Altiplano), que presenta condiciones climáticas y características ecosistémicas singulares asociadas a una mayor aridez. En esta zona, se encontró que la precipitación en años húmedos (intervalo de recurrencia de 20–30 años) desempeña un papel clave en el sostén de estos humedales, ya que permite la recarga de aguas subterráneas (una fuente principal de agua en estos ecosistemas) (De La Fuente et al., 2020; Blin et al., 2022). A su vez, a partir de la variación del NDVI, se determinó que el período entre 2011 y 2017 fue el más productivo de las últimas tres décadas en los humedales ubicados en el Altiplano (área de 63 705 km², por sobre 3700 m s. n. m.) (Chávez et al., 2019).

Por lo antes expuesto, a continuación, se presenta el trabajo propuesto centrado en la caracterización de hidroquímica de cuencas de cabecera andinas y la influencia de las características de las cuencas y variables climáticas. Con un enfoque especial en humedales andinos.

1.3 Estructura del documento

La estructura del presente documento consiste en cuatro capítulos. El CAPÍTULO I corresponde a la introducción donde se describe el planteamiento del problema, además de las hipótesis y de los objetivos. El CAPÍTULO II analiza la hidroquímica de 30 cuencas andinas entre las regiones de Atacama y Ñuble. El CAPÍTULO III Analiza la variabilidad espacio-temporal de una cadena de doce humedales altoandinos de la cuenca del Estero Derecho, valle del Elqui, y la relación entre el estado de la cobertura vegetal, la precipitación, la temperatura y la calidad del agua. En el CAPÍTULO IV se presentan conclusiones y futuras líneas de investigación.

1.4 Hipótesis

H1 En las cuencas de cabecera andinas ente las regiones de Atacama y Ñuble, los factores fluviométricos, de cobertura vegetal y fisiográficos se asocian significativamente con los patrones de comportamiento de los solutos (As, Ca, Cl, Cu, Fe, HCO_3, K, Mg, Na, SO4, NO_3).

1.5 Objetivos.

Objetivo General. Caracterizar la hidroquímica de cuencas andinas con énfasis en la zona semiárida de Chile.

Objetivos Específicos

OE1 Estimar la relación caudal-concentración (c-Q) para diferentes solutos en un transecto de treinta cuencas de cabecera andinas desde la región de Atacama hasta la región del Ñuble.

OE2 Determinar la relación entre el estado de la cobertura vegetal de la cadena de humedales, la precipitación antecedente y la concentración de solutos en el Estero Derecho, cuenca del río Claro, región de Coquimbo.

CAPÍTULO II: Hydrochemistry of Headwater Basins: Streamflow–Concentration Relationships and spatial patterns in Andean Basins of semi-arid region of Chile.

Denisse Duhalde, Jaime Oyarzun, Juan Olivares, Catherina Aldunce, Ricardo Oyarzún, José-Luis Arumí, Consuela Milu

Water 2024, 16(24), 3682; https://doi.org/10.3390/w16243682

2.1 Resultados Clave.

- La química de aguas superficiales está dominada por meteorización de silicatos, principalmente modificada localmente por la litología, volcanismo, drenaje ácido de roca y actividad minera.
- El predominio del régimen de exportación del tipo dilución y el patrón de histéresis antihoraria sugiere fuentes de solutos distantes y escasa disponibilidad de sedimentos finos en el lecho de los ríos.
- Las pruebas no paramétricas aplicadas resultaron útiles, para vincular preliminarmente características de cuencas con la exportación de solutos y resultan una propuesta metodológica simple para estudios de comportamiento de solutos.
- Al incorporar la cobertura vegetal e índice de aridez aportan un marco para anticipar cambios en el comportamiento de solutos bajo escenarios de cambio climático y uso de suelo.
- El análisis de varias cuencas permitió detectar anomalías en la cuenca B12 con respecto al transecto, situación que puso en evidencia la capacidad de la metodología para detectar anomalías a escala regional.

2.2 Resumen extendido.

Las montañas están asociadas al concepto de «torres de agua» por su gran capacidad de almacenamiento y liberación gradual de agua, que sustenta los ecosistemas y las actividades humanas. Por lo que caracterizar las dinámicas hidrológicas e hidroquímicas es fundamental para gestionar el recurso hídrico de las cuencas de montaña. A pesar de su importancia, la compleja interacción de factores naturales y antropogénicos que inciden sobre la calidad de agua genera que aún subsista incertidumbre sobre como las variaciones del uso del suelo y patrones hidrológicos y climáticos pueden alterarla. Brecha de conocimiento que, es aún mayor en las cuencas de montaña, en parte debido a la lejanía y/o el difícil acceso de estos lugares.

En Chile, la cordillera de Los Andes tiene un rol relevante en el suministro de agua, especialmente en las zonas centro-norte y centro de nuestro país, donde se desarrolla más del 75% de la actividad agrícola nacional y una porción significativa de la población urbana. Estas zonas presentan diversas condiciones meteorológicas, de terreno y de uso de suelo, por lo que, además del caudal disponible, la calidad del agua de las cuencas de montañas de estas zonas presenta diferencias.

Adicionalmente, la presión sobre el recurso hídrico en estas zonas ha aumentado considerablemente por factores como el cambio climático, donde las montañas son altamente sensibles a este fenómeno, y los períodos de sequías prolongadas como el fenómeno de megasequía registrado en la última década.

En base al contexto descrito, resulta una oportunidad única caracterizar la hidroquímica de treinta cuencas de cabecera andinas (29°–35°S), basándose en datos de largo plazo y baja frecuencia, mediante la determinación de las relaciones concentración–caudal (c–Q), a través del régimen de exportación y el patrón de histéresis de diez solutos (Ca, Na, Mg, Cl, SO_4, HCO_3, As, Cu, Fe, NO_3). El marco metodológico incluyó: (i) modelos de ley de potencia para definir regímenes de exportación (dilución, constancia, enriquecimiento); (ii) análisis de histéresis (horaria, antihoraria, sin histéresis); (iii) diagramas hidroquímicos (Stiff, Gibbs, relaciones molares normalizadas por Na); y (iv) pruebas de Mann–Whitney U y tamaños de efecto δ de Cliff para relacionar el comportamiento c–Q con atributos de cuenca (área, altitud, pendiente, longitud de cauce, índice de aridez, vegetación, caudal medio). Las series de caudal se obtuvieron de CAMELS-CL y la química del agua de la base de datos DGA–SNIA.

Los datos fueron depurados (valores fuera de rango, valores censurados, balance iónico). La clasificación de regímenes de exportación e histéresis se realizó en base a la metodología propuesta por Pohle et al. (2021). Las características de las cuencas y climáticas se evaluaron estadísticamente en relación con el comportamiento de los solutos.

Los resultados obtenidos son los siguientes: En general en las series temporales del transecto, se identificó una disminución de los caudales y un aumento de las concentraciones. Se identificó un pH neutro a básico en la mayoría de las cuencas, salvo condiciones ácidas en B03 y B21 por alteración argílica y drenaje ácido de roca (DAR). Aplicando el diagrama de Stiff se identificó que el patrón predominante era el enriquecido en los iones Ca–HCO_3 (15/30

cuencas) y Ca–SO_4 (10/30 cuencas). Bajo el diagrama de Gibbs y Na-Normalizado se identificó que los iones provienen principalmente por meteorización de rocas de silicatos.

Con respecto a la relación c-Q se identificó para los iones mayores un comportamiento predominante de dilución para el régimen de exportación y sentido antihorario para la histéresis. El Fe muestra enriquecimiento con histéresis horaria; NO_3 comportamiento mixto; Cu y As con patrones débiles por bajas concentraciones o falta de datos.

En especial las cuencas del sur (B28–B30) mostraron principalmente para todos los solutos comportamiento de dilución. La cuenca B12 presentó comportamiento atípico (Cl, K, Mg, Na), asociado a regulación de caudales y calidad de agua producto de actividad minera.

Con respecto al análisis de la influencia de las características de las cuencas sobre la relación c-Q, en la Histéresis vs. atributos de cuenca: sin resultados significativos ($p \geq 0.05$), pero con tamaños de efecto medianos ($\delta \approx 0.37–0.46$) en pares como Cl–altitud, NO_3–vegetación, K–altitud, Ca–vegetación, SO_4–área. Regímenes de exportación: cinco asociaciones significativas ($p<0.05$, δ medio–alto): Ca–vegetación (+), Ca–altitud (–), K–longitud de cauce, K–pendiente, Mg–pendiente.

El estudio, demostró tener un enfoque práctico para vincular las características de las cuencas y las condiciones climáticas con el comportamiento c–Q a largo plazo, que por su amplia área de estudio y las diversas condiciones presentes en cada una de las treinta cuencas podría resultar útil para estudios similares vinculados al comportamiento de solutos en cursos fluviales. Además, incorporar explícitamente el índice de aridez y la vegetación considerando diversidad que presenta el transecto en estos factores, en un contexto de cambio climático, ofrece una perspectiva novedosa para anticipar cambios en el comportamiento de los solutos bajo patrones de uso de suelo y dinámica hidroclimática en evolución (precipitación y evapotranspiración). Finalmente, se presentaron limitaciones relacionadas con escasez de datos actualizados, por ej de NO_3, soluto relevante para identificar influencia antropogénica y antecedentes para determinar con mayor precisión el origen de las relaciones c–Q observadas. Por lo que posibles líneas de investigación podrían relacionares con ampliar la

caracterización de cada cuenca, con especial atención en actualización datos de parámetros de calidad de agua, monitoreos espacialmente distribuidos en las cuencas, la caracterización físico química de los sedimentos, dinámica nival y los aportes de aguas subterráneas.

2.3. Introduction

Due to their importance in the global freshwater supply for both ecosystems and human well-being, the term "Water Towers" is widely used to describe mountain regions (Immerzeel et al., 2019). This concept is tightly linked to the hydrochemical dynamics of headwater basins, where orographic lifting enhances precipitation and runoff, and where water is additionally stored in snowpacks, glaciers, and wetlands that, in turn, support groundwater recharge (Viviroli et al., 2007; Nauditt et al., 2017; Markovich et al., 2019; Immerzeel et al., 2019). To elucidate how these mountain processes shape downstream chemical signatures and material transport across large watersheds, it is essential to integrate river-chemistry observations with discharge, bedrock, soils, and land-use/land-cover datasets, thereby resolving the effects of spatial heterogeneity in lithology, climate, and land use on overall hydrochemical behavior (Goldrich-Middough et al., 2022; Speir et al., 2023).

In this context, complementing the storage and distribution of water resources, a fundamental factor for the sustenance of ecosystems and human communities is the state and dynamics of river chemistry in headwater basins. Various studies have shown that the lithology and natural terrain conditions significantly shape the baseline hydrochemistry of rivers (Bluth & Kump, 1994; Burns et al., 2019; Zegers et al., 2021; Zhao et al., 2024). Natural factors such as prolonged droughts, floods, and temperature fluctuations, and anthropogenic activities, such as urban development, mining, or agriculture can be altered or even threaten river water quality.

Currently, the natural factors become particularly relevant given that mountain ecosystems, dependent on snow and glacier accumulation and their subsequent melt, are especially vulnerable to climate change, a condition exacerbated by the phenomenon of elevation dependent warming (EDW). The impacts of this phenomenon have intensified over recent decades (Pepin et al., 2015; Markovich et al., 2019; Pörtner et al., 2022).

The naturals and anthropogenic changes can significantly alter physical, chemical, and biological parameters, such as pH, dissolved oxygen, organic matter, total suspended solids (TSS), total dissolved solids (TDS), and nutrient cycles, which, compared to hydrological processes, have received relatively little attention in the scientific literature (Nauditt, 2017; Byrne et al., 2020; Peña-Guerrero et al., 2020; Pohle et al., 2021; Liu et al., 2022; Díaz et al., 2025). Establishing solute-export–based basin typologies enables effective knowledge transfer from data-rich to data-poor systems (Pohle et al., 2021).

Moreover, on a global scale, more than 20% of the global population (approximately 1.9 billion people) directly depends on the hydrological processes that take place in mountain basins (Viviroli et al., 2007; Nauditt et al., 2017; Immerzeel et al., 2019). Understanding the dynamics and behavior of hydrochemical processes is essential for assessing the impacts of both natural and human-induced changes, and for implementing sustainable water management strategies within these basins (Bogena et al., 2018; Kaandorp et al., 2021).

In line with the global context described, the Andes Mountains in Chile constitute the primary water source for the country's most important rivers. Within the transect between 29° and 35°S, over 75% of national agricultural activity and a significant portion of the urban population are concentrated (Vicuña et al., 2013; Garreaud et al., 2017; Peña-Guerrero et al., 2020). This region, being a mountainous ecosystem, presents a characteristic of climate vulnerability for countries linked to the melting of glaciers and changes in precipitation patterns, as evidenced by a prolonged megadrought, accelerated snow and glacier decline, and increasing demand for drinking and industrial water, all contributing to systematic reduced streamflows in the last 15 to 20 years (Garreaud et al., 2019; Muñoz et al., 2020; Peña-Guerrero, 2020; Shaw et al., 2021; Cordero et al., 2024; Ugalde & Sepúlveda, 2025). These impacts are expected to intensify in coming years (Vicuña et al., 2011; Pörtner et al., 2022). This scenario highlights the need to generate detailed knowledge on the state and dynamics of river chemistry, particularly regarding concentration–discharge relationships in headwater basins of north-central Chile.

Analyses of concentration–discharge relationships (c–Q relationships) can quantifie how solute and particulate concentrations vary with streamflow. These relationships allow for the

identification of basins and flow processes that govern solute export patterns (Moatar et al., 2020; Pohle et al., 2021; Liu et al., 2022, Goldrich-Middough et al., 2022).

In general, the causes underlying a given concentration–discharge behavior are not easy to determine, and the mechanisms that explain these behaviors are not yet fully understood. It is quite common to observe contrasting c–Q relationships for different solutes within the same basin, or for the same solute across different Basins (Zhi et al., 2019).

Numerous c–Q method exist, each documenting changes is solute concentration across flow conditions. Three of the most commonly applied c–Q method are: 1. the c–Q slope, 2. the ratio of coefficients of variation for C and Q, and 3. the hysteresis (Speir et al., 2023):

1. The c–Q slope: the Godsey et al. (2009) analyzed c–Q relationships for major cations across 59 watersheds in the United States, with catchment areas ranging from 1.5 to 2,500 km^2. Their results revealed log-linear relationships between discharge (Q) and concentrations (C), suggesting a power-law relationship of the form: $C = aQ^b$. The authors proposed a physical interpretation of the slope "b," associating a value close to zero with chemostatic behavior—i.e., no variation in concentration with changing discharge. Conversely, a slope near −1 reflects dilution processes.

More recently, Hunsaker & Johnson (2017) with an approach similar to that of Godsey et al. (2009) studied c–Q relationships in eight first- and second-order perennial headwater streams of the Sierra Nevada, California (USA), examining solutes including Ca^{2+}, Mg^{2+}, K^+, Na^+, SO_4^{2-}, NO_3^-, Cl^-, NH_4^+, and PO_4^{3-}. They observed near-chemostatic behavior for basic cations as well as for SO_4^{2-} and Cl^-, but noted that differing catchment characteristics—such as soil depth, bedrock geology, vegetation cover, flow pathways, hydrology, and climate—can produce varying c–Q relationships even within the same region. Recently, Kaltenecker et al., 2024 Long-term trends in c-Q relationships for eight water quality variables are studied across Ontario.

2. The ratio of coefficients of variation for C and Q: Musolff et al. (2015) proposed an alternative classification of C–Q relationships as chemostatic or chemodynamic by using the ratio between the coefficients of variation of solute concentrations and discharge (CVC/CVQ).

3. A complementary approach in the c-Q relationship reveals discharge–concentration lags and helps diagnose basins flow pathways (Pohle et al., 2021). Cyclic c–Q trajectories reflect differences in source availability, accessibility, and response times (Klein, 1984; Evans & Davies, 1998; Lloyd et al., 2015; Vaughan et al., 2017, Speir et al., 2023). Event-scale power-law hysteresis analysis is the most commonly applied approach (House & Warwick, 1998; Krueger et al., 2009; Minaudo et al., 2017; Winter et al., 2020; Knapp et al., 2020), whereas a handful of studies have extended this approach to long-term, low-frequency data, notably those of Pohle et al. (2021) and Cairoli et al. (2024). Our work contributes to this limited body of research by providing a comprehensive long-term analysis of concentration–discharge hysteresis across semi-arid Andean basins (Speir, 2023).

Some studies have investigated these topics in selected Chilean basins. Salmon et al. (2001) conducted research in a very small remote forested watershed (1.2 ha) in southern Chile, finding dilution behavior for Ca^{2+} and Si and chemostatic behavior for K^{+}. However, this work was carried out far from the present study area and under entirely different environmental conditions (e.g., precipitation, and soil characteristics).

Flores et al. (2016) analyzed surface discharge–water-quality relationships in the Elqui Basin (north-central Chile) using low-frequency data spanning 30 years from official records of the Chilean Water Authority (Dirección General de Aguas, DGA). They tested several models such as linear, logarithmic, polynomial, power and exponential. They reported inverse c-Q relationships for SO_4^{2-}, direct relationships for Fe, and erratic patterns for As and Cu. Peña-Guerrero et al. (2020) evaluated correlations between daily discharge and surface water constituents in the Maipo River Basin (central Chile) but provided only descriptive c-Q correlations without detailed chemostatic or mathematical analyses. Hernández et al. (2023) studied c–Q relationships in Choapa River headwater basins, focusing on the potential influence of climate change. Finally, Macchioli-Grande et al. (2025) analyzed c-Q relationships in two contrasting central Chilean sub-basins (Maipo Alto and Mapocho Alto). In Maipo Alto, most solutes exhibited dilution with increasing discharge, except in the Melosas stream (enrichment) and the Yeso stream (chemostasis). In Mapocho Alto, solutes were mainly chemostatic or slightly dilutive, while nitrate showed enrichment—patterns attributed to lithology, land use, and local hydrology.

Within this context, we present (i) a hydrochemical characterization across a transect of thirty semi-arid Andean basins and (ii) a framework that applies long-term, low-frequency c–Q relationships to the same transect, complemented by meteorological, terrain, and land-use data.

2.4 Data and Methods

2.4.1 Study area

This study was carried out across a transect of thirty high-Andean headwater basins located in the semi-arid region of Chile, spanning from the Atacama to the Ñuble regions (Figure1). This transect that has been particularly affected in recent years by the megadrought phenomenon (Garreaud, 2019). Table 1 presents the main hydrological and physiographic attributes of the basins.

Based on the updated Köppen–Geiger Climate Classification (Peel et al., 2007), these basins can be classified primarily into two major climate zones: Tundra (ET) and Warm-Summer Mediterranean (CSb), with the exception of the two northernmost basins, which exhibit a Cold Desert Climate (BWk). In addition, a strong climate gradient across the transect is indicated by the aridity index (Evapotranspiration/Precipitation).

Slope ranges of the main river channels in the basins were classified according to the Landform Mapping Systems Subcommittee of the Canada Soil Survey Committee (1976). The average slope of these main channels ranges from 2% to 15%. Most of the basins (15 out of 30, or 50%) have average slopes classified as gentle (Category 4, 5–10%); twelve basins have very gentle average slopes (Category 3, 2–5%), and three basins (B09, B14, B21—10% of the total) exhibit moderatly average slopes (Category 5, 10–15%).

The predominant land covers across the transect are barren areas and shrublands. However, beginning with basin B20 and towards the south, there is a noticeable increase in the coverage of grasslands and natural forest areas.

Regarding lithology, the transect is primarily composed of igneous rocks such as andesites, diorites, tonalites, and granodiorites. Several volcanic complexes are also identified,

spanning from the Metropolitan Region (basin B24) to the Ñuble Region (basin B30) (Sernageomin, 2002).

Table 1. Summary of Hydrological and Physiographic Basin Attributes.

Basin	Area (km²)	Aridity Index	P (median) (mm/year)	Q (median) (m3/s) (m³/s)	Stream Length (km)	Mean Slope (%)	Land Cover (%)				Climate
							Barren	Shrublands	Grasslands	Natural forest	
B01	3039	7,6	77,5	2,1	162,6	2	79,3	19,3	0,5	0,0	BWk
B02	1726	5,2	111,4	1,4	72,6	5	73,8	24,1	0,9	0,0	
B03	467,4	4,9	110,5	0,6	32,9	7	86,8	12,3	0,4	0,0	
B04	338,2	2,9	170,8	0,7	47,3	6	69,0	27,6	1,5	0,1	
B05	672,4	2,1	196,8	1,8	49,6	4	66,5	29,0	2,0	0,1	ET
B06	393,7	1,8	316,1	0,8	42,1	6	66,5	29,0	2,0	0,1	
B07	568,5	2,6	241,7	0,2	59,7	4	66,6	29,6	1,9	0,0	
B08	490,5	3,4	237,3	0,9	47,7	5	46,5	50,3	1,2	0,2	
B09	189	2,7	259,3	60,5	22,2	11	47,3	49,7	1,2	0,3	
B10	557,1	2,4	264,0	0,4	37,1	6	68,4	26,3	2,5	0,3	
B11	243,9	2,9	215,6	0,6	26,5	8	57,2	38,3	1,4	0,3	CSb
B12	368,9	2,8	257,3	16,8	29,0	8	49,0	44,4	1,4	0,5	
B13	1132	2,3	283,1	4,8	51,8	5	63,6	28,7	4,9	0,2	
B14	81,1	2,6	344,2	0,1	11,0	15	27,3	70,9	0,8	0,1	
B15	241,1	2,1	365,0	0,4	31,1	7	39,7	56,8	2,3	0,2	
B16	348	2,2	352,5	0,6	37,3	7	37,0	59,1	2,4	0,3	
B17	885,3	1,8	343,6	4,4	57,7	6	63,7	33,0	2,4	0,1	ET
B18	831,6	1,6	319,7	0,6	63,1	5	70,1	24,1	4,1	0,2	
B19	387,2	1,3	341,4	1,5	24,6	7	73,8	7,1	9,9	0,4	
B20	181	2,2	392,8	0,3	24,2	6	19,6	60,9	19,0	0,2	CSb
B21	110	1	391,1	0,6	22,1	13	69,6	11,4	12,3	0,2	ET
B22	638	1,4	419,7	3,8	39,3	7	51,8	21,4	24,1	0,4	ET/ CSb
B23	541,6	1	359,6	1,3	53,9	6	67,9	4,6	11,6	0,0	ET
B24	1663	1	464,2	22,1	74,6	5	68,3	11,3	11,6	0,2	ET/ CSb
B25	1463	0,6	964,7	5,7	69,6	3	78,8	5,9	11,8	0,1	ET
B26	245	0,5	1345,2	5,4	26,1	8	43,0	30,9	10,3	13,3	CSb
B27	1438	0,5	1348,6	42,0	65,1	4	57,7	19,7	11,3	5,1	ET/ CSb
B28	354,4	0,6	1529,4	15,6	43,2	6	36,4	32,9	11,5	14,5	
B29	1172	0,6	1160,7	39,4	56,5	3	64,9	12,3	16,8	0,4	CSb
B30	128,6	0,4	2423,9	1,4	27,5	5	18,3	28,0	5,8	43,1	

Aridity Index=Evapotranspiración potencial anual/Precipitation

Köppen-Geiger Climate Classification: BWk: Cold Desert Climate; ET: Tundra; CSb: Warm Summer Mediterranean

The complete version of this table is provided in the supplementary materia

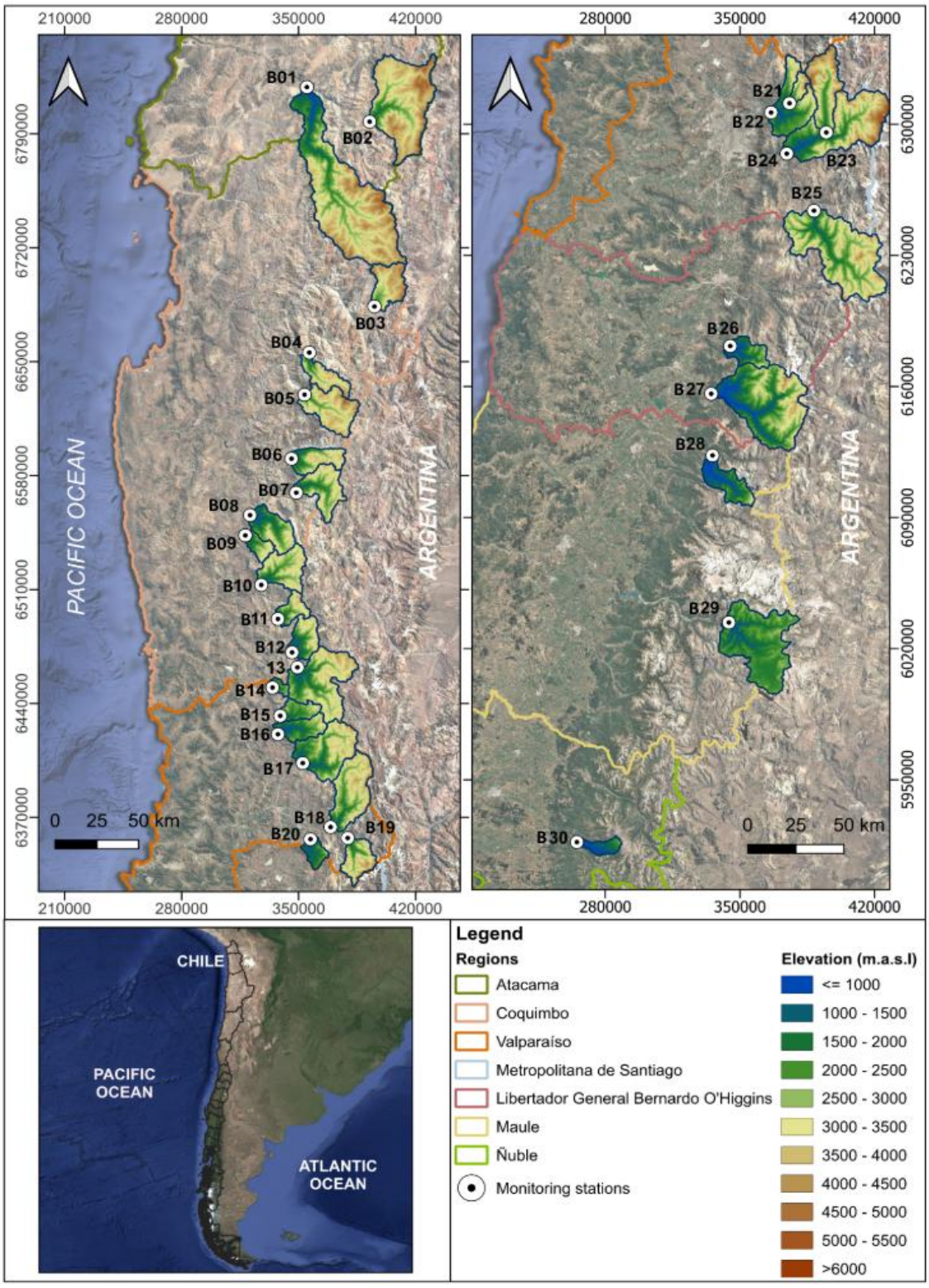

Figure 1. Study area. Maps showing the study basins labeled B01 to B30 along with elevation shading. Monitoring station at the oulet of each basin are labeled with a dot inside open circles. Colored polygons show the regions of Chile.

2.4.2 Historical discharge and water quality data

Discharge data for the basins were obtained from the CAMELS-CL Explorer platform (https://camels.cr2.cl/). Water composition data for arsenic (As), calcium (Ca), chloride (Cl), copper (Cu), iron (Fe), potassium (K), magnesium (Mg), sodium (Na), nitrate ($N–NO_3$), and sulfate (SO_4) were obtained from the historical DGA database, available through the National Water Information System (SNIA) platform (https://snia.mop.gob.cl/BNAConsultas/reportes).

a. Data Preprocessing

To preprocess the database, censored values (i.e., those below the detection limit) and outliers were identified. If censored values represented more than 10% of the total data for a given parameter, values below the detection limit were removed. If they represented less than 10%, these censored values were replaced with the average between zero and the detection limit. The following types of outliers were identified: (a) values measured below the instrument detection limit; (b) extreme values associated with potential measurement, sampling, or data entry errors; and (c) extremely high or low values identified using BoxB and Boxplot functions in RStudio.

After this initial screening, the following criteria were considered: (a) comparison of the parameter under evaluation with records from nearby monitoring stations and similar dates; (b) comparison with directly related parameters (e.g., chloride vs. electrical conductivity); and (c) evaluation of charge balance for major ions. In samples that showed a charge imbalance greater than 10% (positive or negative), the major ions were excluded from the corresponding record date. Finally, outliers that did not meet validation criteria were discarded.

b. Descriptive Analysis

With the cleaned dataset, boxplots were generated for each basin and each studied parameter in order to identify spatiotemporal behavior. This analysis was performed using RStudio, employing the BoxB and Boxplot functions.

To identify the dominant hydrogeochemical processes controlling the mean ionic composition of the study basins, we performed two analyses: (1) The Gibbs diagram

(Gibbs,1971), which differentiates the three principal controls on river-water chemistry-precipitation dominance, water–rock interaction (weathering), and evaporation–crystallization. The diagram plots total dissolved solids (TDS) against the sodium fraction, Na/(Na+Ca) (and, analogously, Cl/(Cl+HCO_3) for anions), delineating the canonical fields for these processes and thereby indicating the primary source of salinity in surface waters and (2) Na-normalized molar ratios diagram (Gaillardet, 1999) for HCO_3^-/Na^+ vs. Ca^{2+}/Na^+ and Mg^{2+}/Na^+ vs. Ca^{2+}/Na^+, to assess the relative contributions of chemical weathering and identify the dominant lithology (evaporites, carbonates, or silicates).

To classify the basin waters into different hydrochemical facies (e.g., calcium–sulfate type water), the classical Stiff diagram (Stiff, 1951) was used, based on major ions, specifically, cations (Ca^{2+}, Mg^{2+}, $Na^+ + K^+$) and anions (Cl^-, HCO_3^-, SO_4^{2-}).

In addition, the statistical analysis of water quality was complemented by data on basin characteristics and information related to anthropogenic activity and geological context within the basins.

2.4.3 Classification of c-Q Relationships

The classification of c–Q relationships was determined based on the methodology proposed by Pohle et al. (2021). These relationships consider the export regime (dilution, constancy, or enrichment) as well as the long-term average hysteresis pattern (clockwise, no hysteresis, or anticlockwise), applied to low-frequency water quality data (Figure 2).

Regarding the export regime: dilution is associated with source-limited mobilization; constancy with a homogeneous distribution of solutes in surface and groundwater flows or in variable source areas; and enrichment with transport-limited mobilization. In terms of hysteresis patterns, a clockwise loop corresponds to a fast response, typically related to nearby sources or high hydrological connectivity; whereas an anticlockwise loop indicates a slow response, associated with distant sources or low connectivity; and no hysteresis reflects an intermediate response, generally linked to medium-distance sources with variable origins and flow paths (Evans & Davies, 1998; Pohle et al., 2021).

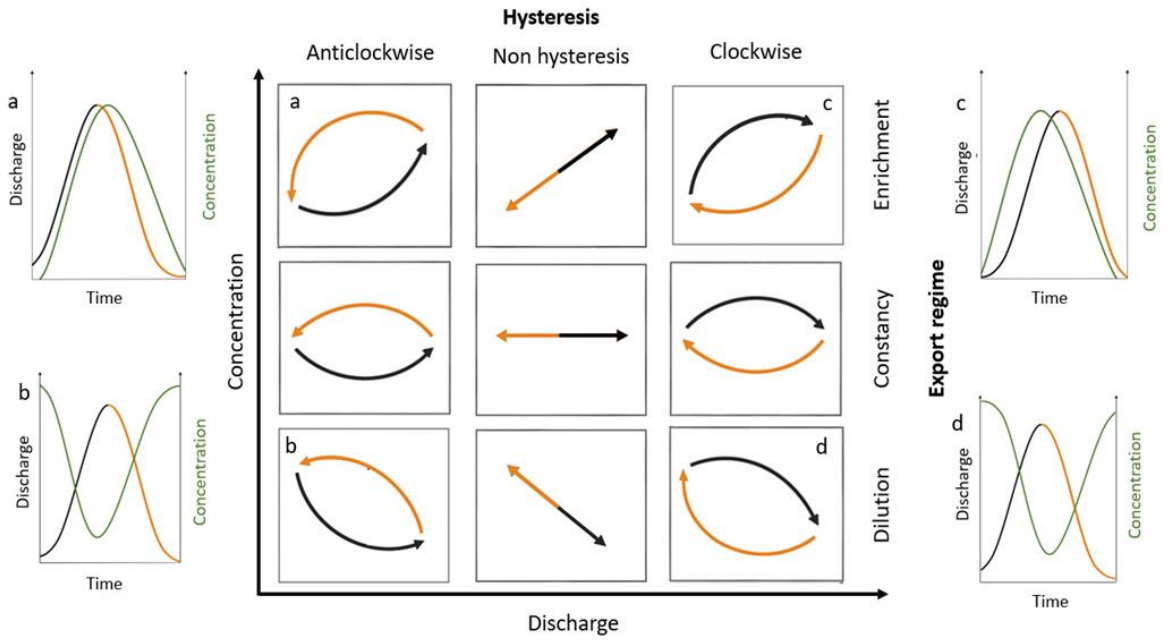

Figure 2. Classification of c–Q relationships based on export regime (enrichment, constancy, dilution) and hysteresis pattern (anticlockwise, clockwise, none). In left and right panels, the concentration curve is shown in green, while the hydrograph is represented in black (rising limb) and orange (falling limb) over time. Panels (a, b, c, d) correspond to the c–Q relationships labeled with the same letters.

The analysis procedure was as follows:

a. **Hydrograph segmentation.** Through baseflow separation, flow events were identified and each record was labeled as "rising", "peak," or "falling."

b. **c–Q parameter fitting.** For the rising, peak and falling subsets, all discharge percentiles (1%–99%) were iterated to determine Q_aut (Caudal en que la relación estadística entre concentración y caudal muestra el cambio más pronunciado). Power-law models of the form $C = aQ^b$ were fitted, and modeled concentration curves were generated over the corresponding discharge hydrograph.

c. **Classification of c–Q type and hysteresis.** Export regime—enrichment, dilution, or constancy—was evaluated using the Mann–Kendall trend test. The Kruskal–Wallis test was applied to identify hysteresis patterns: clockwise, anticlockwise, or no hysteresis.

C–Q relationships were determined using the code developed by Pohle et al. (2021), which was optimized to input and process the database of the thirty basins in the study area.

2.4.4. Influence of Basins Characteristics on Solute Behavior

To assess whether basin characteristics (altitude, area, aridity index, mean discharge Q_mean, vegetation cover, mean slope, and stream length) are associated with c–Q behavior (export regime and hysteresis), we used the non-parametric Mann–Whitney U test (Wilcoxon rank-sum; Mann & Whitney, 1947), implemented in R via wilcox.test(). Statistical significance was set at $p < 0.05$. To complement null-hypothesis testing, we quantified effect sizes with Cliff's delta (δ; Cliff, 1993), in R via Cliff.delta(), a distribution-free measure of stochastic dominance that captures the magnitude and direction of the difference between two groups.

While non-parametric tests (Mann–Whitney U) and effect sizes (Cliff's δ) are routinely reported in aquatic sciences (Hu et al., 2021; Abbott, et al., 2022; Pham & Sokolova, 2023; Ding & Qin; 2024; Jupke, et al., 2024; Waras et al., 2024), our literature survey did not identify studies that apply them directly to solute-export analysis or to the classification of c–Q hysteresis patterns. This gap motivates our approach, which operationalizes these statistics to quantify export regimes and hysteretic behavior in solute–discharge relationships.

2.5. Result and Discussion

2.5.1. Descriptive Data Analysis

Across the transect, time series generally show decreasing discharge (Q) and increasing solute concentrations (Fig.3 a.b.). In the c–Q plots, higher flows are associated with lower concentrations, consistent with dilution. For illustration, Figure 3 presents the discharge and solute dynamics for basins B18 and B27.

Figure 3. Integrated view of stream flow and solutes concentration dynamics in B18: a. streamflow (log) vs time; b. Concentration (log) vs time; c. Concentration (log) vs streamflow.

As expected, the highest streamflows were recorded in the southern part of the transect, consistent with the annual precipitation records. The basins with the highest median flows (above 15.5 m³/s), in descending order, are B27, B29, B24, and B28. Conversely, the basins

with the lowest streamflows, in ascending order, are B14, B12, and B09 (with medians below 0.3 m^3/s). In this case, although these are not the northernmost basins, factors such as basin area (B14 is the smallest in the entire transect, with 81 km^2), basin elevation (B09 and B14 have lower elevations than nearby basins), and anthropogenic influences also affect discharge. This can be explained by the fact that larger and higher-altitude catchments tend to enhance water and/or snow storage, while in the case of human influence, streamflow is affected by consumptive water use.

Regarding streamflow variability, the highest values were observed in the southern basins of the transect (B25, B26, B27, B28, B29) due to lower Aridity index. However, basins B09, B14, B18 and B25 exhibited greater standard deviations that were inconsistent with the behavior of neighboring basins (Figure 4). For B09 and B14, this situation could be associated with their relatively small area and low elevation, which favor rainfall over snowfall, reduce storage capacity, and increase runoff. In contrast, for B18 and B25, with the available information, it was not possible to identify significant differences compared with the nearby catchments.

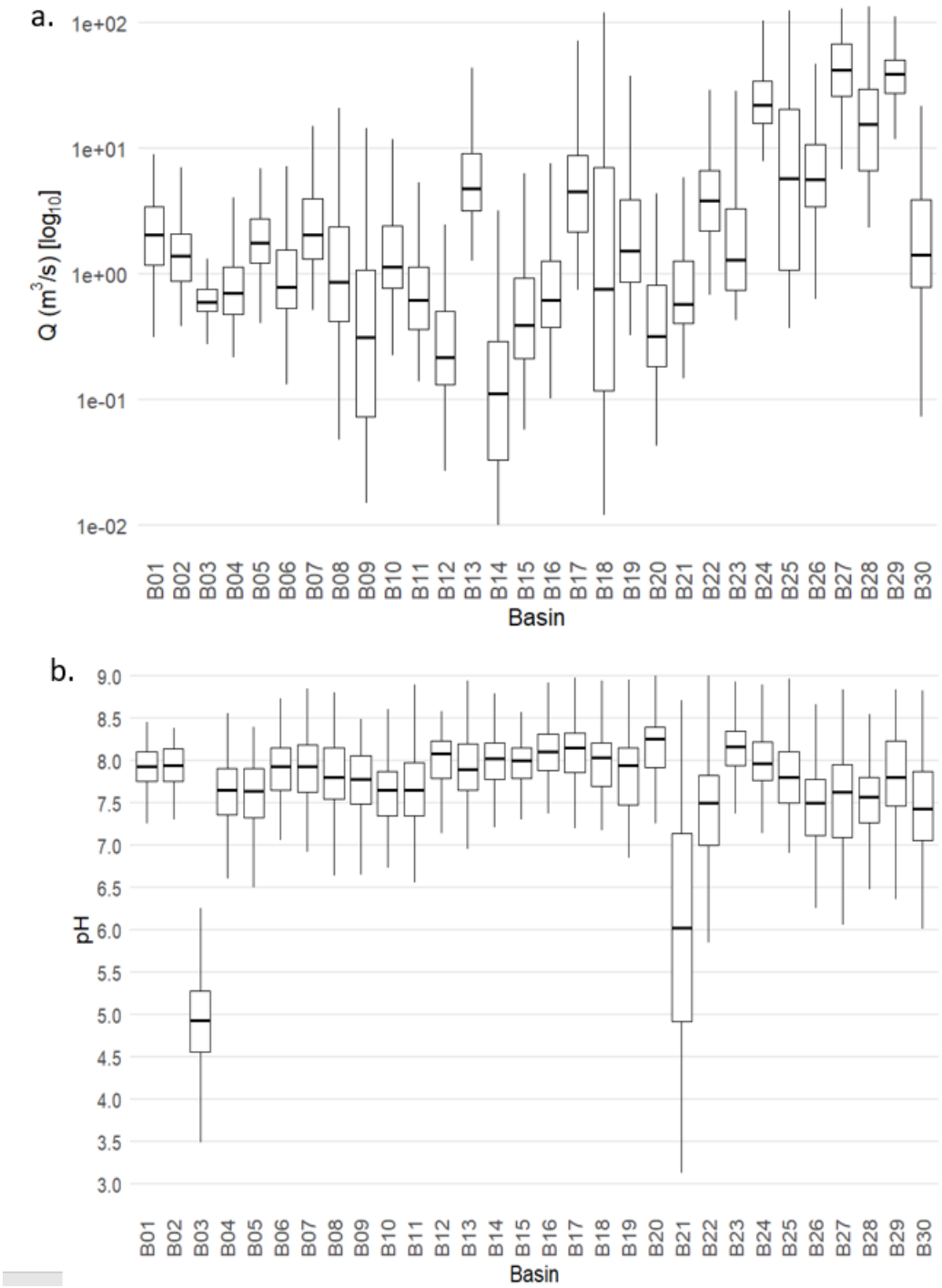

Figure 4. Boxplot: a. streamflow and b. pH for each basin of the transect

In general, the basins exhibit a neutral to slightly basic pH (Figure 4b), associated with the presence of igneous rocks—primarily andesite, diorite, and granodiorite (Sernageomin, 2002). Additionally, along the transect, the Figure 4b shows that pH values tend to be slightly higher in the northern basins than in the southern ones. This pattern is related to the higher

carbonate concentrations found in the more arid northern basins, and to the greater presence of vegetation (organic matter) toward the southern transect, which is linked to the generation of carbonic acid (Moreno & Gibbons, 2007; Senarathne et al., 2024). However, acidic pH values were recorded in basins B03 (pH 4.9) and B21 (pH 6.0), a condition explained by the presence of advanced argillic alteration zones and acid drainage generation processes (Oyarzun et al., 2004; Oyarzun et al., 2006; Orrego-Verdugo et al., 2021).

Solute concentrations (mg/L) (Figure 5) varied across the basins. Notably, Basin B03 generally exhibits the highest concentrations and standard deviations for most solutes, except for HCO_3^- a pattern associated with the previously discussed pH conditions and mineralization processes.

The highest concentrations of major ions are mainly found in B01, B02, B12 and in the basins between B19 and B25, with variable standard deviations. The behavior of major ions in these basins, along with the hydrochemical facies classification, is explained in the following section.

B03, although most of the basins exhibit very low trace element (As, Cu, Fe) concentrations, shows high levels of these elements, associated with mineral deposits and acid rock drainage (ARD).

In addition, the elevated As concentration in B14 may be attributable to: (1) an isolated event, or (2) data recording errors, given that no significant anthropogenic activity has occurred within this basin and that, of the ten measurements obtained during the monitoring period, three showed anomalously high values, all corresponding to consecutive sampling campaigns conducted in February, May, and July 1997, with concentrations of 1.37 mg/L, 0.67 mg/L, and 0.73 mg/L, respectively.

Cu shows elevated concentrations in B21, associated with the contribution of mineral deposits and acidity generated by ARD in the upper part of the basin (Orrego-Verdugo et al., 2021). Basin B22 presents an average concentration of 0.005 mg/L, but one outlier value of 2.434 mg/L stands out from the dataset. This anomaly cannot be attributed to the historical behavior of the basin.

As for Fe, a slight increase in concentration was detected in B01 and in several basins in the central zone (B17–B27), which may be associated with the specific lithology of these basins.

In the case of $N–NO_3^-$, all basins, except for B03, present concentrations below 1 mg/L. Slightly higher concentrations are observed in basins B01, B02, B12, and from B19 to B24 along the transect. This is, in a sense, an expected result, since the headwater catchments studied generally have little to no area allocated to agricultural or residential use.

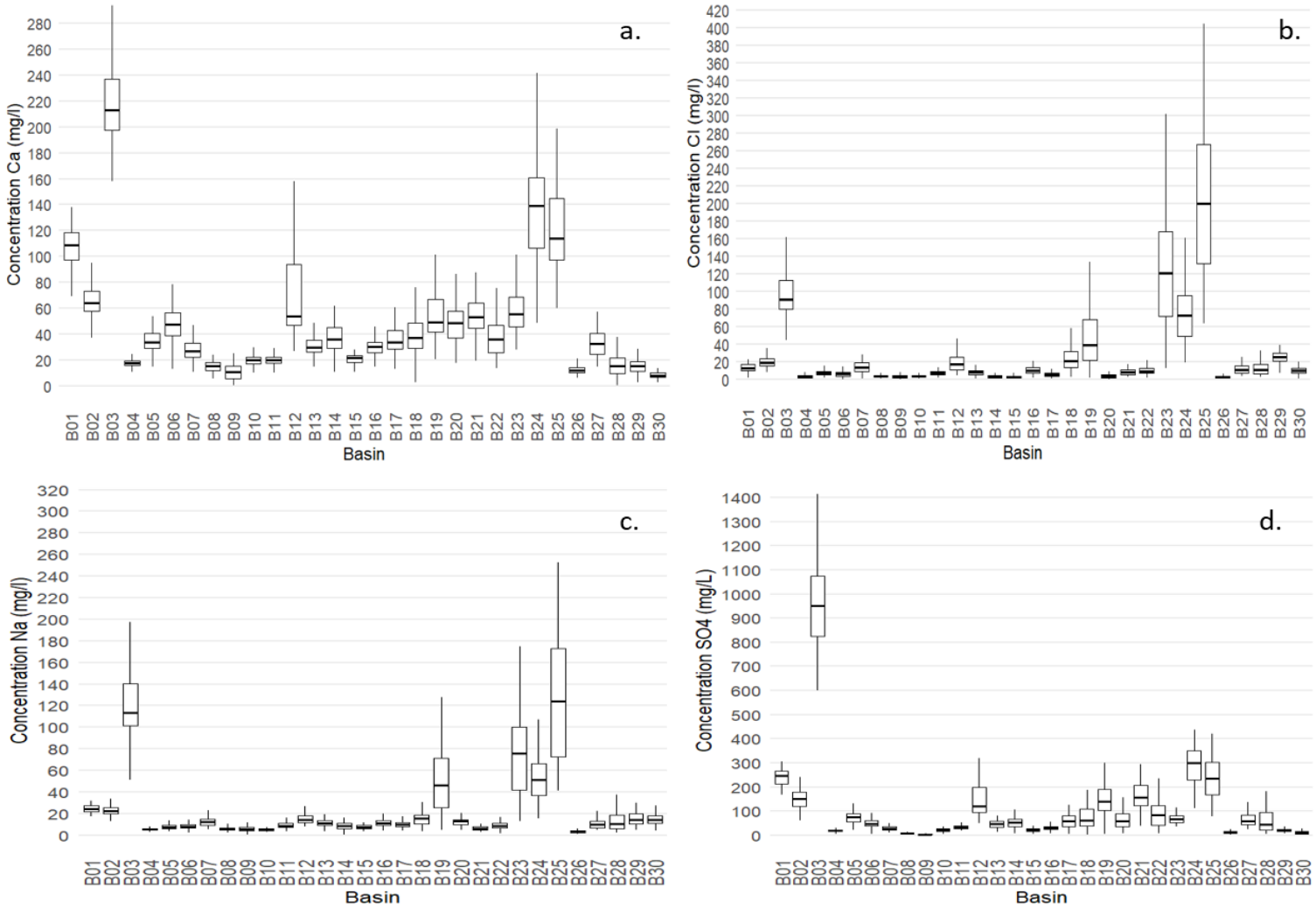

Figure 5: Box plot of the different solutes of the thirty basins of the transect (The boxplot is displayed without outliers): a. Ca (mg/l), b. Cl (mg/l), c. Na (mg/l), d. SO_4 (mg/l). Plots for additional solutes are available in the Supplementary Materials section.

2.5.2. Analysis of ionic water composition

Regarding the analysis of ionic water composition using the Stiff diagram (Figure 6), a predominance of the shape indicating enrichment in Ca^{2+} and CO_3^{2-} ions was identified (14 basins, shown in green). Notably, this type of hydrochemical facies is primarily found between the Coquimbo (north) and Valparaíso (north-central) regions, with the exception of Basin B26, located in the O'Higgins (central) Region. In particular, Basin B26 (Río Claro en hacienda Las Nieves), whose mean elevation is lower than that of the surrounding basins included in the study, shows no significant anthropogenic influence (Sernageomin, 2025; Google Earth, 2025 and SEIA, 2025a.), nor any presence of volcanic or hydrothermal activity. In this context, the hydrochemical composition of the dissolved ions can be predominantly attributed to local lithology.

The second most frequent pattern consists of Ca^{2+} -SO_4^{2-} basins (10 cases, shown in yellow). Within this group, Basin B03 stands out due to its high concentrations of SO_4^{2-} and Ca^{2+}, reaching approximately 20 meq/L and 10 meq/L, respectively a condition linked to advanced argillic alteration and the presence of acid drainage in the basin (Sernageomin, 2002; Parra et al., 2011). In addition, HCO_3^- exhibits a particularly low concentration, attributable to the acidic nature of the stream water (pH close to 4.4). This condition facilitates the formation of carbonic acid (H_2CO_3), thereby reducing the presence of bicarbonate species (Middelburg, 2024). Anthropogenic activities (mining, agriculture, and rural residential) were identified in basins B01 and B02, predominantly in B01. However, both are located in the most arid region of the transect and exhibit low streamflow, a condition that promotes the enrichment of minerals and predominant solutes in the water column. Basin B12 shows elevated concentrations (meq/L) of Ca^{2+} and SO_4^{2-} ions, which are associated with both the basin's natural mineralization and the presence of the large-scale copper mining operation "Minera Los Pelambres". In basins B05 and B18, the land remains with no significant anthropogenic influence or evidence of extrusive volcanic or hydrothermal activity. In this context, the hydrochemical composition of the dissolved ions can be predominantly attributed to the underlying geology of the basins.

In the nested basins B21 and B22, the Stiff diagrams show similar patterns, with both enriched in Ca^{2+} and SO_4^{2-}. However, B22 exhibits lower ionic concentrations. This

difference can be explained by two main factors: (i) in B22, there is no evidence of ARD or other sources of ionic enrichment, unlike B21, which presents hydrothermal argillic alteration and ARD processes; and (ii) The higher discharge in B22 contributes to a significant dilution of the tributary flow from B21. On the other hand, for the nested basins B23 and B24, the Stiff diagrams display different patterns. B23 is enriched in Na^+ and Cl^- ions. The origin of this pattern in B23 remains unclear, because the basin area consists primarily of natural land cover and the lithology is dominated by volcanic rocks (rhyolites and andesites), with volcaniclastic formations and continental sedimentary rocks, which could potentially contribute Na and Cl (Thiele, 1980; Sernageomin,2002). In contrast, B24, enriched in Ca^{2+} and SO_4^{2-}, shows a hydrochemical pattern that can be linked to the presence of the Tupungatito volcanic complex, composed of Nevado sin Nombre, Tupungato, and Tupungatito (the latter still active), the hydrothermal waters of Baños Azules (indicative of hydrothermal activity), and two mining operations that extract gypsum ($CaSO_4 \cdot 2H_2O$) and limestone (primarily composed of $CaCO_3$) (Sernageomin, 2002; SEA, 2025b; SEA, 2025c; CONAF, 2025). Additionally, another relevant factor influencing the hydrochemistry of nested basins B23 and B24 is the presence of the largest glacier surface in the north-central Chilean Andes, and consequently, within the studied transect, which covers approximately 140 km^2 hectares in total (Conaf, 2025).

Basins B19, B25, and B29 also exhibit enrichment in Na^+ and Cl^- ions. In B19, which also shows enrichment in Ca^{2+} and SO_4^{2-}, significant anthropogenic influence was identified. This includes the presence of the Andina copper mine, a large-scale mining operation located throughout nearly the entire basin, as well as an inland fish farm and the town of Río Blanco. These factors may explain the Stiff diagram pattern observed in this basin.

In B25, where the Maipo volcano is located, lithology could be related to the enrichment in Na^+ and Ca^{2+}, as the basin is primarily composed of andesite and dacite rocks (Thiele, 1980; Sernageomin, 2002; Sruoga et al., 2012). Furthermore, the presence of volcanism and the emergence of thermal waters may serve as sources of SO_4^{2-} and Cl^-, as observed in B23, B24, and B25 (Drever & Stillings, 1997; Chiodini et al., 2000; Calmels et al., 2007; Dessert et al., 2008; Gaillardet et al., 2011; Rivé et al., 2013; Perez-Fodich & Derry, 2019; Risacher et al., 2010).

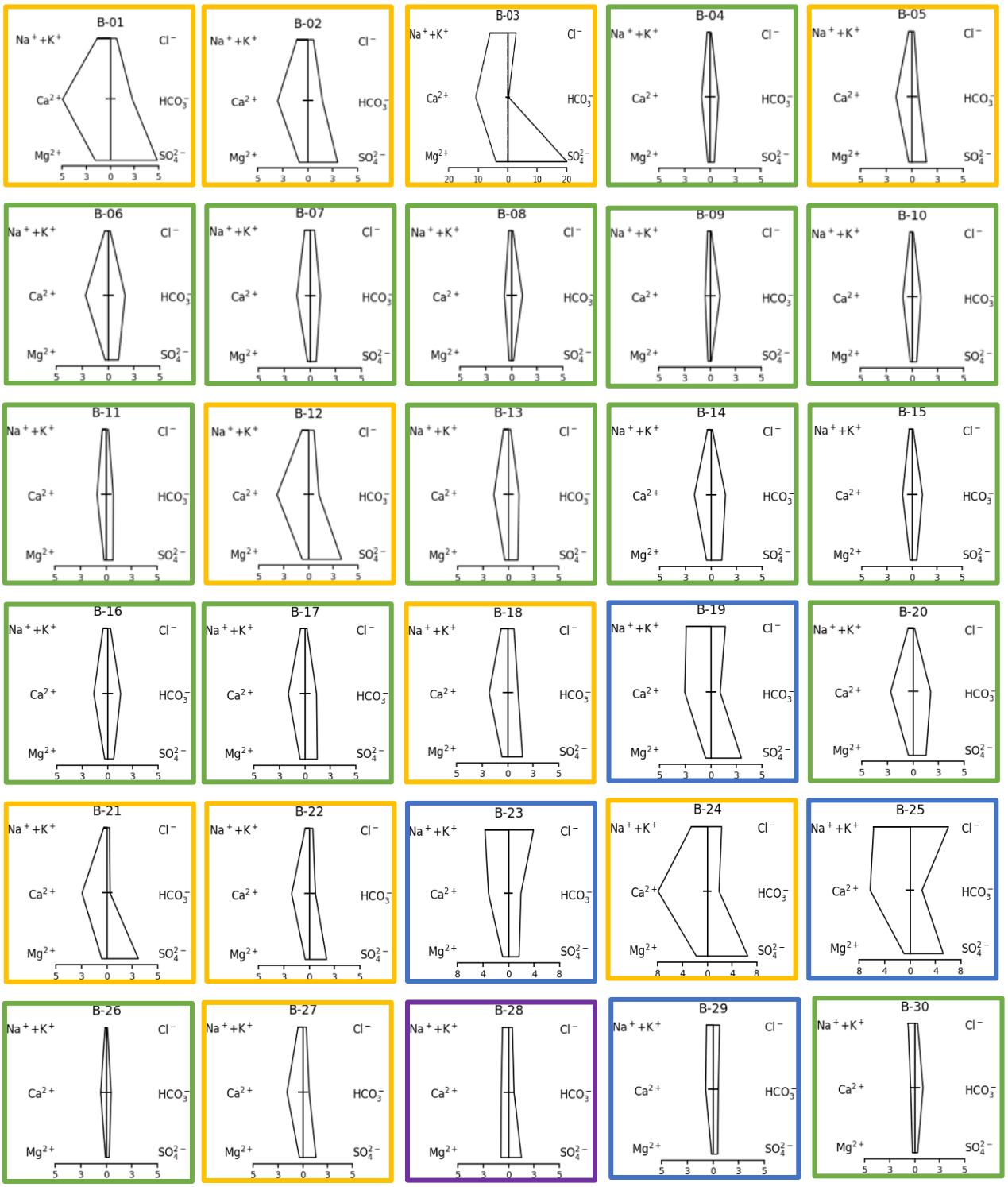

Figure 6. Stiff diagrams of the thirty basins. Yellow box: Ca^{2+} and SO_4^{2-} enrichment; Green box: Ca^{2+} and HCO_3^- enrichment; Blue box: Na^+ and Cl^- enrichment; Purple box: SO_4^{2-} enrichment. The concentration range for B03 is 0 to 20 meq/L; for B23, B24, and B25 it is 0 to 8 meq/L; and for the remaining basins, the range is 0 to 5 meq/L.

In Basin B29, where the Laguna del Maule volcanic complex is located (and where an actual lagoon exists), the only notable anthropogenic activity is a hydroelectric power plant. However, no clear link could be identified to explain the enrichment in Na^+ and Cl^- ions.

Basin B28 shows a distinct pattern, with a rather rectangular shape and very low concentrations, along with the high precipitation levels (approximately 1,500 mm/year on average) and a slight enrichment in sulfate ions. This condition is associated with the active Planchón–Peteroa volcanic complex located within the basin.

Two key observations are made along the transect: (i) The aridity gradient, which is closely related to the amount of precipitation in each basin, is linked to the low ionic concentrations in basins B28, B29, and B30, even though these basins contain active volcanic complexes; (ii) Basins B23, B24, and B25 exhibit a hydrochemical signature with higher solute concentrations compared to other basins in the central part of the transect.

Finally, a dominance of the Ca–SO_4 pattern is observed in the first five basins. Between B06 and B17, a predominance of the Ca–HCO_3 pattern was identified, whereas from B18 to B30 a mixed behavior was evident, with some basins exhibiting enrichment in Na–Cl–Ca–SO_4, which is not observed in the northern sector of the transect.

The role of geological factors in determining the hydrochemical imprint of the rivers in the studied basins is evidenced by the Gibbs diagram and Na-normalized molar ratios diagram shown in Figure 7 and Figure 8.

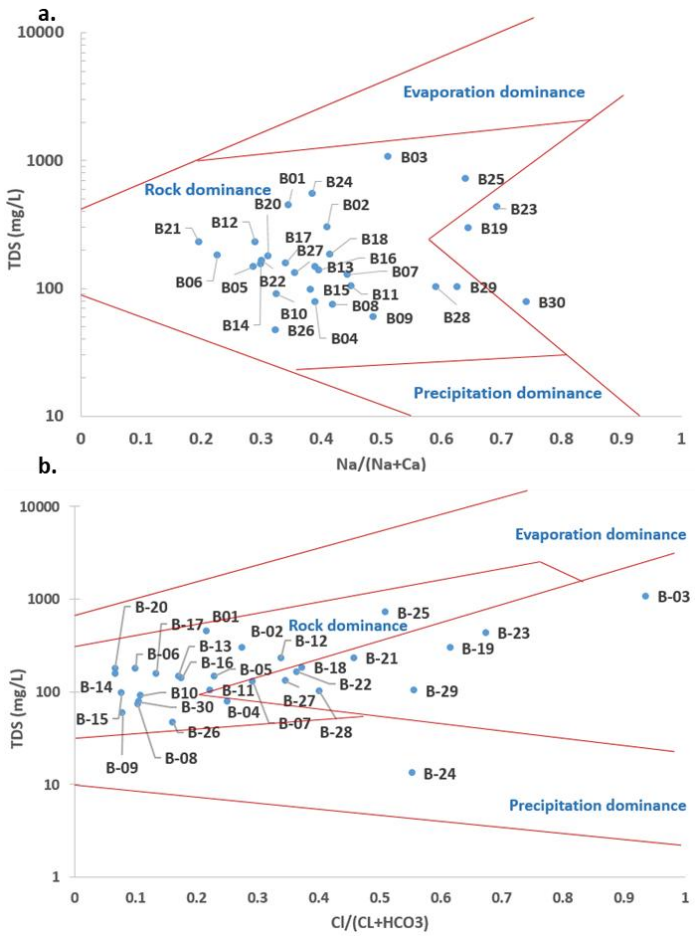

Figure 7. Hydrogeochemical processes of ions (mean) from basins in the study area based on Gibbs diagrams for (a) $Na^+/ (Na^+ + Ca2^+)$ vs. TDS; (b) $Cl^-/ (Cl^- + HCO3^-)$ vs. TDS.

The Gibbs diagrams (Figure 7 a and b) indicate that rock–water interactions are the dominant processes governing surface water chemistry across the transect. Basins located outside the characteristic "boomerang" pattern can be attributed to geology or land-cover of de basins, which are described in detail in the Stiff diagram sections.

To further elucidate the dominant weathering and dissolution processes shaping basin hydrochemistry, the Na-normalized diagram was employed to assess whether water solutes primarily originate from the dissolution of lithological minerals (evaporites, carbonates, and silicates). As shown in Figures 8a and b, the hydrochemical characteristics of most basins are largely controlled by silicate weathering. This situation is consistent with the description provided by Sernageomin (2002).

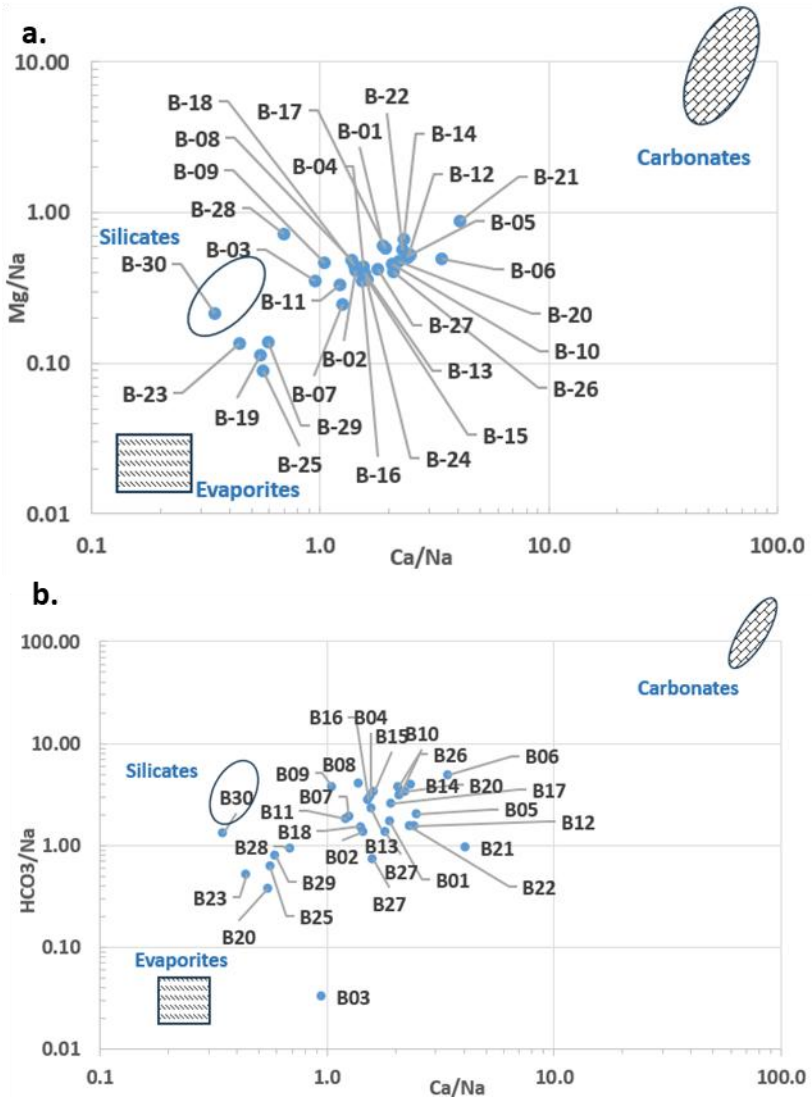

Figure 8. Dominant weathering and dissolution processes shaping basin hydrochemistry in the study area based on Na-normalized molar ratios diagram for (a) (Mg2+/Na+) vs (Ca2+/Na+), (b) (HCO3−/Na+) vs (Ca2+/Na+).

However, in both the Gibbs and Na-normalized diagrams, Basin B03 exhibits a distinct behavior compared to the others: Figure 7b highlights evaporation dominance, whereas Figure 8d indicates a hydrochemical composition strongly influenced by evaporite dissolution. This anomaly can be attributed to acidic pH conditions, which in turn result in low HCO_3 concentrations.

2.5.3. Classification of c-Q relationships

Regarding the concentration–discharge (c–Q) relationship (Figure 9), based on the power-law methodology (dilution–enrichment–constancy), different behaviors were identified across basins and among constituents. A prevalence of dilution behavior and anticlockwise hysteresis was observed for Ca^{2+}, Cl^{-}, K^{+}, Mg^{2+}, Na^{+}, and SO_4^{2-}. For Fe, enrichment behavior and clockwise hysteresis predominated. In the case of $N–NO_3^{-}$, the behavior was predominantly constant (followed by enrichment) with clockwise hysteresis. No non-hysteresis behavior was identified across the transect. These patterns of c-Q relationship align and may be related to the extent and distribution of solute source characteristics, water available for transport, hydrological connectivity and/or availability of fine sediments riverbed within the transect (Klein, 1984; Evans & Davies, 1998; Pohle et al., 2021, Speir et al., 2023). Under anticlockwise hysteresis with dilution, solute sources appear constrained compared with clockwise–enrichment behavior. To resolve the c–Q behavior of each solute with confidence, field-based sediment characterization and solute-source identification, including groundwater contributions, are required in every basin along the transect.

For the trace element As, although enrichment and anticlockwise hysteresis were identified in a greater number of basins, there was no significant difference compared to basins with constant behavior or clockwise hysteresis. A similar situation was observed for Cu, where no dominant pattern emerged, likely due to concentrations near the detection limit and the limited availability of data for this element.

Moreover, basins B28, B29, and B30, which record the highest precipitation levels across the transect, predominantly exhibit dilution behavior, with only Fe showing constancy.

Considering hydrological connectivity in the nested basins B21–B22 and B23–B24, it was found that B21 and B22 exhibit identical hysteresis patterns across all constituents. For B23 and B24, seven coincidences were observed out of eight results (noting that hysteresis could only be determined for eight of the ten analyzed constituents in both basins). Therefore, the hysteresis hydrochemical patterns of these basins are very similar, consistent with a shared solute transport dynamic likely influenced by similar geological, volcanic, or thermal conditions.

Based on the distinctive c–Q relationships (export regime) identified for basin B12 for Cl^{-}, K^{+}, Mg^{2+}, and Na^{+}, we note the presence of a large-scale mining operation with an environmental commitment (Conama, 2004) to manage both discharge and water quality to prevent adverse downstream effects. Such interventions can influence river c–Q behavior and may also occur in other study areas.

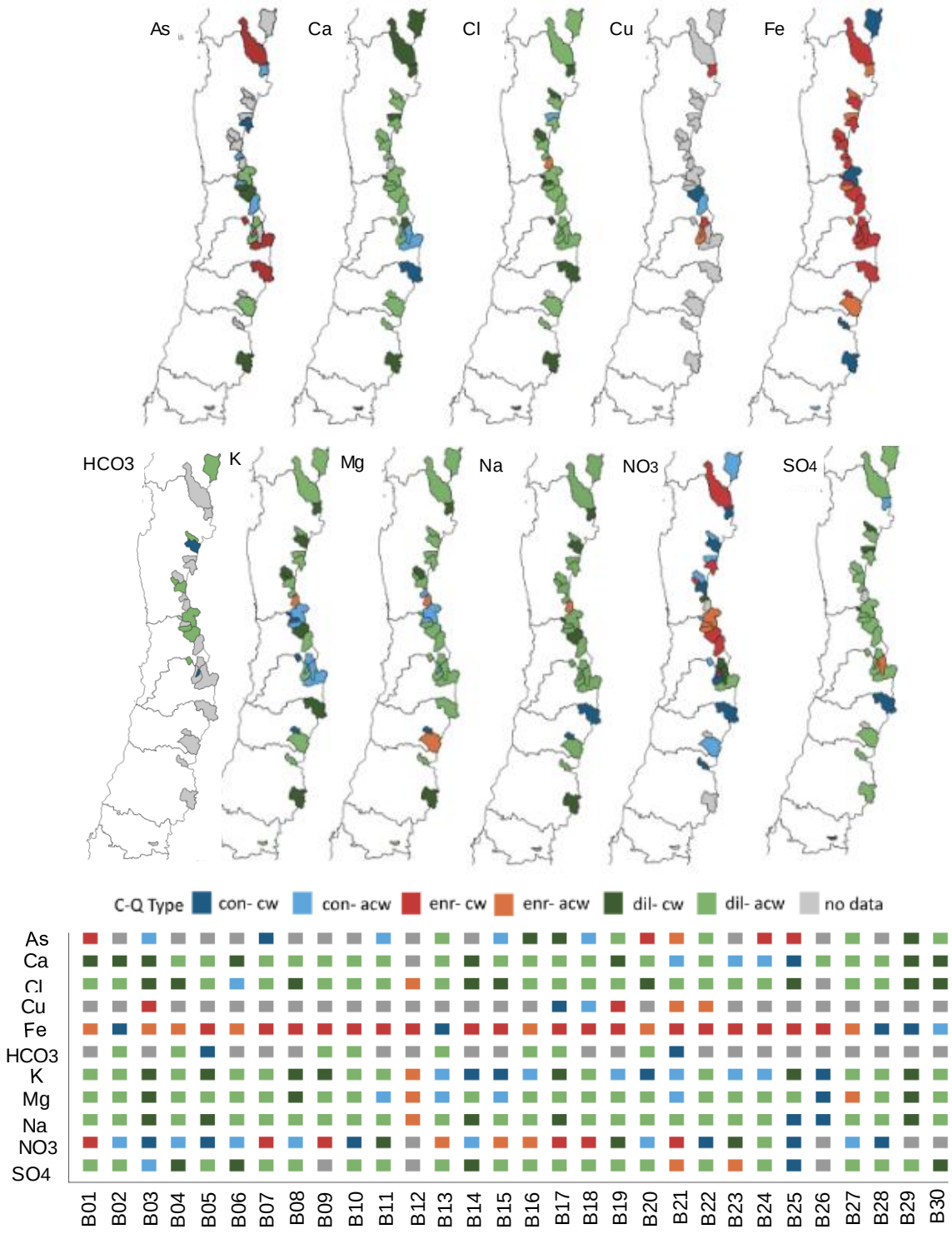

Figure 9. Classification of solutes based on c–Q relationships along the transect. (Export regime: con = constancy, enr = enrichment, dil = dilution; Hysteresis: cw = clockwise, acw = anticlockwise).

2.5.6. Influence of Basins Characteristics on Solute Behavior

When applying the Mann–Whitney U test (Table 2) to contrasts between catchment characteristics and hysteresis classes (clockwise vs. anticlockwise), none of the tests reached the conventional $p < 0.05$ threshold; however, several exhibited medium effect sizes according to Cliff's delta (δ. The effects were for Cl–Altitude ($\delta = 0.46$) and NO_3–Vegetation ($\delta = 0.45$), followed by K–Altitude ($\delta = 0.41$), Ca–Vegetation ($\delta = 0.40$), Cl–Area ($\delta = 0.38$), Cl–mean discharge (Qmean) ($\delta = 0.37$), and SO_4–Area ($\delta = 0.44$). For Fe, effects were negative with Area ($\delta = -0.34$) and Qmean ($\delta = -0.38$). We quantified stochastic dominance between groups using Cliff's δ, fixing the group order as A > C.

Table 2. Influence of Basins Characteristics on Hysteresis of thirty basins (clockwise vs anticlockwise).

Solute	Basin Characteristic	U	p_value	Cliffs delta	Cliffs magnitude
Ca	Vegetation	126	0.094	0.40	medium
Cl	Area	124	0.114	0.38	medium
Cl	Altitude	131	0.056	0.46	medium
Cl	Q mean	123	0.126	0.37	medium
Fe	Area	53	0.186	-0.34	medium
Fe	Q mean	50	0.141	-0.38	medium
K	Altitude	147	0.071	0.41	medium
NO3	Vegetation	120	0.055	0.45	medium
SO4	Area	79	0.142	0.44	medium

Based on, Mann–Whitney U tests applied to each catchment characteristic and export regime (Dilution, Enrichment, Constancy) pair revealed five significant associations ($p < 0.05$), all with medium to large effect sizes according to Cliff's delta. In base the classification (Dilution-constancy) and (Enrichment-constancy) and data per range, the test was applied for Ca, Mg, Fe, K, Na (Table 3).

For Ca, vegetation showed a strong positive effect, whereas altitude exhibited a strong negative effect. For K, significant associations were detected with stream length (medium) and mean slope (large). For Mg, mean slope was also significant (large). Several additional

comparisons were near the conventional significance threshold but displayed notable effect sizes: Ca–aridity index ($\delta = 0.62$; $p = 0.053$), Na–aridity index ($\delta = 0.83$; $p = 0.058$), Mg–stream length ($\delta = 0.51$; $p = 0.082$), and Fe–Q mean ($\delta = -0.50$; $p = 0.089$). Importantly, all significant associations belonged to the Dilution–Constancy export regime, whereas comparisons involving Fe under the Enrichment–Constancy regime did not achieve statistical significance ($p \geq 0.089$).

Determining the relationship between the solutes Ca and Na and the aridity index (potential evapotranspiration/precipitation), is particularly interesting and underexplored topic in comparison to previous studies (Godsey et al., 2019; Ebeling et al., 2021; Pohle et al., 2021), which focused on narrower climatic ranges and generally assumed that basin controls exert uniform influence on mean concentrations and export patterns across different climatic conditions.

Finally, given the documented shifts in vegetation cover in mountain ecosystems driven by climate change (Dhondt, 2003), and the relationships identified in this study between vegetation cover and the solutes Ca (export regime) and NO_3 (hysteresis), it is reasonable to expect that these solutes may exhibit future changes in their c–Q relationship.

Table 3. Influence of Basins Characteristics on export regime (Bold formatting denotes parameters with p-values below the 0.05).

Solute	Basin Characteristic	U	p-value	Cliffs Delta	Cliffs Magnitude	Regimen-Export
Ca	**Altitude**	15.5	**0.032**	-0.69	**large**	Dilution-Constancy
Ca	Aridity Index	81	0.053	0.62	large	Dilution-Constancy
Ca	**Vegetation**	39	**0.010**	0.82	**large**	Dilution-Constancy
Fe	Mean Slope	88	0.107	0.47	medium	Enrichment-Constancy
Fe	Q mean	30	0.089	-0.50	large	Enrichment-Constancy
K	Area	136	0.063	0.43	medium	Dilution-Constancy
K	**Stream Length**	139	**0.046**	0.46	**medium**	Dilution-Constancy
K	**Mean Slope**	45.5	**0.023**	-0.52	**large**	Dilution-Constancy
Mg	Area	84	0.119	0.46	medium	Dilution-Constancy
Mg	Stream Length	87	0.082	0.51	large	Dilution-Constancy
Mg	**Mean Slope**	24.5	**0.048**	-0.57	**large**	Dilution-Constancy
Na	Aridity Index	49.5	0.058	0.83	large	Dilution-Constancy
Na	Q mean	10	0.156	-0.63	large	Dilution-Constancy

2.6. Conclusions

We conducted a comprehensive hydrochemical assessment of ten solutes—major ions (Ca^{2+}, Na^{+}, Mg^{2+}, Cl^{-}, HCO_3^{-}, SO_4^{2-}), trace elements (As, Cu, Fe), and nitrate (NO_3^{-})—to characterize mountain-river behavior across thirty Andean headwater basins. Basin attributes explained spatial variability in mean concentrations and in concentration–discharge (c–Q) relationships (hysteresis and export regime), as well as climatic gradients along the transect. Joint application of Gibbs diagrams and Na-normalized molar-ratio diagrams indicate that silicate rock–water interactions are the dominant processes governing surface-water chemistry across the study area. Stiff diagrams showed that most basins are enriched in Ca^{2+}–HCO_3^{-} (15/30) and Ca^{2+}–SO_4^{2-} (10/30). In general, concentrations were < 5 meq L^{-1}; elevated SO_4^{2-} was associated with mining activity, volcanism, and hydrothermal inputs. Increased precipitation toward the southern transect was accompanied by lower solute concentrations.

From low-frequency, long-term observations of c–Q, ions were predominantly characterized by dilution behavior and anticlockwise hysteresis, suggesting generally low hydrological connectivity in these headwaters, solute sources, and/or limited availability of fine sediments riverbed. In contrast, Fe exhibited mainly enrichment with clockwise hysteresis, whereas NO_3^{-} showed mixed responses. To determine the c–Q pattern of each solute with confidence, it would be necessary to conduct in-field sediment characterization and identification of solute sources in the basins along the transect.

The c–Q analysis also revealed a distinct behavior for most solutes in basin B12; a targeted literature review pointed to an authorized river-management intervention by a mining operator affecting discharge and water quality. Identifying such an anomalous basin within a large set highlights the utility of this approach for screening and hypothesis generation in multi-basin studies.

To test associations between c–Q metrics (export regime, hysteresis) and basin characteristics, we applied non-parametric Mann–Whitney U tests and Cliff's delta. Contrasts between basin attributes and hysteresis direction (clockwise vs anticlockwise) did

not reach conventional significance ($p \geq 0.05$) but consistently yielded medium effect sizes for several pairs (e.g. Cl–altitude; NO_3^-–vegetation; K–altitude; Ca–vegetation; Cl–area; Cl–mean discharge; SO_4^{2-}–area). In contrast, five significant associations ($p < 0.05$) with medium-to-large effects emerged for export-regime pairings, concentrated on the Dilution–Constancy axis: Ca–vegetation, Ca–altitude, K–stream length, K–mean slope, and Mg–mean slope. Near-threshold signals ($p \approx 0.05$–0.09) with large δ were observed for Ca and Na versus aridity index (ET/P), for Mg versus stream length, and for Fe versus mean discharge.

This straightforward non-parametric framework proved practical for linking basin characteristics and climate conditions to c–Q behavior and may be useful for similar solute-response studies. Moreover, explicitly incorporating aridity index and vegetation across a wide regional gradient, within a climate-change context, offers a novel lens to anticipate shifts in solute behavior under evolving land use and hydroclimatic patterns (precipitation and evapotranspiration). Finally, to more accurately determine the origin of the observed c–Q relationships, it would be necessary to expand the characterization of each catchment, with particular attention to the assessment of sediment properties and groundwater contributions.

ACKNOWLEDGEMENTS

We thank Dr. Ina Pohle, James Hutton Institute, for sharing the base code for the concentration–discharge (c–Q) relationship analyses.

CRHIAM Centro de Recursos Hídricos para la Agricultura y la Minería ANID/FONDAP/23A0001

Fondecyt Proyect ANID/FONDECYT/1210177.

Data Availability Statement

The data that support the findings of this study are available from the corresponding author upon reasonable request.

Supplementary Material Basins.xlsx

Declaration of generative AI and AI-assisted technologies in the writing process

During the preparation of this work the author(s) used Chat GPT in order to improve language and readability. After using this tool/service, the author(s) reviewed and edited the content as needed and take(s) full responsibility for the content of the publication.

REFERENCES

Abbott, K. M., Zaidel, P. A., Roy, A. H., Houle, K. M., & Nislow, K. H. (2022). Investigating impacts of small dams and dam removal on dissolved oxygen in streams. Plos one, 17(11), e0277647.

Bluth, G.J.S.& Kump, L.R. Lithologic and Climatologic Controls of River Chemistry. Geochimica Et Cosmochimica Acta 1994, 58, 2341–2359, doi:10.1016/0016-7037(94)90015-9.

Bogena, H.R.; Montzka, C.; Huisman, J.A.; Graf, A.; Schmidt, M.; Stockinger, M.; Von Hebel, C.; Hendricks-Franssen, H.J.; Van Der Kruk, J.; Tappe, W.; et al. The TERENO-Rur Hydrological Observatory: A Multiscale Multi-Compartment Research Platform for the Advancement of Hydrological Science. Vadose Zone Journal 2018, 17, 1–22, doi:10.2136/vzj2018.03.0055.

Burns, D.A.; Pellerin, B.A.; Miller, M.P.; Capel, P.D.; Tesoriero, A.J.; Duncan, J.M. Monitoring the Riverine Pulse: Applying High-frequency Nitrate Data to Advance Integrative Understanding of Biogeochemical and Hydrological Processes. Wiley Interdisciplinary Reviews Water 2019, 6, doi:10.1002/wat2.1348.

Byrne, P.; Onnis, P.; Runkel, R.L.; Frau, I.; Lynch, S.F.L.; Edwards, P. Critical Shifts in Trace Metal Transport and Remediation Performance under Future Low River Flows. Environmental Science & Technology 2020, 54, 15742–15750, doi:10.1021/acs.est.0c04016.

Calmels, D.; Gaillardet, J.; Brenot, A.; France-Lanord, C. Sustained Sulfide Oxidation by Physical Erosion Processes in the Mackenzie River Basin: Climatic Perspectives. Geology 2007, 35, 1003, doi:10.1130/g24132a.1.

Canada, A. and A.-F. Chapter 18: Landform Classification Available online: https://sis.agr.gc.ca/cansis/taxa/cssc3/chpt18.html.

Cairoli, M., Souza, F., Stroomberg, G., Postma, G., Buydens, L., & Jansen, J. (2024). BAHYS—A Bayesian Modeling Framework for Long-Term Concentration-Discharge Hysteresis: A Case Study on Chloride. Water Resources Research, 60(6). https://doi.org/10.1029/2023wr035427

Chiodini, G.; Frondini, F.; Cardellini, C.; Parello, F.; Peruzzi, L. Rate of Diffuse Carbon Dioxide Earth Degassing Estimated from Carbon Balance of Regional Aquifers: The Case of Central Apennine, Italy. Journal of Geophysical Research Atmospheres 2000, 105, 8423–8434, doi:10.1029/1999jb900355.

Cliff, N. (1993). Dominance statistics: Ordinal analyses to answer ordinal questions. Psychological Bulletin, 114(3), 494–509. https://doi.org/10.1037/0033-2909.114.3.494

Conaf, 2025. Informe Técnico Para La Ampliación Del Parque Nacional Glaciares de Santiago y La Creación Del Área de Conservación de Múltiples Usos "Olivares-Colorado" En La Región Metropolitana (accessed on 03 May 2025)

Conama, 2004. Ficha Del Proyecto: Proyecto Integral de Desarrollo Available online: https://seia.sea.gob.cl/expediente/ficha/fichaPrincipal.php?id_expediente=6243. (accessed on 24 May 2025).

Cordero, R.R.; Feron, S.; Damiani, A.; MacDonell, S.; Carrasco, J.; Pizarro, J.; Karas, C.; Jorquera, J.; Sepulveda, E.; Cabello, F.; et al. Rapid Decline in Extratropical Andean Snow Cover Driven by the Poleward Migration of the Southern Hemisphere Westerlies. Scientific Reports 2024, 14, doi:10.1038/s41598-024-78014-0.

Dessert, C.; Gaillardet, J.; Dupre, B.; Schott, J.; Pokrovsky, O.S. Fluxes of High- versus Low-Temperature Water–Rock Interactions in Aerial Volcanic Areas: Example from the Kamchatka Peninsula, Russia. Geochimica Et Cosmochimica Acta 2008, 73, 148–169, doi:10.1016/j.gca.2008.09.012.

Dhondt, K.; Boeckx, P.; Van Cleemput, O.; Hofman, G. Quantifying Nitrate Retention Processes in a Riparian Buffer Zone Using the Natural Abundance of 15N in NO3−. Rapid Communications in Mass Spectrometry 2003, 17, 2597–2604, doi:10.1002/rcm.1226.

Díaz, J.A.; Montecinos, M.; Vega, A.; Gironás, J.; Molinos, M.; Pastén, P. Impacts of Droughts on Water Quality: Processes and Monitoring. In Global issues in water policy; 2025; pp. 89–124.

Ding, K., & Qin, B. (2024). Global Drivers of Algal Bloom Occurrence: The Role of Climate, Hydrology, and Morphometry. Water, 16(24), 3624. https://doi.org/10.3390/w16243624

Drever, J.I.; Stillings, L.L. The Role of Organic Acids in Mineral Weathering. Colloids and Surfaces a Physicochemical and Engineering Aspects 1997, 120, 167–181, doi:10.1016/s0927-7757(96)03720-x.

Ebeling, P.; Kumar, R.; Weber, M.; Knoll, L.; Fleckenstein, J.H.; Musolff, A. Archetypes and Controls of Riverine Nutrient Export across German Catchments. Water Resources Research 2021, 57, doi:10.1029/2020wr028134.

Evans, C.& Davies, T.D. Causes of Concentration/Discharge Hysteresis and Its Potential as a Tool for Analysis of Episode Hydrochemistry. Water Resources Research 1998, 34, 129–137, doi:10.1029/97wr01881.

Farley, K.A.; Piñeiro, G.; Palmer, S.M.; Jobbágy, E.G.; Jackson, R.B. Stream Acidification and Base Cation Losses with Grassland Afforestation. Water Resources Research 2008, 44, doi:10.1029/2007wr006659.

Flores, M.; Núñez, J.; Oyarzún, J.; Freixas, G.; Maturana, H.; Oyarzún, R. Surface Water Quality in a Sulfide Mineral-rich Arid Zone in North-Central Chile: Learning from a Complex Past, Addressing an Uncertain Future. Hydrological Processes 2016, 31, 498–513, doi:10.1002/hyp.11086.

Floury, P.; Bouchez, J.; Druhan, J.L.; Gaillardet, J.; Blanchouin, A.; Gayer, É.; Ansart, P. Linking Dynamic Water Storage and Subsurface Geochemical Structure Using High-Frequency Concentration-Discharge Records. Water Resources Research 2024, 60, doi:10.1029/2022wr033999.

Gaillardet, J.; Louvat, P.; Lajeunesse, E. Rivers from Volcanic Island Arcs: The Subduction Weathering Factory. Applied Geochemistry 2011, 26, S350–S353, doi:10.1016/j.apgeochem.2011.03.057.

Garreaud, R.D.; Alvarez-Garreton, C.; Barichivich, J.; Boisier, J.P.; Christie, D.; Galleguillos, M.; LeQuesne, C.; McPhee, J.; Zambrano-Bigiarini, M. The 2010–2015 Megadrought in Central Chile: Impacts on Regional Hydroclimate and Vegetation. Hydrology and Earth System Sciences 2017, 21, 6307–6327, doi:10.5194/hess-21-6307-2017.

Garreaud, R.D.; Boisier, J.P.; Rondanelli, R.; Montecinos, A.; Sepúlveda, H.H.; Veloso-Aguila, D. The Central Chile Mega Drought (2010–2018): A Climate Dynamics Perspective. International Journal of Climatology 2019, 40, 421–439, doi:10.1002/joc.6219.

Godsey, S.E.; Hartmann, J.; Kirchner, J.W. Catchment Chemostasis Revisited: Water Quality Responds Differently to Variations in Weather and Climate. Hydrological Processes 2019, 33, 3056–3069, doi:10.1002/hyp.13554.

Godsey, S.E.; Kirchner, J.W.; Clow, D.W. Concentration–Discharge Relationships Reflect Chemostatic Characteristics of US Catchments. Hydrological Processes 2009, 23, 1844–1864, doi:10.1002/hyp.7315.

Goldrich-Middaugh, G.M.; Ma, L.; Engle, M.A.; Ricketts, J.W.; Soto-Montero, P.; Sullivan, P.L. Regional Drivers of Stream Chemical Behavior: Leveraging Lithology, Land Use, and Climate Gradients Across the Colorado River, Texas USA. Water Resources Research 2022, 58, doi:10.1029/2022wr032155.

Google Earth. (2025). [Andean catchment transect; 29°-35°S]. Digital map, accessed 15 April 2025, https://earth.google.com/web/

Hernandez, V.; Arumí, J.L.; Boll, J.; Duhalde, D.; MacDonell, S.; Oyarzún, R. Streamflow–Concentration Relationships of Surface Water in the Choapa Basin: Historical Analysis and Projections under Climate Change. Hydrological Sciences Journal 2023, 68, 1250–1263, doi:10.1080/02626667.2023.2212167.

Hofmeister, K.L.; Nave, L.E.; Drevnick, P.; Veverica, T.; Knudstrup, R.; Heckman, K.A.; Riha, S.J.; Schneider, R.L.; Walter, M.T. Seasonal Dynamics and Exports of Elements from a First-order Stream to a Large Inland Lake in Michigan. Hydrological Processes 2019, 33, 1476–1491, doi:10.1002/hyp.13416.

House, W.A.& Warwick, M.S. Hysteresis of the Solute Concentration/Discharge Relationship in Rivers during Storms. Water Research 1998, 32, 2279–2290, doi:10.1016/s0043-1354(97)00473-9.

Hu, P.; Feng, L. The Risk of Water Quality Deterioration with Urban Flood Control—A Case in Wuxi. Sustainability 2023, 16, 185, doi:10.3390/su16010185.

Hunsaker, C.T.; Johnson, D.W. Concentration-discharge Relationships in Headwater Streams of the Sierra Nevada, California. Water Resources Research 2017, 53, 7869–7884, doi:10.1002/2016wr019693.

Immerzeel, W.W.; Lutz, A.F.; Andrade, M.; Bahl, A.; Biemans, H.; Bolch, T.; Hyde, S.; Brumby, S.; Davies, B.J.; Elmore, A.C.; et al. Importance and Vulnerability of the World's Water Towers. Nature 2019, 577, 364–369, doi:10.1038/s41586-019-1822-y.

Jupke, J.F., Sinclair, T., Maltby, L. et al. Europe-wide spatial trends in copper and imidacloprid sensitivity of macroinvertebrate assemblages. Environ Sci Eur 36, 124 (2024). https://doi.org/10.1186/s12302-024-00944-3

Kaandorp, V.P.; Broers, H.P.; Van Der Velde, Y.; Rozemeijer, J.; De Louw, P.G.B. Time Lags of Nitrate, Chloride, and Tritium in Streams Assessed by Dynamic Groundwater Flow Tracking in a Lowland Landscape. Hydrology and Earth System Sciences 2021, 25, 3691–3711, doi:10.5194/hess-25-3691-2021.

Kaltenecker, M.G.; Mitchell, C.P.J.; Howell, E.T.; Arhonditsis, G. Long-Term Trends in Water Quality and C-Q Relationships Reveal Complex Interactions between Changing Land Uses and Climate. Journal Of Hydrology 2024, 132511, doi:10.1016/j.jhydrol.2024.132511.

Klein, M. Anti Clockwise Hysteresis in Suspended Sediment Concentration during Individual Storms. CATENA 1984, 11, 251-257, doi:10.1016/s0341-8162(84)80024-7.

Knapp, J.L.A.; Von Freyberg, J.; Studer, B.; Kiewiet, L.; Kirchner, J.W. Concentration–Discharge Relationships Vary among Hydrological Events, Reflecting Differences in Event Characteristics. Hydrology And Earth System Sciences 2020, 24, 2561-2576, doi:10.5194/hess-24-2561-2020.

Krueger, T.; Quinton, J.N.; Freer, J.; Macleod, C.J.A.; Bilotta, G.S.; Brazier, R.E.; Butler, P.; Haygarth, P.M. Uncertainties in Data and Models to Describe Event Dynamics of Agricultural Sediment and Phosphorus Transfer. Journal of Environmental Quality 2009, 38, 1137–1148, doi:10.2134/jeq2008.0179.

Liu, S.; Dupas, R.; Guo, D.; Lintern, A.; Minaudo, C.; Bende-Michl, U.; Zhang, K.; Duvert, C. Controls on Spatial Variability in Mean Concentrations and Export Patterns of River

Chemistry across the Australian Continent. Water Resources Research 2022, 58, doi:10.1029/2022wr032365.

Lloyd, C.E.M.; Freer, J.E.; Johnes, P.J.; Collins, A.L. Using Hysteresis Analysis of High-Resolution Water Quality Monitoring Data, Including Uncertainty, to Infer Controls on Nutrient and Sediment Transfer in Catchments. The Science of the Total Environment 2015, 543, 388–404, doi:10.1016/j.scitotenv.2015.11.028.

Macchioli-Grande, M.; Soto-Maass, A.; Pfeiffer, M.; Covarrubias, J.I.; Peña-Echeverría, A.; Perez-Fodich, A. Solute Generation and Transport in Semiarid Mountain Catchments of the Central Chilean Andes. Earth Systems and Environment 2025, doi:10.1007/s41748-025-00642-x.

Mann, H. B., & Whitney, D. R. (1947). On a Test of Whether one of Two Random Variables is Stochastically Larger than the Other. The Annals of Mathematical Statistics, 18(1), 50–60. https://doi.org/10.1214/aoms/1177730491

Markovich, K.H.; Manning, A.H.; Condon, L.E.; McIntosh, J.C. Mountain-Block Recharge: A Review of Current Understanding. Water Resources Research 2019, 55, 8278–8304, doi:10.1029/2019wr025676.

Middelburg, J.J. Closing the Inland Water Carbon Cycle. Science Advances 2024, 10, doi:10.1126/sciadv.adt3893.

Minaudo, C.; Dupas, R.; Gascuel-Odoux, C.; Fovet, O.; Mellander, P.; Jordan, P.; Shore, M.; Moatar, F. Nonlinear Empirical Modeling to Estimate Phosphorus Exports Using Continuous Records of Turbidity and Discharge. Water Resources Research 2017, 53, 7590–7606, doi:10.1002/2017wr020590.

Moatar, F.; Floury, M.; Gold, A.J.; Meybeck, M.; Renard, B.; Ferréol, M.; Chandesris, A.; Minaudo, C.; Addy, K.; Piffady, J.; et al. Stream Solutes and Particulates Export Regimes: A New Framework to Optimize Their Monitoring. Frontiers in Ecology and Evolution 2020, 7, doi:10.3389/fevo.2019.00516.

Moreno, T.& Gibbons, W. (Eds.) The Geology of Chile; Geological Society of London: London, UK, 2007.

Muñoz, A.A.; Klock-Barría, K.; Alvarez-Garreton, C.; Aguilera-Betti, I.; González-Reyes, Á.; Lastra, J.A.; Chávez, R.O.; Barría, P.; Christie, D.; Rojas-Badilla, M.; et al. Water Crisis in Petorca Basin, Chile: The Combined Effects of a Mega-Drought and Water Management. Water 2020, 12, 648, doi:10.3390/w12030648.

Musolff, A.; Schmidt, C.; Selle, B.; Fleckenstein, J.H. Catchment Controls on Solute Export. Advances in Water Resources 2015, 86, 133–146, doi:10.1016/j.advwatres.2015.09.026.

Nauditt, A.; Birkel, C.; Soulsby, C.; Ribbe, L. Conceptual Modelling to Assess the Influence of Hydro-Climatic Variability on Runoff Processes in Data Scarce Semi-Arid Andean Catchments. Hydrological Sciences Journal 2016, 62, 515–532, doi:10.1080/02626667.2016.1240870.

Orrego-Verdugo, R.; Abarca-Del-Rio, R.; Lara-Uribe, C. Spatial Dynamics and Consistency of Agroclimatic Trends in Chile during 1985-2015 to the Köppen- Geiger Climate Classification. Chilean Journal of Agricultural Research 2021, 81, 618–629, doi:10.4067/s0718-58392021000400618.

Oyarzun, R.; Guevara, S.; Oyarzún, J.; Lillo, J.; Maturana, H.; Higueras, P. The As-Contaminated Elqui River Basin: A Long Lasting Perspective (1975–1995) Covering the Initiation and Development of Au–Cu–As Mining in the High Andes of Northern Chile. Environmental Geochemistry and Health 2006, 28, 431–443, doi:10.1007/s10653-006-9045-1.

Oyarzun, R.; Lillo, J.; Higueras, P.; Oyarzún, J.; Maturana, H. Strong Arsenic Enrichment in Sediments from the Elqui Watershed, Northern Chile: Industrial (Gold Mining at El Indio–Tambo District) vs. Geologic Processes. Journal of Geochemical Exploration 2004, 84, 53–64, doi:10.1016/j.gexplo.2004.03.002.

Parra, A., Oyarzún, J., Maturana, H., Kretschmer, N., Meza, F., & Oyarzún, R. (2011). Natural factors and mining activity bearings on the water quality of the Choapa basin, North Central Chile: insights on the role of mafic volcanic rocks in the buffering of the acid drainage process. Environmental Monitoring and Assessment, 181, 69–82. https://doi.org/10.1007/s10661-010-1814-8

Peel, M.C.; Finlayson, B.L.; McMahon, T.A. Updated World Map of the Köppen-Geiger Climate Classification. Hydrology and Earth System Sciences 2007, 11, 1633–1644, doi:10.5194/hess-11-1633-2007.

Peña-Guerrero, M. D., Nauditt, A., Muñoz-Robles, C., Ribbe, L., & Meza, F. (2020). Drought impact on water quality and potential implications for agricultural podruction in the Maipo River Basin, Central Chile. Hydrological Sciences Journal, 65(6), 1005-1021. https://doi.org/10.1080/02626667.2020.1711911

Pepin, N.; Bradley, R.S.; Diaz, H.F.; Baraer, M.; Caceres, E.B.; Forsythe, N.; Fowler, H.; Greenwood, G.; Hashmi, M.Z.; Liu, X.D.; et al. Elevation-Dependent Warming in Mountain Regions of the World. Nature Climate Change 2015, 5, 424–430, doi:10.1038/nclimate2563.

Perez-Fodich, A.; Derry, L.A. Organic Acids and High Soil CO2 Drive Intense Chemical Weathering of Hawaiian Basalts: Insights from Reactive Transport Models. Geochimica Et Cosmochimica Acta 2019, 249, 173–198, doi:10.1016/j.gca.2019.01.027.

Pham, D. N., & Sokolova, I. M. (2023). Dissecting integrated indices of multiple biomarker responses: Think before use. Integrated Environmental Assessment and Management, 19(2), 302-311.

Pohle, I.; Baggaley, N.; Palarea-Albaladejo, J.; Stutter, M.; Glendell, M. A Framework for Assessing Concentration-Discharge Catchment Behavior from Low-Frequency Water Quality Data. Water Resources Research 2021, 57, doi:10.1029/2021wr029692.

Pörtner, H.-O.; Roberts, D.C.; Adams, H.; Adelekan, I.; Adler, C.; Adrian, R.; Aldunce, P.; Ali, E.; Bednar-Friedl, B.; Begum, R.A.; et al. 2022: Technical Summary. In Climate Change 2022: Impacts, Adaptation, and Vulnerability. Contribution of Working Group II to the Sixth Assessment Report of the Intergovernmental Panel on Climate Change; Pörtner, H.-O., Roberts, D.C., Tignor, M., Poloczanska, E.S., Mintenbeck, K., Alegría, A., Craig, M., Langsdorf, S., Löschke, S., Möller, V., et al., Eds.; Cambridge University Press: Cambridge, UK; New York, NY, USA, 2022; pp. 37–118.

Risacher, F.; Fritz, B.; Hauser, A. Origin of Components in Chilean Thermal Waters. Journal of South American Earth Sciences 2010, 31, 153–170, doi:10.1016/j.jsames.2010.07.002.

Rivé, K.; Gaillardet, J.; Agrinier, P.; Rad, S. Carbon Isotopes in the Rivers from the Lesser Antilles: Origin of the Carbonic Acid Consumed by Weathering Reactions in the Lesser Antilles. Earth Surface Processes and Landforms 2013, 38, 1020–1035, doi:10.1002/esp.3385.

Roberts, W.M.; Couldrick, L.B.; Williams, G.; Robins, D.; Cooper, D. Mapping the Potential for Payments for Ecosystem Services Schemes to Improve Water Quality in Agricultural Catchments: A Multi-Criteria Approach Based on the Supply and Demand Concept. Water Research 2021, 206, 117693, doi:10.1016/j.watres.2021.117693.

Saavedra, F.A.; Musolff, A.; Von Freyberg, J.; Merz, R.; Basso, S.; Tarasova, L. Disentangling Scatter in Long-Term Concentration–Discharge Relationships: The Role of Event Types. Hydrology and Earth System Sciences 2022, 26, 6227–6245, doi:10.5194/hess-26-6227-2022.

Salmon, C.D.; Walter, M.T.; Hedin, L.O.; Brown, M.G. Hydrological Controls on Chemical Export from an Undisturbed Old-Growth Chilean Forest. Journal of Hydrology 2001, 253, 69–80, doi:10.1016/s0022-1694(01)00447-4.

SEA, 2025a. Sistema de Evaluación de Impacto Ambiental Available online: https://seia.sea.gob.cl/busqueda/buscarProyectoResumen.php. (accessed on 15 April 2025).

SEA, 2025b. Ficha Del Proyecto: Planta Paneles de Yeso y Ampliación Cantera Rubí Available online: https://seia.sea.gob.cl/expediente/ficha/fichaPrincipal.php?modo=normal&id_expediente=2161701083. (accessed on 11 February 2025).

SEA, 2025c. Ficha Del Proyecto: Proyecto Minero La Perla Available online: https://seia.sea.gob.cl/expediente/expedientesEvaluacion.php?id_expediente=220&idExpediente=220. (accessed on 11 February 2025).

Senarathne, S.; Van Geldern, R.; Chandrajith, R.; Barth, J.A.C. Unexpected Contributions by Carbonates and Organic Matter in a Silicate-Dominated Tropical Catchment: An Isotope

Approach. The Science of the Total Environment 2024, 948, 174651, doi:10.1016/j.scitotenv.2024.174651.

SERNAGEOMIN. Mapa Geológico de Chile: Versión Digital. 2002. Available online: https://tiendadigital.sernageomin.cl/es/geologia-basica/3273-mapa-geologico-de-chile-version-digital.html (accessed on 17 March 2025).

SERNAGEOMIN, 2025. Catálogo Nacional de Información Geológica y Minera Available online: https://portalgeomin.sernageomin.cl/ (accessed on 15 April 2025).

Shaw, T.E.; Ulloa, G.; Farías-Barahona, D.; Fernandez, R.; Lattus, J.M.; McPhee, J. Glacier Albedo Reduction and Drought Effects in the Extratropical Andes, 1986–2020. Journal of Glaciology 2020, 67, 158–169, doi:10.1017/jog.2020.102.

Speir, S.L.; Rose, L.A.; Blaszczak, J.R.; Kincaid, D.W.; Fazekas, H.M.; Webster, A.J.; Wolford, M.A.; Shogren, A.J.; Wymore, A.S. Catchment Concentration–Discharge Relationships across Temporal Scales: A Review. Wiley Interdisciplinary Reviews Water 2023, 11, doi:10.1002/wat2.1702.

Sruoga, P., Etcheverría, M. P., Feineman, M., Rosas, M., Bukert, C., & Ibañes, O. (2012). Complejo Caldera Diamante-volcán Maipo (34° 10'S, 69º50'O): Evolución volcanológica y geoquímica e implicancias en su peligrosidad. Revista de la Asociación Geológica Argentina, 69(4), 508-530.

Stiff, H.A. The Interpretation of Chemical Water Analysis by Means of Patterns. Journal of Petroleum Technology 1951, 3, 15–3, doi:10.2118/951376-g.

Su, H.; Cheng, L.; Wu, Y.; Qin, S.; Liu, P.; Zhang, Q.; Cheng, S.; Li, Y. Extreme Storm Events Shift DOC Export from Transport-Limited to Source-Limited in a Typical Flash Flood Catchment. Journal of Hydrology 2023, 620, 129377, doi:10.1016/j.jhydrol.2023.129377.

Sudduth, E.B.; Perakis, S.S.; Bernhardt, E.S. Nitrate in Watersheds: Straight from Soils to Streams? Journal of Geophysical Research Biogeosciences 2013, 118, 291–302, doi:10.1002/jgrg.20030.

Thiele, R., 1980. Hoja Santiago: región metropolitana: carta geológica de Chile escala 1: 250.000. Instituto de Investigaciones Geológicas, Chile.

Ugalde, F.& Sepúlveda, S.A. Susceptibility Assessment for Glacier Hazards in the Volcán Catchment (33.82°S/70.00°W), Central Andes of Chile. Journal of South American Earth Sciences 2025, 105581, doi:10.1016/j.jsames.2025.105581.

Ulloa-Cedamanos, F.; Probst, J.L.; Probst, A. Medium Term Hydrochemical and CO2 Responses to Anthropogenic and Environmental Changes in Karst Headwater Streams. The Science of the Total Environment 2024, 957, 177614, doi:10.1016/j.scitotenv.2024.177614.

Vaughan, M.C.H.; Bowden, W.B.; Shanley, J.B.; Vermilyea, A.; Sleeper, R.; Gold, A.J.; Pradhanang, S.M.; Inamdar, S.P.; Levia, D.F.; Andres, A.S.; et al. High-frequency Dissolved Organic Carbon and Nitrate Measurements Reveal Differences in Storm Hysteresis and Loading in Relation to Land Cover and Seasonality. Water Resources Research 2017, 53, 5345–5363, doi:10.1002/2017wr020491.

Vicuña, S.; Garreaud, R.D.; McPhee, J. Climate Change Impacts on the Hydrology of a Snowmelt Driven Basin in Semiarid Chile. Climatic Change 2010, 105, 469–488, doi:10.1007/s10584-010-9888-4.

Vicuña, S.; Gironás, J.; Meza, F.J.; Cruzat, M.L.; Jelinek, M.; Bustos, E.; Poblete, D.; Bambach, N. Exploring Possible Connections between Hydrological Extreme Events and Climate Change in Central South Chile. Hydrological Sciences Journal 2013, 58, 1598–1619, doi:10.1080/02626667.2013.840380.

Viviroli, D.; Dürr, H.H.; Messerli, B.; Meybeck, M.; Weingartner, R. Mountains of the World, Water Towers for Humanity: Typology, Mapping, and Global Significance. Water Resources Research 2007, 43, doi:10.1029/2006wr005653.

Wali, S.U.; Umar, K.J.; Abubakar, S.D.; Ifabiyi, I.P.; Dankani, I.M.; Shera, I.M.; Yauri, S.G. Hydrochemical Characterization of Shallow and Deep Groundwater in Basement Complex Areas of Southern Kebbi State, Sokoto Basin, Nigeria. Applied Water Science 2019, 9, doi:10.1007/s13201-019-1042-5.

Waras, M.N.; Zabidi, M.A.; Ismail, Z.; Sangaralingam, M.; Gazzali, A.M.; Harun, M.S.R.; Aziz, M.Y.; Mohamed, R.; Najib, M.N.M. Comparative Analysis of Water Quality Index and River Classification in Kereh River, Penang, Malaysia: Impact of Untreated Swine Wastewater from Kampung Selamat Pig Farms. Water Environment Research 2024, 96, doi:10.1002/wer.11095

Winter, C.; Lutz, S.R.; Musolff, A.; Kumar, R.; Weber, M.; Fleckenstein, J.H. Disentangling the Impact of Catchment Heterogeneity on Nitrate Export Dynamics from Event to Long-Term Time Scales. Water Resources Research 2020, 57, doi:10.1029/2020wr027992.

Zegers, G.; Navarro-Valdivia, L.; Lagos-Zuñiga, M.; Navarrete-Calvo, A.; Caraballo, M.A.; Niño, Y.; McPhee, J.; Montserrat, S. An Integrated Modeling Approach for Mineral and Metal Transport in Acidic Rivers at High Mountainous Porphyry Cu Systems. Journal of Hydrology 2021, 602, 126718, doi:10.1016/j.jhydrol.2021.126718.

Zhao, X.; Wu, L.; Dong, Z.; Zhang, Z.; Wu, K.; Wei, A.; Wang, Y. Hydrochemical Characteristics and Controlling Factors of the Mingyong River Water of the Meili Snow Mountains, China. Sustainability 2024, 16, 6174, doi:10.3390/su16146174.

Zhi, W.; Li, L.; Dong, W.; Brown, W.; Kaye, J.; Steefel, C.; Williams, K.H. Distinct Source Water Chemistry Shapes Contrasting Concentration-Discharge Patterns. Water Resources Research 2019, 55, 4233-4251, doi:10.1029/2018wr024257.

CAPÍTULO III. Exploring the Behavior of the High-Andean Wetlands in the Semi-Arid Zone of Chile: The Influence of Precipitation and Temperature Variability on Vegetation Cover and Water Quality

Denisse Duhalde, Javiera Cortés, José-Luis Arumí, Jan Boll and Ricardo Oyarzún
Water **2024**, *16*(24), 3682; **https://doi.org/10.3390/w16243682**

3.1 Resultados Clave:

- La precipitación y el estado de la cobertura vegetal de la cadena de humedales, estimada mediante NDVI y NDMI, muestran tendencias temporales negativas, y se identificó un mayor deterioro de la cobertura en el período de la megasequía (2019).
- Se identificó correlaciones temporales significativas entre la precipitación y los índices NDVI y NDMI, siendo la fuerza de correlación "fuerte" para un año de desface entre las variables y "media" con dos años de desface.
- La cobertura vegetal de los humedales es espacialmente heterogénea, influenciada por la altitud, características del terreno y aportes hídricos locales provenientes de glaciares y acumulación en abanicos aluviales.
- Se identificó correlaciones significativas entre la cobertura vegetal y la calidad de agua, siendo el NDMI el índice que presentó correlaciones con más solutos y con mayor fuerza de correlación.

3.2 Resumen extendido:

En las últimas décadas, los ecosistemas del planeta han enfrentado transformaciones significativas asociadas al cambio climático, entre ellas una creciente variabilidad en la precipitación y en los patrones de disponibilidad hídrica. Estos cambios no son homogéneos, sino que se expresan de manera particular en ecosistemas frágiles y sensibles como los humedales altoandinos, donde el agua cumple un rol esencial para el mantenimiento de la biodiversidad, los procesos ecológicos y los servicios ecosistémicos que sustentan a las comunidades humanas y naturales.

En regiones semiáridas como el centro-norte de Chile, donde la disponibilidad de agua es limitada y se encuentra sometida a presiones tanto naturales como antrópicas, los humedales de altura son reservorio de agua natural que regulan flujos hídricos, almacenan carbono, sirven de refugio a especies endémicas y proporcionan agua de calidad a comunidades aguas

abajo. Sin embargo, su funcionamiento depende críticamente del régimen de precipitaciones, de los aportes hídricos laterales y subterráneos, y de la capacidad de la cobertura vegetal para responder y adaptarse a condiciones de estrés.

El presente estudio se centró en una cadena de doce humedales altoandinos localizados en el Santuario de la Naturaleza Estero Derecho, en la cabecera del río Elqui, región de Coquimbo, Chile. Además, la cuneca del Estero Derecho se ha identificado de especial interés para estudios hidrológicos por presentar la densidad poblacional más alta en las cuencas andinas del valle del Elqui, tener actividades económicas relevantes como agricultura y turismo. Todo lo anterior en un contexto de escasez hídrica y afectación por el fenómeno de Megasequía (Garreaud et al. 2019). El objetivo principal fue analizar las dinámicas espacio-temporales del estado de la cubertura vegetal y su relación con la precipitación y la calidad del agua.

El estudio utilizó series de tiempo satelitales obtenidas desde Landsat 5 (1986- 2011) y Landsat 8 (2013-2023), mediante los cuales se obtuvieron los índices normalizados: NDVI (Normalized Difference Vegetation Index), indicador de vigor y densidad de la vegetación y NDMI (Normalized Difference Moisture Index), indicador del contenido de humedad en la vegetación. Dado que se usó dos satélites (Landsat 5 y Landsat 8) para la obtención de los índices y que, además, no se registran tiempos comunes de funcionamiento entre ambos satélites, para asegurar una adecuada interpretación de los valores observados, se aplicó una técnica de armonización usando el satélite Landsat 7 como detector común entre los valores obtenidos de los índices desde los satélites Landsat 5 y Landsat 8. La precipitación y temperatura fue obtenida desde la plataforma CAMELS-CL. Las concentraciones de los solutos se obtuvieron desde la página del Sistema Nacional de Información Ambiental (SINIA): CE, Ca, Cl, Fe, K, Mg, Na, SO_4. Para el análisis satelital se desarrolló un código en Google Earth Engine. En base a las series de tiempo se identificaron tendencias en el período de estudio, análisis de diagramas de caja (boxplots) para explorar la variabilidad del estado de la cobertura vegetal entre los humedales y se aplicó correlación lineal (Spearman (no requiere distribución normal de las series) y Pearson (requiere distribución normal de ambas variables)) para evaluar las relaciones entre índices de vegetación, precipitación, temperatura y parámetros de calidad de agua. Finalmente, se realizó un análisis sobre características del terreno para identificar las diferencias entre los humedales.

Los resultados mostraron tendencias negativas tanto en la precipitación como en los índices NDVI y NDMI durante el período analizado. Esto se asocia a un decrecimiento de los valores de las variables analizadas en el periodo estudiado a diferencia de la temperatura, que mostró una tendencia positiva. Además, se detectó entre la precipitación y los índices de vegetación correlaciones significativas, con fuerza de correlación "fuerte" con un desfase de un año entre variables y "media" con dos años de desfase.

En el análisis por humedal, se detectó que los humedales emplazados a mayor altura (W10, W11, W12) presentan un menor valor histórico de índices y que los factores identificados, falla Las Gualtatas, roca basal de baja permeabilidad (rocas andesíticas, basálticas y graníticas/riolíticas), aportes de agua desde los glaciares (rocosos) y presencia de abanicos aluviales pueden influir en el estado diferenciado de la cobertura vegetal de los humedales.

Finalmente, se identificaron más correlaciones significativas y con mayor fuerza de correlación entre el NDMI y la concentración de solutos (CE, Cl, Mg, Na, Fe) que con NDVI (Cl y Na), sugiriendo una mayor relación entre ambas variables. Los resultados pueden incorporarse directamente a los planes de manejo del Santuario y apoyar procesos de conservación liderados por comunidades locales.

Esta investigación relacionada con un análisis exploratorio de los efectos de la precipitación sobre la vegetación mediante el uso de teledetección ha resultado especialmente valioso para caracterizar la dinámica espacio-temporal de la cadena de humedales de montaña y su influencia sobre la calidad del agua, ecosistema de montaña único y remoto con accesibilidad limitada. Asimismo, ha permitido identificar ciertos factores ambientales, de terreno y de calidad del agua que influyen en estos humedales. El enfoque presentado, ofrece un marco metodológico y resultados que puede ser extrapolados y aplicados a investigaciones similares en otras regiones.

No obstante, este estudio enfrentó limitaciones relacionadas con la disponibilidad espacial de datos de terreno, tales como información detallada para cada humedal, caracterizaciones de calidad de agua específicas por humedal y descripciones hidrológicas de los aportes superficiales y subterráneos. Además, se identificó la necesidad de incrementar la frecuencia de monitoreo de parámetros químicos y de mediciones de caudal.

En cuanto al trabajo futuro, se ha presentado a la comunidad agrícola administradora del Santuario de la Naturaleza una propuesta para realizar análisis hidrológicos e hidroquímicos basados en programas de monitoreo en terreno y ampliar análisis SIG que consideren caracterización de la calidad de agua y caudal en la cadena de humedales, caracterización físico química de sedimentos, influencia de la cobertura nival y glaciares en la dinámica hidroquímica y aportes de agua subterránea. Estos esfuerzos buscan mejorar la comprensión espacio-temporal de la cadena de humedales y abordar las brechas de información identificadas.

3.3. Introduction

Wetlands are areas that retain and store water and that provide fundamental ecosystem services for wildlife and vegetation dynamics [1,2]. The ecological importance of wetlands for the planet is widely recognized, as they can store carbon, regulate the water cycle, and sustain approximately 40% of global biodiversity [3-5].

Many different types of wetlands are recognized, including coastal wetlands, high altitude wetlands (called bofedales in the Andes), peat bogs, mangrove forests, estuarine wetlands, salt marshes, and others. High-altitude wetlands are considered complex ecosystems that are generally located at least at 3000 m.a.s.l. Conservation of these wetlands is of particular interest because they are among the main water sources in headwater basins, and they play a fundamental hydrological role as water reservoirs and regulators of water quality as sinks for sediments, pollutants (including certain metals), and excess nutrients [6–13]. They also host a large amount of diversity, including endemic species that are especially essential in arid and semi-arid zones. In this regard, the sustainability of these wetlands is closely linked to water availability, and is significantly influenced by precipitation variability, which is a key climate factor that impacts both the associated downstream ecosystems and the human activities that depend on them [3,14–22].

Studies on vegetation cover behavior and water quality under the influence of different climate factors (such as precipitation variation, including drought periods) have been carried out more often in the northern hemisphere [23]. Because these high-altitude wetlands are located in remote mountain areas, remote sensing and normalized indices such as the NDVI

(normalized difference vegetation index) have proven to be especially useful for generating spatio-temporal datasets that would otherwise be unattainable or challenging to obtain through conventional field methods [18,19,21,24–29]. In addition, the NDMI (normalized difference moisture index), which is used specifically to analyze vegetation cover water stress, is relevant to water resources and vegetation management [24,30], making the NDMI particularly useful for understanding wetland behavior in areas with water scarcity.

Analyses of precipitation–vegetation time-series dynamics have identified various vegetation cover behaviors related to the occurrence of precipitation and drought events in mountain ecosystems, including high-altitude wetlands. Based on the NDVI, general increases in greening were detected in the Western Alps and in Switzerland (including mountain systems) due to climate variables (including precipitation) and it was found that precipitation was rarely significant [31,32]. Research undertaken in the Koshi River Basin (Himalayas) revealed an increase in vegetation productivity from 1982 to 1994, aligning with previous studies across Eurasia. However, at a smaller temporal scale, the authors detected a sudden decrease in productivity between 1994 and 2000, followed by an increase from 2000 to 2011 [33]. In addition, precipitation proved to have an influence on vegetation cover behavior. Moreover, a rapid expansion of wetlands was identified on the Tibetan Plateau between 1990 and 2019, which was associated with an increase in precipitation amid climate change [34]. Moreover, the study was carried out in a mountainous area of the Yangguan National Nature Reserve, where it was observed that the presence and accumulation of precipitation are important factors in the high NDVI levels associated with the vegetation in these wetlands [35].

The use of remote sensing techniques for understanding the complex interactions between changes in vegetation cover reflectance and water quality concentrations is relatively new [29]. In the Everglades National Park, Florida, USA, it was identified that long-term mangrove water quality (mayor ions, nitrate, and phosphate) was correlated

with the biophysical reflectance indices (like the NDVI and EVI) of the vegetation cover [36]. In Xinjiang and Tibet in western China, it was determined that a significant correlation exists between major ion concentrations and the NDVI [37]. Utilizing an approach that

predicts Araçuaí river water quality in a semi-arid area through the NDVI of the vegetation cover basin demonstrated the potential of this index to predict water quality [38].

In Chile, there are approximately 17,000 wetlands, which account for an area of about14,604 km^2 [39]. High-altitude wetlands and groups of wetlands in the Andes (known in Chile as "high-Andean") are mainly flood meadows [23,39,40]. Like other terrestrial and aquatic ecosystems, they are impacted by climate change [41,42]. In the Maipo Valley of Chile, using remote sensing complemented by data from study area, the Andean Wetlands of this Valley were identified and mapped. The research revealed that the approach using remote sensing was particularly valuable for monitoring high-mountain wetland areas with limited accessibility, such as is the case in the Andes [43].

Studies on high-Andean wetland dynamics and the influence of the climate in Chile have been focused on the far north of the country (the Altiplano), which has unique climate conditions and ecosystem characteristics that are associated with greater aridity. In this area, it was found that precipitation in wet years (20–30 years recurrence interval) played a key role in sustaining these wetlands, as it allows for groundwater recharge (a main water source in these ecosystems) [19,44]. Meanwhile, via NDVI variation, it was determined that the period between 2011 and 2017 was the most productive period in the last three decades in the wetlands located in the Altiplano (area of 63,705 km^2, above 3700 m.a.s.l) [45].

In north-central Chile, the main impact of climate change has been a decrease in precipitation in terms of both frequency and intensity as part of a megadrought phenomenon [46,47]. We are not aware of any previous studies on the impacts of climate change on the high-Andean wetlands in this region. Therefore, the main goal of this study is to present a spatiotemporal analysis of the vegetation cover behavior dynamics in a chain of twelve high-Andean wetlands in the Elqui Valley in the semi-arid zone of Chile, and relate these vegetation cover dynamics to precipitation and water quality in the Claro River. To address this main goal, the following specific objectives have been established: first, to assess the influence of precipitation variability on vegetation cover dynamics across the chain of wetlands using a time series of biophysical indices (NDVI and NDMI); second, to analyze the correlation between these biophysical indices and key water quality parameters, and third, to identify

factors, such as the altitude, slope, and additional water inputs from streams, that relate to differences in the index values between the wetlands in the chain.

3.4. Materials and Methods

3.4.1. Study Area

This study was carried out in a chain of twelve high-Andean wetlands (about 364 ha) located in the Estero Derecho Nature Sanctuary (Private Protected Area (PPA)), in the Claro River basin (Elqui River headwater basin), north-central Chile, Coquimbo Region (Figure 10 and Table 4).

Table 4. Characterization of twelve high-Andean wetlands.

Code	Wetland	Area (ha)	Altitude (m.a.s.l)	Slope (%)
W01	Bofedal 1	2.06	2751–2795	14
W02	Bofedal 2	2.76	2796–2823	10
W03	Los Corralitos	10.57	2848–2884	5
W04	Los Toros	6.94	2884–2921	8
W05	Bofedal 5	8.80	2923–2967	7
W06	Candelilla	2.13	2956–2988	9
W07	El Chañar	18.90	2984–3034	5
W08	Bofedal 8	5.21	3029–3057	6
W09	Piuquenes	49.73	3050–3198	5
W10	Llareta	20.68	3263–3314	3
W11	Bofedal 11	119.46	3329–3515	3
W12	Bofedal 12	116.40	3488–3659	5

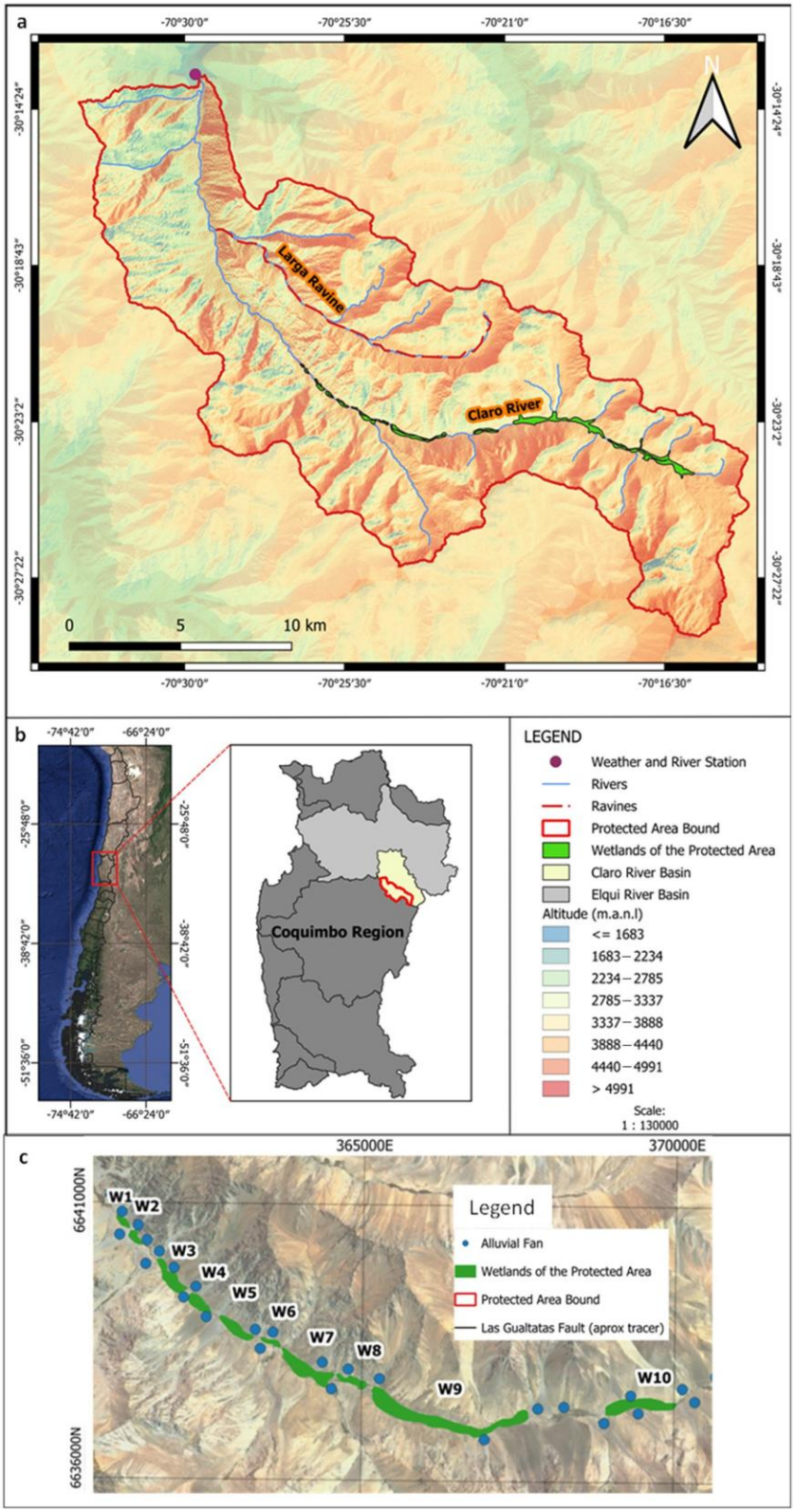

Figure 10. Study area: (a) location of Claro River basin, (b) Claro River basin and chain of wetlands—Estero Derecho Nature Sanctuary, and (c) interaction of alluvial fans with wetlands (W1–W10).

In this sanctuary, both conservation and small-scale grazing of large livestock are carried out. Grazing is a historical–cultural tradition of the members of "Estero Derecho" Agricultural Community, who manage the sanctuary and are in charge of the sanctuary management plan [48].

The Claro River basin (338 km^2) has a semi-arid climate, in which precipitation, snowmelt, and ENSO (El-Niño Southern Oscillation) play an important role in the Elqui River headwater basins [49]. This basin presents a snow-dominated hydrological regime with greater precipitation during the winter months (June, July, and August). Average annual precipitation is 237 mm, and the recorded streamflow of the Claro River averages 1.17 m3/s [50,51]. Moreover, in the Claro River basin, 4.31 km^2 of rock glaciers and 4.01 km^2 of protalus lobes have been identified [52], which add as water reservoirs to the snowpack.

The geology of the Claro River is composed mainly of andesitic, basaltic, and granitic/ rhyolitic rocks that are primarily of plutonic origin. Intrusive igneous rocks (granites, granodiorites, monzogranites, tonalites, and diorites) account for approximately 63% of the geological composition of the study area. Volcanic and volcano-sedimentary rocks (tuffs and rhyolitic lavas, sedimentary breccias, and conglomerate) comprise 10%, while alluvial, colluvial, and fluvioglacial sediment accounts for 23% and metamorphic rocks (schists, slates, and meta-sandstones) make up the remaining 4% [3,50,52,53]. (Geological and 12 wetland alluvial fan maps can be found in Supplementary Files).

The morphology of the upper part of the basin, where the chain of wetlands is located, is characterized by narrow valleys with steep slopes that are associated with high runoff and erosion, which are conditions that promote the formation of wetlands [54]. In the study area, the formation of alluvial fans has been observed from the upper part of the basin to the base of the valley, where the chain of wetlands is located. These geomorphological structures have been found to be a factor that promotes the formation of wetlands due to their ability to retain and distribute surface water courses and contribute to groundwater recharge [55]. Figure 10c shows the alluvial fans and their shaping influence on the studied wetlands, which is a more notable condition in the downstream wetlands of the chain.

Due to the lack of information on the specific characteristics of all wetlands in the study area, the description of the Piuquenes wetland (49.7 ha), which is part of the wetland chain (code W9 in this study), provides an approximate idea of the general formation of the chain of wetlands [23]. Moreover, this description indicated that the wetland consists of layers of saturated unconsolidated sediments with a low clay content, including sands, gravels, and silt beds. These layers are expected to extend to a depth of approximately 10 m. The morphology of the bofedal resembles that of a basin-shaped landform, exhibiting thicker sediment accumulation downstream compared to upstream. The boundary of its lower portion is delineated by a rock barrier. The water retention capacity of this alluvial-filled structure is estimated at 2000 mm per m2 of bofedal area [23].

3.4.2. Satellite Data

Satellite images are from the Landsat 5 Level 2, Collection 2, Level 2 (available from 1986 to 2011) and Landsat 8 Level 2, Collection 2, Level 2 (available from 2013 onward), with a temporal resolution of 16 days and a spatial resolution of 30 m. Images were selected from 1986 to 2023 in the southern hemisphere summer (from December to March), which represents the vegetation growing season, on days with no or minimal cloud cover in the study area. They were provided by the GEE cloud platform.

3.4.3. Historical Precipitation and Water Quality Data

Monthly precipitation data from 1986 to 2019 for the Claro River basin were downloaded from the CAMELS-CL explorer platform (https://camels.cr2.cl/) (accessed on 2 October 2023). In order to extend the analysis of the time-series graph, as a reference, precipitation data from the years 2020, 2021, and 2022 from La Laguna weather station (30◦12′7″ S and 70◦2′28″ W), a DGA mountain station located in the Elqui River basin, were used. It is the closest mountain weather station to the Claro River basin with temporal records in the aforementioned years (omitted for the correlation analyses explained below). For water quality, CE, Ca, Cl, K, Mg, Na, SO4, and Fe data were taken from the historical database of the General Water Directorate (DGA) National Water Information System (SNIA) platform (https://snia.mop.gob.cl/BNAConsultas/reportes) (accessed on 27 April 2023).

3.4.4. Normalized Difference Indices

Vegetation cover behavior was quantified based on the spatiotemporal variation of the time series of the normalized difference vegetation index (NDVI) and the normalized difference moisture index (NDMI).

The NDVI index represents vegetation greening and is useful for understanding vegetation density and assessing changes in plant vigor. NDVI values range from +1.0 to −1.0. Areas of bare rock or snow usually present with very low NDVI values (for example, 0.1 or less). The NDVI is calculated as a ratio between the red (R) (band 3 for Landsat5 and band 4 for Landsat 8) and near infrared (NIR) values (band 4 for Landsat5 and band 5 for Landsat 8) [56,57]:

$$NDVI = (NIR - RED)/(NIR + RED) \quad (1)$$

The NDMI index is used specially to determine water content in vegetation and is useful for determining water stress and canopy cover. NDMI values range from +1.0 to −1.0; values near the limits may be associated with waterlogging/complete cover and water stress/bare soil. This index is used in drought monitoring because it is a reliable indicator for water stress in vegetation cover, detecting it even at an early stage. The NDMI is calculated as a function of the surface reflectance bands in Landsat 5 (NIR is band 4 and SWIR is band 5) and Landsat 8 (NIR is band 5 and SWIR is band 6) [58,59].

$$NDMI = (NIR - SWIR)/(NIR + SWIR) \quad (2)$$

3.4.5. Time-Series Analysis

A spatiotemporal analysis during the 1986–2023 period was carried out based on NDVI and NDMI values for the vegetation cover in the chain of wetlands and annual precipitation data from the basin. Satellite images were processed to determine the median values for the normalized indices for both the entire chain and for each wetland by year, in order to identify vegetation cover variability patterns and possible trends related to hydrological and climate dynamics. The code that was used to determine the NDVI and NDMI was created in GEE (the code is available in the Supplementary Materials).

The cropped geometry was downloaded from the National Wetland Inventory (https: //humedaleschile.mma.gob.cl/inventario-humadales/) (accessed on 4 March 2023).

All images stored in the GEE program were preprocessed in order to guarantee quick and efficient access. GEE, and particularly the data related to surface reflectance (SR), were generated with specific algorithms that atmospherically correct each image in the collection. In addition, shade, ice, cloud, and spray masks were applied to the satellite collection to avoid alterations in the calculation of the indices (NDVI and NDMI).

To determine the time series of the NDVI (associated with vegetation cover greening) and NDMI (moisture levels in vegetation cover), Landsat 5 TM and 8 OLI satellite images were used, covering the 1986–2023 period (December, January, February, and March). The initial set consisted of 150 images (103 Landsat 5 and 47 Landsat 8). The first step was to discard images due to defects and cloudiness in the study area (22 images). Thus, the final database consisted of 138 images (85 Landsat 5 and 53 Landsat 8). Then, the median NDVI and NDMI during the study period (37 years) were calculated and harmonized for the chain of wetlands, in accordance with the explanation above.

Two spatial approaches were used for the study: (a) the chain of wetlands as a whole and (b) each individual wetland. To analyze the entire time series, and because the image set with which the indices were calculated is from two Landsat satellites (TM and OLI), a harmonization procedure was applied to the images [60–62]. Due to the fact that the operational periods of Landsat 5 and Landsat 8 do not overlap, the data from the images from both satellites were transformed to Landsat 7 (ETM) for the harmonization procedure. For each pair of images, 217 points were selected (those outside the confidence interval were removed). Using the selected sampling points, two scatter plots were created for each index (TM vs. ETM and OLI vs. ETM). The corresponding fitting equations were obtained using the least squares linear regression method. The harmonization equations are as follows:

NDVI harmonization:

$$ETM = 1.0218 \times OLI - 0.0465 \quad (3)$$

$$\mathbf{ETM = 1.0377 \times TM + 0.0012} \quad (4)$$

NDMI harmonization:

$$ETM = 0.9966 \times OLI - 0.0249 \quad (5)$$

$$ETM = 1.0137 \times TM + 0.0058 \quad (6)$$

3.4.6. Boxplot Analysis

The spatial behavior of the indices was analyzed using boxplots created in RStudio with the ggplot2 package for each of the twelve wetlands.

3.4.7. Least-Squares Regression Analysis

To identify possible relationships between vegetation cover behavior and precipitation and water quality in the Claro river, least-squares regression was performed for the following variables: (a) NDVI/NDMI and annual precipitation records and (b) NDVI/NDMI and selected water quality parameters (CE, Ca, Cl, K, Mg, Na, SO4, and Fe) [31–33,38,63].

To this end, first, the Shapiro–Wilk normality test was applied to the datasets associated with each variable. If the data for both variables presented with a normal distribution, the Pearson correlation coefficient was calculated. If the data for at least one of the variables presented with a non-normal distribution, the Spearman correlation coefficient was calculated. The ranges used for the strength of the correlation are as follows: None [0.0–0.1); Low [0.1–0.3); Medium [0.3–0.5); Strong [0.5–0.7); and Very Strong [0.7–1.0].

A methodological summary with the main activities associated with obtaining spatiotemporal series and correlation results is presented below (Figure 11).

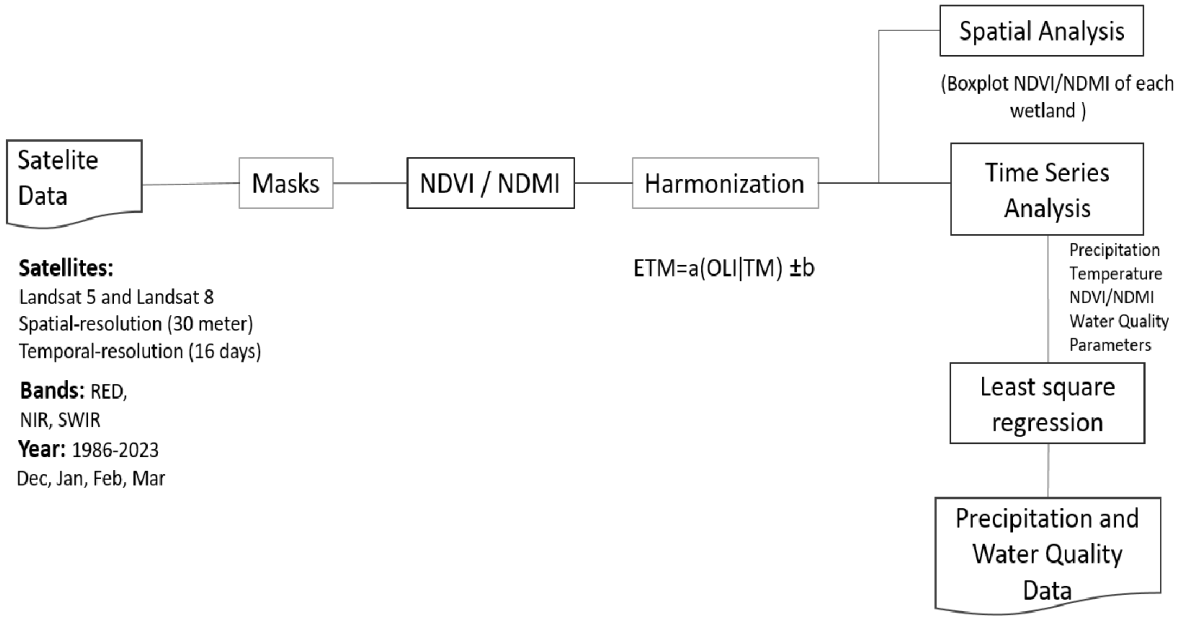

Figure 11. The analytical framework of the study.

3.5 Results and Discussion

3.5.1. Analysis of Temporal Behavior of Indices with Respect to Wetland Chain Precipitation

In general, the time-series data show a marked congruence between the cumulative annual precipitation time series and the temporal variability of the NDVI and NDMI, with a one-year lag (Figure 12). Cyclical behavior and coincidence in the occurrence of the maximum (MAXNDVI: 0.584 and MAXNDMI: 0.232) and minimum values (MINNDVI: 0.280 and MINNDMI: −0.189) is present in the time series of the two indices. The highest precipitation values were recorded in 1987 and 1997 and the highest index values were found in 1988 and 1998. As mentioned earlier, the indices were not determined in 2003, 2012, or 2013 due to a lack of images.

Of note is the 2017–2022 period, in which the longest sustained decrease in the time series for both indices were evident, which coincides temporally with the megadrought phenomenon. The megadrought is closely related to climate change and represents a precipitation deficit of approximately 30%, which is extraordinary for its prolonged duration within the historical record [46,47]. Our result is in contrast with studies carried out in the

wetlands of the Altiplano, which detected greater vegetation cover productivity in this period [19,44,45].

The increase in NDMI values in 1993 and 2020 was not detected in the NDVI, which may be explained by the occurrence of summer rainfall in December 1992, February 1993, and January 2020, respectively, allowing for an increase in vegetation cover moisture but no variation in the NDVI.

A few times, increases or decreases in precipitation caused contradictory responses in the vegetation indices (with a one-year lag). One notable case is that of 1993/1994, when the precipitation in 1993 surpassed that of 1994, but the 1994 indices were lower than those of 1995. This could be explained by the temporal distribution of the rainfall: in 1993 the main precipitation events occurred early, concentrated in April and May, representing an anomaly in the study zone. In contrast, in 1994, the precipitation was concentrated between June and August, during the southern hemisphere winter, which facilitates snow storage, boosting the availability of water resources in the wetlands.

A similar situation was observed in 1988 and 1998, when there was less precipitation than in 1989 and 1999, but the data show higher indices in 1989 and 1999 compared to 1990 and 2000. In this case, no significant variations in precipitation in the pairs of years were detected, although historical maxima were recorded in 1987 and 1997, which would have allowed for the accumulation of snow reserves that were sufficient to supply the wetlands in subsequent years.

To complement the analysis of the influence of climatic variables on vegetation cover, the temporal variations in the annual average temperature during the period of 1986–2019 were included. In Figure 12b, the time-series data do not show a marked congruence between the annual average temperature and the temporal variability in the NDVI and NDMI. Moreover, a marked increasing temperature value was observed in the period between 2014 and 2019, which is a phenomenon that can be linked to climate change [41]. This result (over long periods) is in contrast with studies carried out in the Alpes, where it has been identified that a rise in average temperatures favors an increase in NDVI values [31,32].

The determination of the linear relationships in the historical data for the time series suggests a slight decreasing trend in both precipitation and the NDVI and NDMI and a slight increasing trend in the temperature over the years. However, the low R2 values in all cases indicate a limited fit with the observed variability. In particular, the NDMI presents with a more marked temporal trend than the NDVI and precipitation, which could be linked to the greater sensitivity of moisture content to long-term changes. In addition to precipitation variability, other factors that can influence vegetation cover include glacial melt contributions, groundwater input, snowmelt timing and grazing.

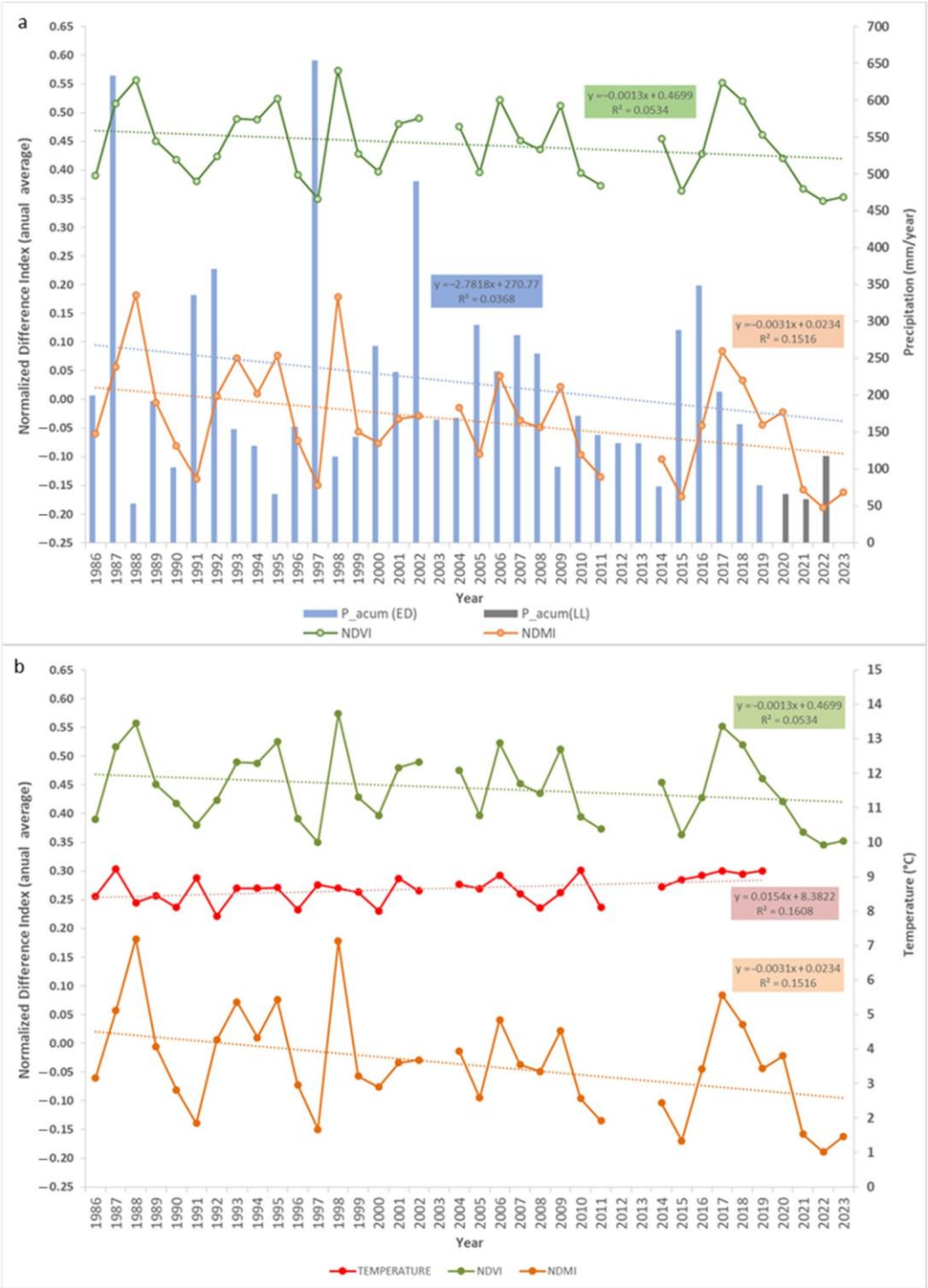

Figure 12. The temporal variations in vegetation cover in the chain of wetlands: NDVI and NDMI time series (summer—annual average) and meteorological variables: (a) annual precipitation (1986–2019): Estero Derecho station (ED) and (2020–2022): La Laguna station (LL), used as a reference in the absence of data from the station in the basin in which the wetlands are located) and (b) annual average temperature (1986–2019): Estero Derecho station (ED).

The Spearman correlation coefficients (after confirming the normal distribution of the data for all the variables) also showed significant least-squares linear relationships for each index (NDVI and NDMI) with respect to annual precipitation (Table 5). In accordance with the classification, a high correlation ($\rho > 0.6$) was identified for both indices with a one-year lag (precipitation from a year before the indices) and a medium correlation ($\rho > 0.4$) with a two-year lag [64]. The correlation was not statistically significant for the same year, as in general precipitation occurs in the fall and winter in the southern hemisphere (May to August), following the austral summer (Dec, Jan, Feb, Mar), the months for which the vegetation cover indices were determined.

Table 5. Spearman's rank correlation coefficient between cumulative precipitation–temperature and NDVI/NDMI.

Variable		**NDVI**		**NDMI**	**Strength of Correlation**
Precipitation	**ρ**	**p-value**	**ρ**	**p-value**	
P (year n)	0.28	0.128	−0.138	0.436	None
P (year n − 1)	0.654	5.58 × 10−5 *	0.637	9.66 × 10−5 *	Strong
P (year n − 2)	0.471	7.05 × 10−3 *	0.42	1.75 × 10−3 *	Medium
Temperature	**r**	**p-value**	**r**	**p-value**	
T (year n)	0.280	0.128	0.074	0.691	None
T (year n − 1)	−0.049	0.791	−0.138	0.459	None
T(year n − 2)	0.135	0.468	0.168	0.364	None

Note: * Correlation significant ($\alpha = 0.05$; two-tailed).

The Pearson correlation coefficients (after confirming the normal distribution of the data for all the variables) showed no statistically significant least-squares linear relationships for each index (NDVI and NDMI) with the annual mean temperature (Table 5).

To complement the analysis of the chain of wetlands as a whole, the results of the spatiotemporal analysis of the vegetation cover behavior by year for the entire chain of wetlands is shown in Figure 13. This analysis was based on pixel value classification in

accordance with the ranges defined for each index in EOS [56,58]. In general, both temporal and spatial (area in hectares) congruence was observed for the variability of the state of vegetation cover between the two indices, and precipitation variability was also observed (Figure 13). These results show the greatest number of hectares with the highest NDVI (dark green) and NDMI values (yellow) in 1988 and 1998, which coincide with the rainiest years in the study period with a one-year lag (1987 and 1997). Meanwhile, after 2010, years that can be linked to the megadrought phenomenon, the greatest number of hectares linked to the lowest ranges of the indices (NDVI below 0.4 and NDMI below zero) are presented. Between 2017 and 2022, a sustained decrease in greening and moisture was identified, representing a unique behavior in the time series.

As a reference, Figure 13 includes images of 18 January1988 and 20 March 2022, which represent the days with the greatest and lowest indices, respectively. In both cases, these images show a predominance of greater values in the downstream wetlands (left side of each image) and lower index values upstream (right side of each image).

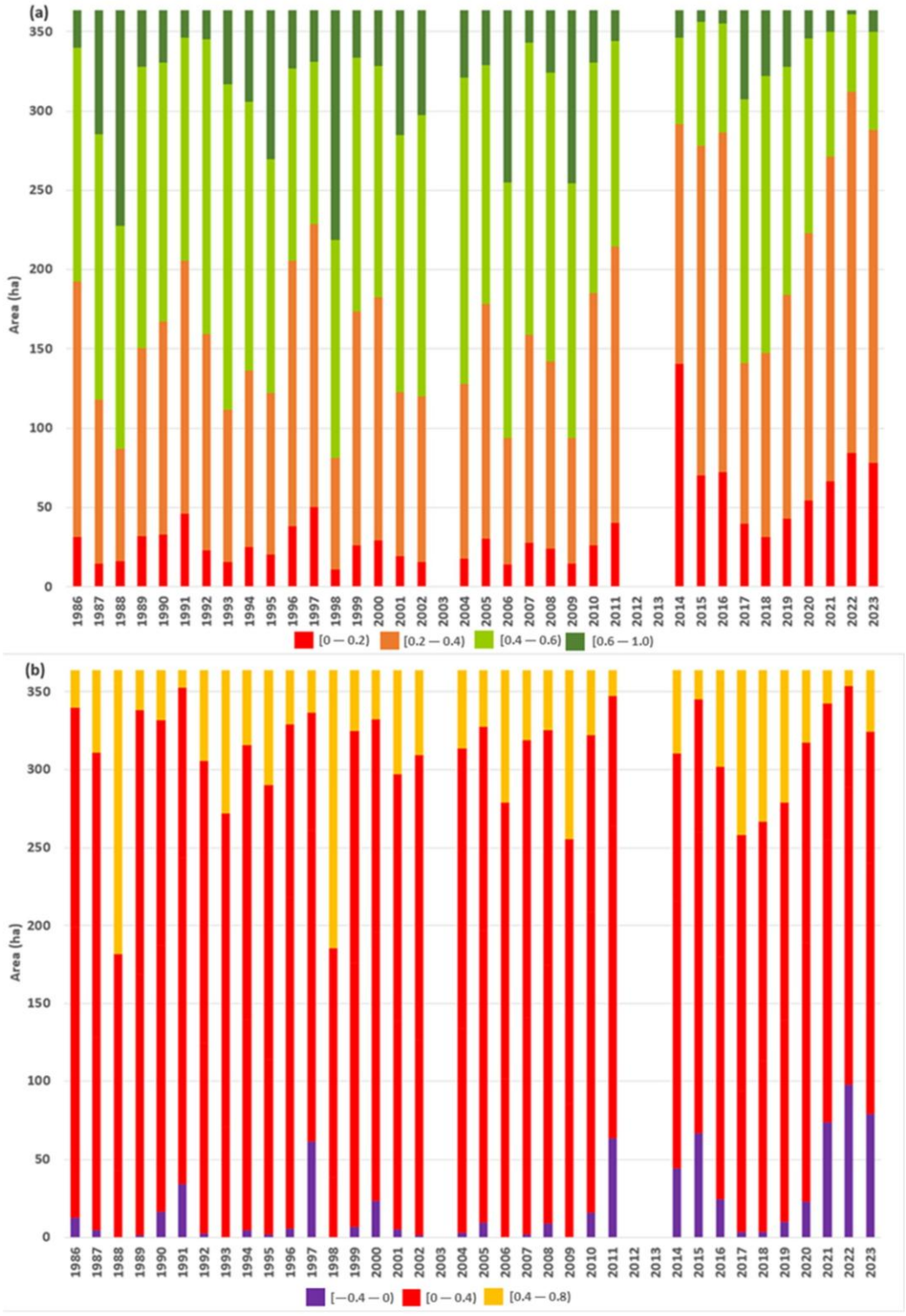

Figure 13. The temporal variability in the vegetation cover of the chain of wetlands according to the classification of the indices: (a) NDVI and (b) NDMI.

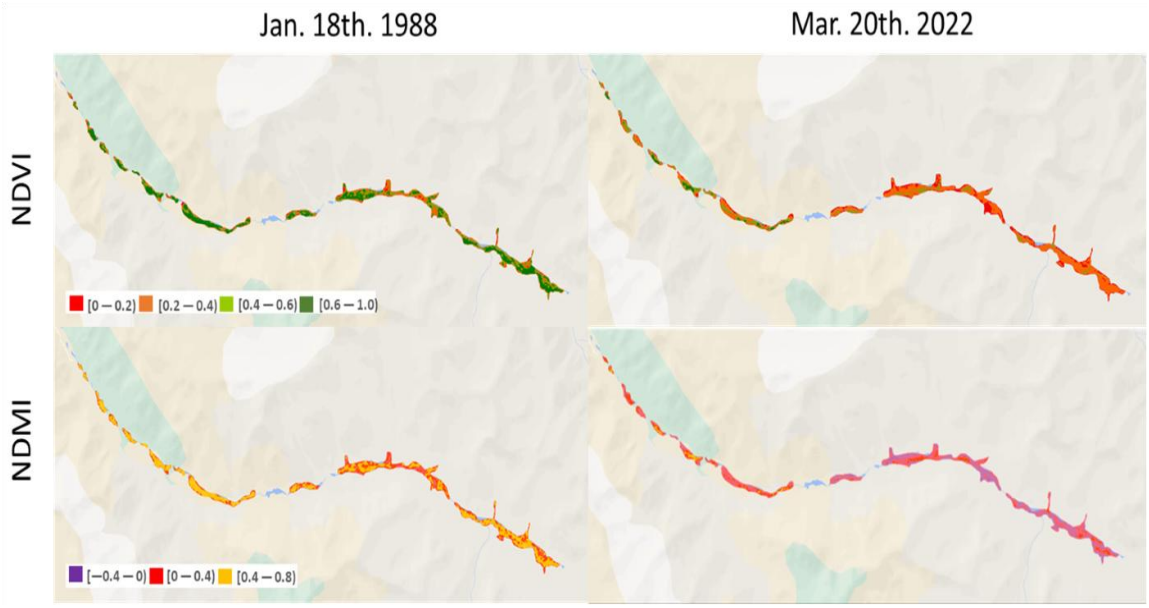

Figure 14. NDVI and NDMI maps (18 January 1988: highest index values; 20 March 2022: lowest index values).

3.5.2. Spatial Analysis of Vegetation Cover by Wetland

The boxplot analyses (Figure 15) for each wetland showed evidence of the vegetation cover behavior in each, revealing that the NDVI and NDMI remained consistently lower in the wetlands located at altitudes higher than 3200 m.a.s.l., (W11, W10, W12), in contrast with W03 and W02, which were located below 2800 m.a.s.l, and followed by W07 and W06. This behavior could be explained by altitude-related environmental conditions [32]. Besides, for the wetlands with the highest median index values, the satellite images showed tributary streams, which, in addition to the Claro River, directly contribute water to these wetlands, resulting in greater index values in runoff periods.

Meanwhile, the interquartile range proved to be lower for the NDVI than for the NDMI; this situation can be linked to the ranges in which the NDVI (0–1.0) and NDMI data are distributed (−0.4 a 0.8). In addition, the interquartile ranges for both indices presented with a greater amplitude in wetlands W10 and W6, and the smallest amplitude in W9, which are associated with more or less vegetation cover behavior variability, respectively. In the case of W6, the conditions favoring high variability could be related to the following: (a) the steep terrain slope (9%) where the wetland is located, which limits water storage, and (b) the presence of a tributary stream with intermittent runoff, which in periods of abundant

precipitation would provide a greater streamflow for a longer duration, unlike in drier periods, during which the contribution of the stream would be lower or nonexistent. No particular conditions were identified for W10.

In the case of W09, the greater variation seen with both indices, which indicates greater stability in the vegetation cover behavior over time, could be influenced by the gentle terrain slope (5%) and the relatively large size of the wetland (50 ha) compared to most of the wetlands in the chain. These conditions promote water storage in the wetland, allowing the vegetation cover to maintain its greening and moisture longer.

From the analysis of the NDVI/NDMI time series stratified by wetland, a general congruence was identified between the indices' values and precipitation patterns. Notably, despite the overall decline in the indices since 2017 and the low precipitation recorded during those years, the indices for wetlands W1–W8 exhibited unusually high values between 2017 and 2019. In this context, although no long-term association with temperature was identified, the historical increase in temperature observed since 2014 could potentially influence this phenomenon [31,32].

A linear regression analysis for each wetland (indices vs time) revealed that, among the twelve wetlands, those exhibiting a positive slope were as follows: NDVI: W1–W8, W11 (close to zero), and NDMI: W2–W5, W7, and W8. On the other hand, the wetlands showing a negative slope were as follows: NDVI: W9, W10, and W12, and NDMI: W1, W6, and W9–12. The analysis highlights a general trend (related to the altitude) of increasing indices from W1 to W8, and a decreasing trend from W9 to W12, with W1 and W6 showing distinct patterns in their trend lines. Both W1 and W6 have the smallest areas and the steepest slopes among the entire wetland chain.

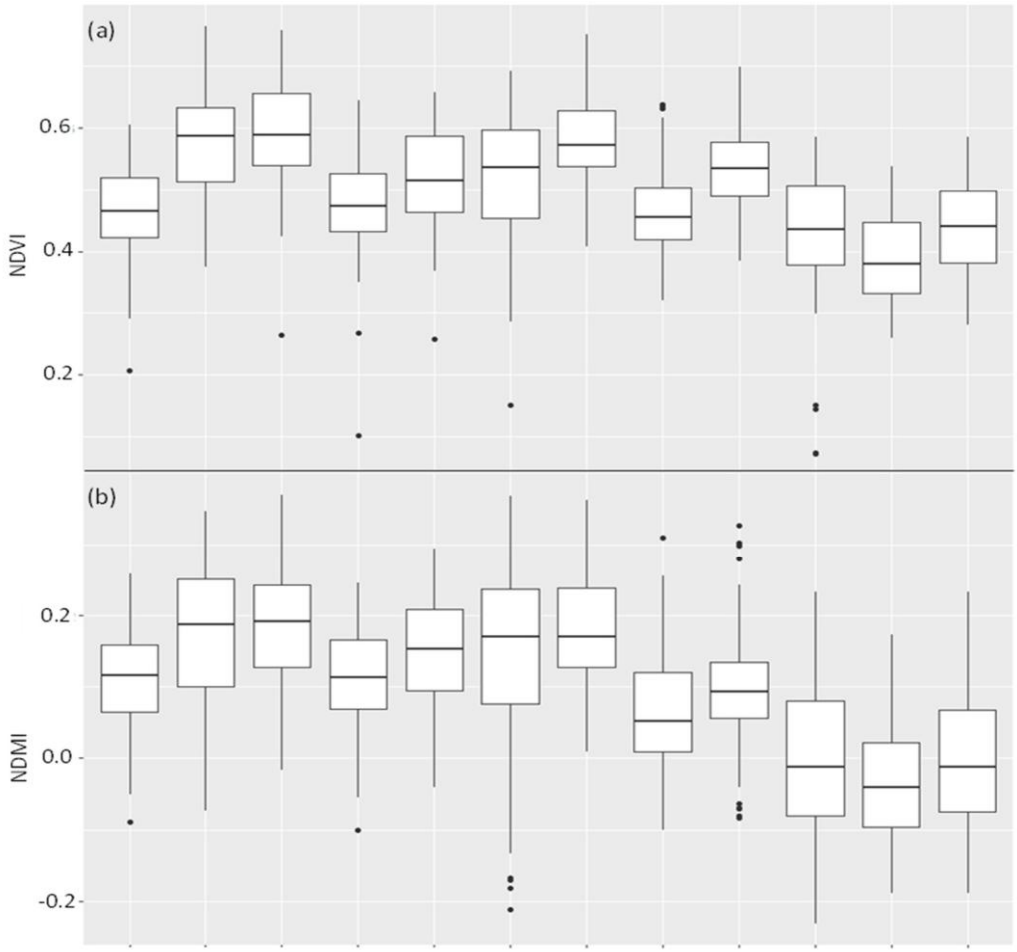

		W01	W02	W03	W04	W05	W06	W07	W08	W09	W10	W11	W12
NDVI	Me	0.464	0.587	0.589	0.473	0.515	0.535	0.572	0.455	0.534	0.436	0.379	0.441
	σ	0.097	0.120	0.116	0.093	0.123	0.143	0.091	0.084	0.085	0.128	0.117	0.116
NDMI	Me	0.116	0.188	0.191	0.113	0.153	0.171	0.170	0.053	0.094	−0.013	−0.041	−0.012
	σ	0.094	0.151	0.115	0.097	0.114	0.160	0.111	0.111	0.078	0.161	0.118	0.143

Figure 15. Vegetation cover behavior in the study area disaggregated by wetland, generated based on the median index of each image during the summer season: (a) NDVI and (b) NDMI.

3.5.3 Influence of Terrain Characteristics on the Wetlands

To identify the potential influence of terrain factors for each wetland (average altitude, slope, and area), a combined analysis of these variables was carried out (Figure 16). A pattern associated with altitude was observed: higher altitudes corresponded to lower index values, and was possibly linked to climatic variables (e.g., temperature). A key factor explaining the lower vegetation cover in high-Andean zones compared with lowland areas is the greater

persistence of snow. Snow accumulation reduces both air and soil temperatures, delaying the onset of the growing season and collectively limiting vegetation development.

Regarding slope, wetlands with slopes below 5% were found to exhibit lower index values, while those with slopes above 5% showed higher values. However, this relationship might appear counterintuitive, as lower slopes are traditionally associated with a higher water storage capacity, which would typically result in higher index values. This discrepancy could be attributed to other factors that are intrinsic to each wetland (e.g., altitude and soil water retention capacity, among others).

For wetlands with a slope of exactly 5%, a descending order of index values was identified as the wetland area increased. However, this trend coincided with an ascending order of altitude for these wetlands: W3, W7, W9, and W12. In terms of the wetland area, no clear behavioral pattern was identified overall. While the two largest wetlands recorded the lowest index values, this may be related to their altitude.

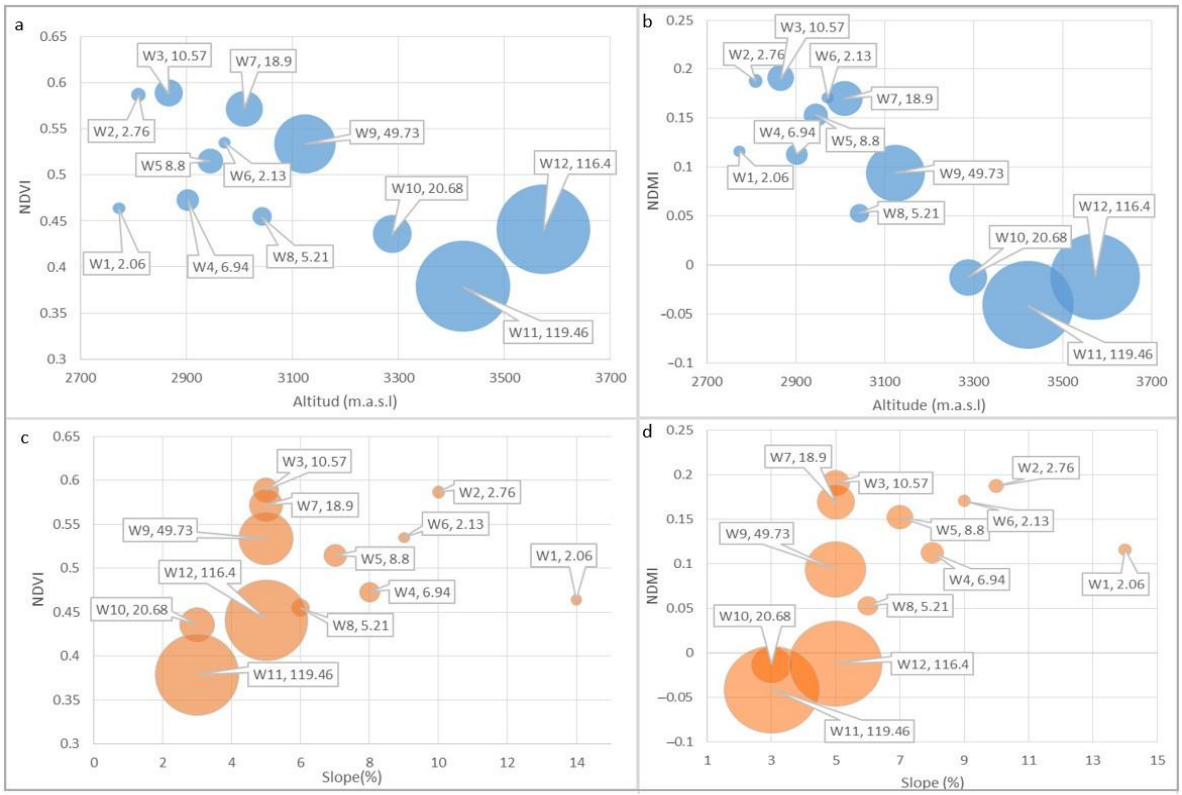

Figure 16. Bubble plot showing relationship between vegetation indices (NDVI and NDMI) and wetland characteristics: (a) altitude vs. NDVI area as bubble size; (b) altitude vs. NDMI area as bubble size; (c) slope vs. NDVI area as bubble size; and (d) slope vs. NDMI area as bubble size.

Another factor potentially influencing the vegetation dynamics of the wetlands in the study area is groundwater contribution. Although no field data are currently available for this factor, the local geology provides the following insights: a. Geological Characterization: the Claro River basin predominantly features crystalline basement blocks and metamorphic rocks. As a result, the study area is characterized by generally low permeability, limiting subsurface water flow and water storage, and therefore reducing water availability for vegetation during summer periods or droughts. b. Exogenous Processes: Freeze–thaw cycles, associated with the presence of rock glaciers and snowfields in the upper basin, are notable in this region. Snow in high mountain environments plays a critical role in controlling alpine vegetation dynamics, particularly in arid and semi-arid ecosystems, as it constitutes the primary water source and regulates the length of the growing season, soil microbial composition, temperature, soil moisture, and runoff, conditions essential for plant development. Early melt events may promote an earlier onset of vegetation growth; however, in the absence of subsequent recharge, water availability for plants later in the season is substantially reduced. c. Structural Control: The Gualtatas Fault, identified within the study area, could exert significant geological control. This fault may either act as a barrier to groundwater flow or enhance infiltration, depending on its structural and hydraulic characteristics. Furthermore, fluvial and alluvial processes have facilitated the formation of colluvial and alluvial fans, structures that are widely recognized for their capacity to promote water infiltration, thereby enhancing water availability for vegetation during summer or dry periods (Geological and 12 wetland alluvial fan maps can be found in the Supplementary Files).

3.5.4. Linear Relationships Between Vegetation Cover and Selected Water Quality Parameters

The linear relationships between the NDVI and NDMI indices that were derived from the satellite images and water quality parameters with a maximum lag of 15 days revealed that the Na and Fe data presented with a non-normal distribution based on the Shapiro–Wilk test. Therefore, the least-squares fit between these elements and the indices was determined using the Spearman coefficient. For all the other variables (indices and water quality parameters),

the least-squares fit was determined with Pearson coefficients, as the data followed a normal distribution (Table 6).

The results show that the NDVI has significant correlations with fewer water quality parameters than the NDMI, and the correlation coefficients are lower, which suggests a more robust relationship between the NDMI and water quality parameters. For the NDVI, significant medium correlations with CE, Cl, and Na were identified. For the NDMI, medium correlations with CE, Cl, and Mg were found, along with high correlations with Na and Fe. These correlations were only positive with Fe, whereas for the other parameters, they were negative. The significant correlation with CE could be linked to the presence of dissolved ions in the water (e.g., chlorides).

Table 6. Correlation analysis for NDVI, NDMI, and selected water quality parameters.

Parameter	NDVI			NDMI		
	Coefficient	p-value		Coefficient	p-value	
CE	-0.374	0.095		-0.500	0.021	*
Ca	-0.072	0.756		-0.429	0.052	
Cl	-0.403	0.035	*	-0.470	0.032	*
K	-0.036	0.877		0.009	0.969	
Mg	-0.167	0.468		-0.457	0.037	*
Na	-0.449	0.041	*	-0.541	0.011	*
SO_4	0.211	0.358		-0.103	0.658	
Fe	0.386	0.084		0.588	0.005	*

*Significant Correlation: α= 0.05 (two-tailed)

Coefficient: Spearman (ρ): CE, Ca, Cl, K, Mg, SO_4; Pearson (R): Na, Fe.

Notes: Significant Correlation: α = 0.05 (two-tailed), Coefficient: Spearman (ρ): CE, Ca, Cl, K, Mg, SO4; Pearson (R): Na, Fe.

These negative correlations may be explained by the increased greening and moisture content that is associated with increased canopy coverage and healthier/low water stress vegetation cover [56,58]. These situations are related to an increase in the absorption of ions dissolved in the water, in contrast with situations in which the indices (NDVI/NDMI) are lower [36,37]. Regarding the positive correlation between Fe and the NDMI, it could be related to the

resuspension of sediment containing poorly soluble iron precipitates, caused by an increase in runoff into the wetlands [65,66].

Unlike the wetlands of the Chilean Altiplano, which exhibit characteristics of salt flats with high concentrations of water quality parameters, the concentrations in the Claro River are considerably lower and do not reach levels that are toxic to plants. This is particularly true for sodium (Na+), which, while beneficial to plants at low concentrations, is a well-documented toxic element at high concentrations. For example, Na+ toxicity levels are 1.5–2.9 g/L, which are far above the concentrations observed in the study area. In Figure 17, the temporal dynamics of the water-quality parameters that were statistically correlated with vegetation-cover status are presented.

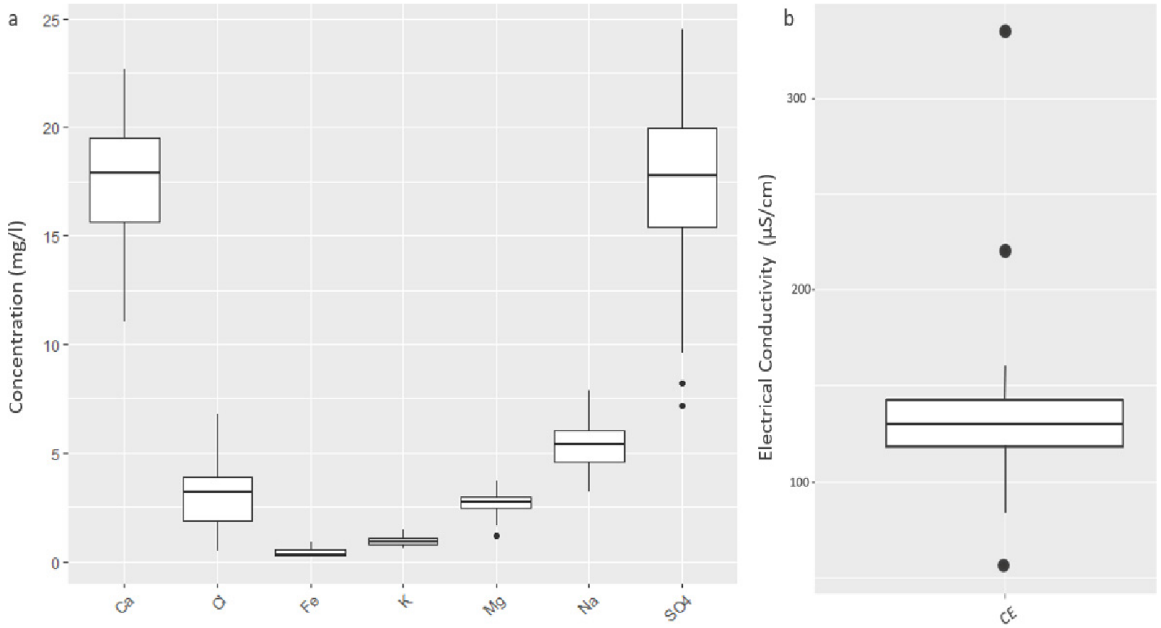

Figure 17. Water quality parameters at Claro River Station: (a) mayor ion and iron concentrations, and (b) electrical conductivity.

3.6. Conclusions

North-central Chile, due to its semi-arid climate conditions, is especially sensitive to precipitation variability and drought events, where headwater basin water reservoirs, such as high-altitude wetlands, play an important role in both water dynamics and the functioning of the mountain ecosystems downstream of the basin. In conditions of field information scarcity, remote sensing tools proved to be of great utility in order to assess the influence of precipitation on the vegetation cover behavior of a chain of 12 high-Andean bofedales and to identify the role of the alluvial fans in each high-altitude wetland in our study domain. We used the NDVI and NDMI time series (1986–2023) to assess the relationships between precipitation variability and vegetation cover in the complete chain of wetlands (greening and moisture content).

Our time-series analysis using a linear regression of the 37 years of Landsat imagery for both indices and precipitation presented with a negative slope, which relates to the megadrought experienced in Chile. In addition, our analysis of the time series and a correlation analysis showed that the state of vegetation cover in the chain of wetlands is strongly related to the amount of precipitation recorded the previous year. Some differences between the two indices are of interest, as it was determined that upward variations in the NDMI, which were not detectable in the NDVI, could be associated with summer precipitation, which is infrequent in the study area. In general, the state of the vegetation cover showed a progressive decrease in both greening and moisture content in the wetlands, which was likely caused by the megadrought. This phenomenon can be linked to climate change.

Our spatial analysis using boxplots confirmed differences in vegetation cover behavior among the wetlands, and a bubble plot analysis of terrain factors for each wetland (average altitude, average slope, and area) identified a marked influence associated with wetland altitudes.

From the review of the geological background, it was identified that due to the low permeability of the predominant rocks in the study area, there is generally low permeability. However, factors such as the alluvial fans and the Las Gualtatas fault could facilitate groundwater discharge to the wetland chain.

Regarding the temperature, no long-term relationship could be determined with the NDVI/NDMI index values for the wetland chain. However, an analysis stratified by wetland identified unusually high values for wetlands W1–W8 between 2017 and 2019, a period that coincides with the megadrought and a rise in the historical average temperature (since 2014). This phenomenon can be linked to climate change.

Our spatial analysis using boxplots confirmed differences in vegetation cover behavior among the wetlands, which could be related to factors such as the altitude, terrain slope, additional water contributions from streams (associated with alluvial fans), and wetland size.

Meanwhile, significant correlations (high and medium) between the indices and several water quality parameters (CE, Cl, Mg, Na, and Fe), were found, with the NDMI having a more robust association with the parameters compared to the NDVI. These negative correlations with CE, Cl, Mg, and Na could be linked to increased absorption of dissolved elements when there is more greening and moisture in the vegetation cover, while positive correlations could be related to the resuspension of Fe precipitates.

Considering that the studied bofedales are protected within the Estero Derecho Nature Sanctuary due to their ecological value, the information obtained in this study is highly useful for conservation activities related to this ecosystem. At the study site, our findings may be formally incorporated into the management plan for the nature sanctuary, focusing on the characterization and monitoring of environmental parameters, the development of specific management programs for wetlands, as well as water resource conservation and environmental education. It is important to highlight that the management plan is overseen by the "Estero Derecho" Agricultural Community, making these results a meaningful contribution to this community. More broadly, given the ecological importance of wetlands, particularly high-altitude ones, the methodological approach in this study could contribute to other wetland management and conservation efforts. This would be especially valuable for communities connected to remote or hard-to-reach areas, such as the Andes Mountain Range.

This exploratory analysis of the impacts of precipitation on vegetation using remote sensing has proven particularly valuable for characterizing the spatiotemporal dynamics of the wetland chain, which is a unique and remote mountainous ecosystem with limited

accessibility. It has also facilitated the identification of certain environmental, terrain, and water quality factors that influence the wetlands. However, this study faced limitations related to the spatial availability of field data, such as detailed information for individual wetlands, water quality characterizations specific to each wetland, and hydrological characterizations of both surface and subsurface contributing flows. Additionally, the need for an increased monitoring frequency for chemical parameters and flow measurements has been identified.

Regarding future work, the agricultural community managing the Nature Sanctuary has been approached with a proposal to conduct hydrological and hydrochemical analyses based on field monitoring programs. These efforts aim to enhance the spatiotemporal understanding of the wetland chain and address the identified data gaps.

Supplementary Materials: The following supporting information can be downloaded at https: //www.mdpi.com/article/10.3390/w16243682/s1, NDVI and NDMI time series for each wetland; Geological map of the Claro River basin and alluvial fans related to the wetland chain; Time series for water quality parameters. GEE code, NDVI: L5: https://code.earthengine.google.com/a651 eb4b155afc6c273a629c7f001c76, L8: https://code.earthengine.google.com/8f6614eb130614f555c5 664557fa3888; NDMI: L5: https://code.earthengine.google.com/0494d9bede80f3caf994fed5a66109 02, L8: https://code.earthengine.google.com/e26188743f68cd06c0aa792e76d62794 (all accessed on 8 December 2024).

Nota. La versión de este trabajo, incluida en la presente tesis, difiere de la publicada, ya que se incluyeron modificaciones indicadas por la comisión revisora.

References

1. Barducci, A.; Guzzi, D.; Marcoionni, P.; Pippi, I. Aerospace wetland monitoring by hyperspectral imaging sensors: A case study in the coastal zone of San Rossore Natural Park. J. Environ. Manag. 2009, 90, 2278–2286. [CrossRef] [PubMed]
2. Yager, K.; Prieto, M.; Meneses, R.I. Reframing Pastoral Practices of Bofedal Management to Increase the Resilience of Andean Water Towers. Mt. Res. Dev. 2021, 41, A1–A9. [CrossRef]
3. Ramsar Convention Secretariat. Manual de la Convención de Ramsar, 6th ed.; Secretaría de la Convención de Ramsar: Gland, Switzerland, 2013. Available online:

https://www.ramsar.org/sites/default/files/documents/library/manual6-2013-sp.pdf (accessed on 11 March 2024).
4. U.S. Environmental Protection Agency. Why Are Wetlands Important? Available online: https://www.epa.gov/wetlands/whyare-wetlands-important (accessed on 9 November 2024).
5. U.S. Geological Survey. Why Are Wetlands Important? Available online: https://www.usgs.gov/faqs/why-are-wetlandsimportant (accessed on 11 March 2024).
6. Mitsch, W.J.; Bernal, B.; Hernandez, M.E. Ecosystem Services of Wetlands. Int. J. Biodivers. Sci. Ecosyst. Serv. Manag. 2015, 11, 1–4. [CrossRef]
7. Marton, J.M.; Chowdhury, R.R.; Craft, C.B. A Comparison of the Spatial Variability of Denitrification and Related Soil Properties in Restored and Natural Depression Wetlands in Indiana, USA. Int. J. Biodivers. Sci. Ecosyst. Serv. Manag. 2014, 11, 36–45. [CrossRef]
8. Evenson, G.R.; Golden, H.E.; Lane, C.R.; McLaughlin, D.L.; D'Amico, E. Depressional Wetlands Affect Watershed Hydrological, Biogeochemical, and Ecological Functions. Ecol. Appl. 2018, 28, 953–966. [CrossRef]
9. Lane, C.R.; Leibowitz, S.G.; Autrey, B.C.; LeDuc, S.D.; Alexander, L.C. Hydrological, Physical, and Chemical Functions and Connectivity of Non-Floodplain Wetlands to Downstream Waters: A Review. JAWRA J. Am. Water Resour. Assoc. 2018, 54, 346–371.
[CrossRef] [PubMed]
10. Cheng, F.Y.; Van Meter, K.J.; Byrnes, D.K.; Basu, N.B. Maximizing US Nitrate Removal through Wetland Protection and Restoration. Nature 2020, 588, 625–630. [CrossRef]
11. Fritz, K.M.; Schofield, K.A.; Alexander, L.C.; McManus, M.G.; Golden, H.E.; Lane, C.R.; Kepner, W.G.; LeDuc, S.D.; DeMeester, J.E.; Pollard, A.I. Physical and Chemical Connectivity of Streams and Riparian Wetlands to Downstream Waters: A Synthesis. JAWRA J. Am. Water Resour. Assoc. 2018, 54, 323–345. [CrossRef] [PubMed]
12. Lu, S.; Li, J.; Si, J.; Miao, Y.; Qi, X.; Zhang, X.; Bao, W.; Zhang, X.; Zhou, S.; Jin, C.; et al. Evaluation and Prediction of Water Quality of Typical Wetlands in the Source Region of the Yangtze River. Water 2023, 15, 1612. [CrossRef]
13. Qiu, J.; Shen, Z.; Xie, H. Drought Impacts on Hydrology and Water Quality under Climate Change. Sci. Total Environ. 2022, 858, 159854. [CrossRef] [PubMed]
14. Squeo, F.A.; Warner, B.G.; Aravena, R.; Espinoza, D. Bofedales: High Altitude Peatlands of the Central Andes. Rev. Chil. Hist. Nat. 2006, 79, 245–255. [CrossRef]
15. Hribljan, J.A.; Cooper, D.J.; Sueltenfuss, J.; Wolf, E.C.; Heckman, K.A.; Lilleskov, E.; Chimner, R.A. Carbon Storage and Long-Term Rate of Accumulation in High-Altitude Andean Peatlands of Bolivia. Mires Peat 2015, 15, 1–14.
16. Aponte-Saravia, J.; Ospina-Noreña, J.E. Evaluando El Desempeño de Índices Espectrales Para Identificar Humedales Alto Andinos. Rev. Teledetec. 2019, 53, 59–72. [CrossRef]

17. Anderson, T.G.; Christie, D.A.; Chávez, R.O.; Olea, M.; Anchukaitis, K.J. Spatiotemporal Peatland Productivity and Climate Relationships across the Western South American Altiplano. J. Geophys. Res. Biogeosci. 2021, 126, e2020JG005994. [CrossRef] 18. Ashok, A.; Rani, H.P.; Jayakumar, K.V. Monitoring of Dynamic Wetland Changes Using NDVI and NDWI Based Landsat Imagery. Remote Sens. Appl. Soc. Environ. 2021, 23, 100547. [CrossRef]
19. De La Fuente, A.; Meruane, C.; Suárez, F. Long-Term Spatiotemporal Variability in High Andean Wetlands in Northern Chile. Sci. Total Environ. 2020, 756, 143830. [CrossRef]
20. Uribe-Álvarez, M.C.; Prieto, M.; Meseguer-Ruiz, O. Bofedal Response to Climate Variability, Local Management, and Water Extraction: A Case Study of Chucuyo, Northern Chile. J. Mt. Sci. 2021, 19, 241–252. [CrossRef]
21. Chávez, R.O.; Meseguer-Ruiz, O.; Olea, M.; Calderón-Seguel, M.; Yager, K.; Meneses, R.I.; Lastra, J.A.; Núñez-Hidalgo, I.; Sarricolea, P.; Serrano-Notivoli, R.; et al. Andean Peatlands at Risk? Spatiotemporal Patterns of Extreme NDVI Anomalies, Water Extraction and Drought Severity in a Large-Scale Mining Area of Atacama, Northern Chile. Int. J. Appl. Earth Obs. Geoinf. 2022, 116, 103138. [CrossRef]
22. Luo, N.; Yu, R.; Wen, B. Characteristics of Changes in Typical Mountain Wetlands in the Middle and High Latitudes of China over the Past 30 Years. Land 2024, 13, 1124. [CrossRef]
23. Valois, R.; Schaffer, N.; Figueroa, R.; Maldonado, A.; Yáñez, E.; Hevia, A.; Carrizo, G.Y.; MacDonell, S. Characterizing the Water Storage Capacity and Hydrological Role of Mountain Peatlands in the Arid Andes of North-Central Chile. Water 2020, 12, 1071. [CrossRef]
24. Guo, M.; Li, J.; Sheng, C.; Xu, J.; Wu, L. A Review of Wetland Remote Sensing. Sensors 2017, 17, 777. [CrossRef]
25. Ju, Y.; Bohrer, G. Classification of Wetland Vegetation Based on NDVI Time Series from the HLS Dataset. Remote Sens. 2022, 14, 2107. [CrossRef]
26. Jombo, S.; Adelabu, S. Evaluating Landsat-8, Landsat-9 and Sentinel-2 Imageries in Land Use and Land Cover (LULC) Classification in a Heterogeneous Urban Area. GeoJournal 2023, 88, 377–399. [CrossRef]
27. Rapinel, S.; Panhelleux, L.; Gayet, G.; Vanacker, R.; Lemercier, B.; Laroche, B.; Chambaud, F.; Guelmami, A.; Hubert-Moy, L. National Wetland Mapping Using Remote-Sensing-Derived Environmental Variables, Archive Field Data, and Artificial Intelligence. Heliyon 2023, 9, e13482. [CrossRef]
28. Zhang, H.; Guo, J.; Li, X.; Liu, Y.; Wang, T. Spatiotemporal Variation in and Responses of the NDVI to Climate in Western Ordos and Eastern Alxa. Sustainability 2023, 15, 4375. [CrossRef]
29. Mashala, M.J.; Dube, T.; Mudereri, B.T.; Ayisi, K.K.; Ramudzuli, M.R. A Systematic Review on Advancements in Remote Sensing for Assessing and Monitoring Land Use

and Land Cover Changes Impacts on Surface Water Resources in Semi-Arid Tropical Environments. Remote Sens. 2023, 15, 3926. [CrossRef]
30. Monteiro, A.T.; Arenas-Castro, S.; Punalekar, S.M.; Cunha, M.; Mendes, I.; Giamberini, M.; Da Costa, E.M.; Fava, F.; Lucas, R. Remote Sensing of Vegetation and Soil Moisture Content in Atlantic Humid Mountains with Sentinel-1 and 2 Satellite Sensor Data. Ecol. Indic. 2024, 163, 112123. [CrossRef]
31. Filippa, G.; Cremonese, E.; Galvagno, M.; Isabellon, M.; Bayle, A.; Choler, P.; Carlson, B.Z.; Gabellani, S.; Morra di Cella, U.; Migliavacca, M. Climatic Drivers of Greening Trends in the Alps. Remote Sens. 2019, 11, 2527. [CrossRef]
32. Obuchowicz, C.; Poussin, C.; Giuliani, G. Change in Observed Long-Term Greening across Switzerland—Evidence from a Three Decades NDVI Time-Series and Its Relationship with Climate and Land Cover Factors. Big Earth Data 2023, 8, 1–32. [CrossRef]
33. Zhang, Y.; Gao, J.; Liu, L.; Wang, Z.; Ding, M.; Yang, X. NDVI-Based Vegetation Changes and Their Responses to Climate Change from 1982 to 2011: A Case Study in the Koshi River Basin in the Middle Himalayas. Glob. Planet. Chang. 2013, 108, 139–148. [CrossRef]
34. Li, Y.; Hou, Z.; Zhang, L.; Qu, Y.; Zhou, G.; Lin, J.; Li, J.; Huang, K. Long-term spatio-temporal changes of wetlands in Tibetan Plateau and their response to climate change. Int. J. Appl. Earth Obs. Geoinf. 2023, 121, 103351. [CrossRef]
35. Pan, F.; Xie, J.; Lin, J.; Zhao, T.; Ji, Y.; Hu, Q.; Pan, X.; Wang, C.; Xi, X. Evaluation of Climate Change Impacts on Wetland Vegetation in the Dunhuang Yangguan National Nature Reserve in Northwest China Using Landsat Derived NDVI. Remote Sens. 2018, 10, 735. [CrossRef]
36. Lagomasino, D.; Price, R.M.; Whitman, D.; Campbell, P.K.E.; Melesse, A. Estimating Major Ion and Nutrient Concentrations in Mangrove Estuaries in Everglades National Park Using Leaf and Satellite Reflectance. Remote Sens. Environ. 2014, 154, 202–218. [CrossRef]
37. Liu, X.; Zhou, Z.; Ding, Y. Vegetation Coverage Change and Erosion Types Impacts on the Water Chemistry in Western China. Sci. Total Environ. 2021, 772, 145543. [CrossRef] [PubMed]
38. Vieira, F.R.; Christofaro, C. Contributions of the Vegetation Index (NDVI) in Water Quality Prediction Models in a Semi-Arid Tropical Watershed. J. Arid Environ. 2024, 220, 105122. [CrossRef]
39. Vivanco, E. Humedales y Turberas en Chile. Available online: https://obtienearchivo.bcn.cl/obtienearchivo?id=repositorio/1022 1/24257/2/Humedales_y_turberas_en_Chile_CMA_2017_FINAL.pdf (accessed on 24 March 2024).
40. Convención de Ramsar y EHAA. Estrategia Regional para la Conservación y Uso Sostenible de Humedales Altoandinos; Gobiernos de Ecuador y Chile, CONDESAN y TNC-Chile. Available online: https://humedaleschile.mma.gob.cl/wp-content/ uploads/2018/04/ERHAA_espanol.pdf (accessed on 24 March 2024).

41. Pörtner, H.-O.; Roberts, D.C.; Adams, H.; Adelekan, I.; Adler, C.; Adrian, R.; Aldunce, P.; Ali, E.; Bednar-Friedl, B.; Begum, R.A.; et al. 2022: Technical Summary. In Climate Change 2022: Impacts, Adaptation, and Vulnerability. Contribution of Working Group II to the
Sixth Assessment Report of the Intergovernmental Panel on Climate Change; Pörtner, H.-O., Roberts, D.C., Tignor, M., Poloczanska, E.S., Mintenbeck, K., Alegría, A., Craig, M., Langsdorf, S., Löschke, S., Möller, V., et al., Eds.; Cambridge University Press: Cambridge, UK; New York, NY, USA, 2022; pp. 37–118. [CrossRef]
42. Salimi, S.; Almuktar, S.A.A.A.N.; Scholz, M. Impact of Climate Change on Wetland Ecosystems: A Critical Review of Experimental Wetlands. J. Environ. Manag. 2021, 286, 112160. [CrossRef] [PubMed]
43. Araya-López, R.A.; Lopatin, J.; Fassnacht, F.E.; Hernández, H.J. Monitoring Andean High Altitude Wetlands in Central Chile with Seasonal Optical Data: A Comparison between Worldview-2 and Sentinel-2 Imagery. ISPRS J. Photogramm. Remote Sens. 2018, 145, 213–224. [CrossRef]
44. Blin, N.; Hausner, M.; Leray, S.; Lowry, C.; Suárez, F. Potential Impacts of Climate Change on an Aquifer in the Arid Altiplano, Northern Chile: The Case of the Protected Wetlands of the Salar Del Huasco Basin. J. Hydrol. Reg. Stud. 2022, 39, 100996. [CrossRef]
45. Chávez, R.O.; Christie, D.A.; Olea, M.; Anderson, T.G. A Multiscale Productivity Assessment of High Andean Peatlands across the Chilean Altiplano Using 31 Years of Landsat Imagery. Remote Sens. 2019, 11, 2955. [CrossRef]
46. Garreaud, R.; Alvarez-Garreton, C.; Barichivich, J.; Boisier, J.P.; Christie, D.; Galleguillos, M.; LeQuesne, C.; McPhee, J.; Zambrano-Bigiarini, M. The 2010–2015 mega drought in Central Chile: Impacts on regional hydroclimate and vegetation. Hydrol. Earth Syst. Sci. Discuss. 2017, 21, 6307–6327. [CrossRef]
47. Garreaud, R.D.; Boisier, J.P.; Rondanelli, R.; Montecinos, A.; Sepúlveda, H.H.; Veloso-Aguila, D. The Central Chile Mega Drought (2010–2018): A Climate Dynamics Perspective. Int. J. Climatol. 2019, 40, 421–439. [CrossRef]
48. Comunidad Agrícola Estancia Estero Derecho. Plan de Manejo para la Conservación del Área Protegida Privada y Santuario de la Naturaleza Estero Derecho. 2017. Available online: https://www.esteroderecho.cl/PMC2017/PMC%20APP%20y%20SN%20Estero%20Derecho%2020170515.pdf (accessed on 3 April 2024).
49. Souvignet, M.; Oyarzún, R.; Verbist, K.M.J.; Gaese, H.; Heinrich, J. Hydro-Meteorological Trends in Semi-Arid North-Central Chile (29–32◦S): Water Resources Implications for a Fragile Andean Region. Hydrol. Sci. J. 2012, 57, 479–495. [CrossRef]
50. Alvarez-Garreton, C.; Mendoza, P.A.; Boisier, J.P.; Addor, N.; Galleguillos, M.; Zambrano-Bigiarini, M.; Lara, A.; Puelma, C.;
Cortes, G.; Garreaud, R.; et al. The CAMELS-CL Dataset: Catchment Attributes and Meteorology for Large Sample Studies—Chile Dataset. Hydrol. Earth Syst. Sci. 2018, 22, 5817–5846. [CrossRef]

51. Barría, P.; Sandoval, I.B.; Guzman, C.; Chadwick, C.; Alvarez-Garreton, C.; Díaz-Vasconcellos, R.; Ocampo-Melgar, A.; Fuster, R. Water Allocation under Climate Change. Elem. Sci. Anthr. 2021, 9, 00131. [CrossRef]
52. Merino, R.N.; Pino, C. Criósfera del río Cochiguaz y Cuenca Superior del río Claro o Derecho, Región de Coquimbo: Geomorfología Periglaciar e Inventario de Glaciares Rocosos; Servicio Nacional de Geología y Minería: Santiago, Chile, 2020; Informe Registrado IR-20-80; 85p.
53. SERNAGEOMIN. Mapa Geológico de Chile: Versión Digital. Available online: https://tiendadigital.sernageomin.cl/es/geologiabasica/3273-mapa-geologico-de-chile-version-digital.html (accessed on 2 April 2024).
54. Harvey, A. Alluvial Fans. In Reference Module in Earth Systems and Environmental Sciences; Elsevier: Amsterdam, The Netherlands, 2018; ISBN 978-0-12-409548-9. [CrossRef]
55. Stock, J.D. Waters Divided: A History of Alluvial Fan Research and a View of Its Future. In Treatise on Geomorphology; Shroder, J.F., Ed.; Academic Press: San Diego, CA, USA, 2013; pp. 413–458. ISBN 978-0-08-088522-3. [CrossRef]
56. EOS. NDVI FAQ: All You Need to Know About NDVI. 2024. Available online: https://eos.com/blog/ndvi-faq-all-you-need-toknow-about-ndvi/ (accessed on 9 April 2024).
57. USGS. Landsat Normalized Difference Vegetation Index. 2024. Available online: https://www.usgs.gov/landsat-missions/ landsat-normalized-difference-vegetation-index (accessed on 9 April 2024).
58. EOS. NDMI: A Comprehensive Guide to NDMI Analysis. 2024. Available online: https://eos.com/make-an-analysis/ndmi/ (accessed on 11 April 2024).
59. USGS. Landsat Normalized Difference Moisture Index. 2024. Available online: https://www.usgs.gov/landsat-missions/ normalized-difference-moisture-index (accessed on 11 April 2024).
60. Li, P.; Jiang, L.; Feng, Z. Cross-Comparison of Vegetation Indices Derived from Landsat-7 Enhanced Thematic Mapper Plus (ETM+) and Landsat-8 Operational Land Imager (OLI) Sensors. Remote Sens. 2013, 6, 310–329. [CrossRef]
61. Roy, D.P.; Kovalskyy, V.; Zhang, H.K.; Vermote, E.F.; Yan, L.; Kumar, S.S.; Egorov, A. Characterization of Landsat-7 to Landsat-8
Reflective Wavelength and Normalized Difference Vegetation Index Continuity. Remote Sens. Environ. 2016, 185, 57–70. [CrossRef]
62. Gavilán, V.; Lillo-Saavedra, M.; Holzapfel, E.; Rivera, D.; García-Pedrero, A. Seasonal Crop Water Balance Using Harmonized Landsat-8 and Sentinel-2 Time Series Data. Water 2019, 11, 2236. [CrossRef]
63. Ghebrezgabher, M.G.; Yang, T.; Yang, X.; Sereke, T.E. Assessment of NDVI Variations in Responses to Climate Change in the Horn of Africa. Egypt. J. Remote Sens. Space Sci. 2020, 23, 249–261. [CrossRef]
64. Klatetzki, T.; Schimank, U. Perspektiven der Gesellschaftstheorie: Sozialität, Kulturalität, Materialität; Springer: Berlin/Heidelberg, Germany, 2013. [CrossRef]

65. Hove, M.; Van Hille, R.P.; Lewis, A.E. Mechanisms of Formation of Iron Precipitates from Ferrous Solutions at High and Low pH. Chem. Eng. Sci. 2008, 63, 1626–1635. [CrossRef]
66. Peña-Guerrero, M.D.; Nauditt, A.; Muñoz-Robles, C.; Ribbe, L.; Meza, F. Drought Impacts on Water Quality and Potential Implications for Agricultural Production in theMaipo River Basin, Central Chile. Hydrol. Sci. J. 2020, 65, 1005–1021. [CrossRef]

CAPÍTULO IV: CONCLUSIONES GENERALES

4.1 Conclusiones

La investigación se centró en el estudio con datos a largo plazo de la hidroquímica de cuencas de cabecera de montaña e identificó factores incidentes en el comportamiento de parámetros de calidad de agua mediante dos enfoques: a) Determinación de la relación c-Q de un transecto de 30 cuencas andinas (29°-35°S) y b) Exploración del efecto del estado de la cobertura vegetal de una cadena de doce humedales altoandinos sobre la calidad del agua del Estero Derecho (Cuenca B04 del transecto).

En el enfoque relacionado con el estudio del transecto de cuencas, se identificó, mediante los diagramas de Gibbs y Na-Normalizado, que el aporte principal de solutos a los ríos se originaba de la meteorización de rocas ígneas silíceas. Luego, la determinación de la relación c-Q de las 30 cuencas, mediante la propuesta de Phole et al 2021, se identificó un patrón predominante de la relación c-Q (escorrentía-histéresis) de dilución-antihorario para los iones mayores, sugiriendo fuentes de solutos lejanas y/o limitadas y baja presencia de sedimentos finos, mientras que para el hierro se determinó un comportamiento predominante de enriquecimiento-horario identificando mayor disponibilidad de los solutos.

Por otra parte, los principales resultados del análisis de la influencia de características de las cuencas sobre el comportamiento de los solutos en el transecto de cuencas, mediante la interpretación de los resultados de los diagramas de Stiff y factores naturales, como magmatismo, y antropogénicos como emplazamiento de actividades industriales permitió caracterizar las singularidades de las cuencas que podrían influir en el comportamiento de los solutos. Además, se aplicaron test no-parametricos (Mann–Whitney U y el delta de Cliff). Se identificaron cinco asociaciones significativas ($p < 0,05$), con efectos de medianos a grandes, para el par Dilución–Constancia: Ca–vegetación, Ca–altitud, K–longitud del cauce, K–pendiente media y Mg–pendiente media.

Aunque los resultados de la relación ente la cobertura vegetal y los solutos fueron concluyentes solo para el Ca y no fueron concluyentes para el índice de aridez, incorporar en

el análisis estos índices a lo largo de un amplio gradiente regional, en un contexto de cambio climático, ofrece un enfoque novedoso para anticipar cambios en el comportamiento de los solutos bajo patrones de uso del suelo e hidroclimáticos en evolución.

Además, aunque la aplicación de los test U-Mann y Delta de Cliff ha sido limitada en otras áreas de la hidrología, no se encontraron aplicaciones en estudios sobre comportamiento de solutos, por lo que podría ser útil para estudios hidroquímicos

Para el segundo enfoque (cadena de humedales en la cuenca B04 Estero Derecho), los resultados del estado de la cobertura vegetal a largo plazo identificaron una correlación estadísticamente significativa entre la cantidad de la precipitación y el estado de la cobertura vegetal (NDVI/NDMI) con respuestas diferenciadas por humedal. Situación que identifica vulnerabilidad del humedal, dada la presencia del fenómeno de megasequía y cambio climático, donde, en los últimos años, la cobertura mostró los menores valores de índice del período estudiado. El estado de la cobertura vegetal en la cadena de humedales no fue uniforme; la altitud demostró ser una característica notablemente influyente en su condición.

Con respecto a la influencia entre el estado de la cobertura vegetal y la calidad de agua, se identificaron correlaciones significativas entre los índices y parámetros de calidad del agua (CE, Cl, Mg, Na y Fe), siendo el NDMI el que presentó mayor relación. Las correlaciones negativas con CE, Cl, Mg y Na sugieren mayor absorción de los solutos por la vegetación con mayor contenido de humedad y verdor, mientras que la correlación positiva podría vincularse a la resuspensión de Fe desde los sedimentos.

En general, de manera integrada la investigación ha logrado resultados que ofrecen una caracterización de la dinámica hidroquímica de las cuencas estudiadas que mejoran la comprensión de la relación c-Q y la influencia de factores naturales como la cubertura vegetal y condiciones del terreno y antropogénicos sobre el comportamiento de los parámetros de la calidad del agua en una amplia escala espacial. La relación identificada entre el comportamiento de los solutos, el índice de aridez y la cobertura vegetal permite, en un escenario de cambio climático, proyectar posibles cambios en la hidroquímica de los ríos que sirvan de insumo para tomas de decisión en la gestión de cuencas.

En base a las secciones precedentes y la hipótesis establecida se verifica que para el área de estudio los factores considerados como: fluviométricos, de cobertura vegetal y fisiográficos, están relacionados, con significancia estadística (p value< 0.05) con los patrones de comportamiento de los solutos estudiados en casos específicos como Ca, K, Mg. Para el transecto y Cl, Mg, Na y Fe Al para el Humedal Estero Derecho. Una limitación relevante se relacionó con la escasez datos, lo cual fue especialmente notorio en el caso de As, Cu, HCO_3 y NO_3.

En virtud de la investigación realizada, que abarca un transecto amplio (29°-35°S) y las diversas condiciones que presentan las cuencas, incluyendo una cadena de humedales de altura, los métodos usados y resultados obtenidos de la influencia de los diferentes factores naturales y antrópogénicos sobre el comportamiento de los solutos, este estudio entrega información diversa y valiosa que puede ser transferida a otras cuencas y ser comparada con hallazgos de estudios futuros similares, especialmente los realizados en zonas semiáridas y/o cuencas de cabeceras ubicadas en las montañas.

Al respecto, se plantean otras líneas de investigación tendientes a mejorar la comprensión de los factores clave que influyen sobre el comportamiento de los solutos y las proyecciones de escenarios futuros del comportamiento de los solutos en los cursos de agua de cuencas de cabecera. Primero se plantea caracterizar las fuentes específicas de los solutos mediante recolección de datos de terreno y el análisis SIG; identificar el aporte de aguas subterráneas en las cuencas, por ejemplo, mediante análisis isotópico (Rn+222), analizar la dinámica nival en la cordillera y su influencia en el comportamiento hidroquímico de las cuencas de cabecera y realizar una caracterización física y química de los sedimentos. Otro aspecto, relevante en un escenario de escasez hídrica, sería estudiar la influencia antropogénica temporal y espacial sobre la calidad de agua en las cuencas de cabecera. Lo anterior con el fin de modelar escenarios hidroquímicos futuros basados en la información generada.

En particular, el estudio de la cadena de humedales tuvo una aplicación directa a la comunidad debido a que la información generada será considerada para actualizaciones del plan de manejo y educación ambiental del Santuario.

Referencias

Ali, G., Wilson, H., Elliott, J., Penner, A., Haque, A., Ross, C., & Rabie, M. (2017). Phosphorus export dynamics and hydrobiogeochemical controls across gradients of scale,

topography and human impact. Hydrological Processes, 31(18), 3130–3145. https://doi.org/10.1002/hyp.11258

Anderson, T. G., Christie, D. A., Chávez, R. O., Olea, M., & Anchukaitis, K. J. (2021). Spatiotemporal Peatland Productivity and Climate Relationships Across the Western South American Altiplano. Journal Of Geophysical Research Biogeosciences, 126(6). https://doi.org/10.1029/2020jg005994

Aponte-Saravia, J., & Ospina-Noreña, J. E. (2019). Evaluando el desempeño de índices espectrales para identificar humedales alto andinos. Revista de Teledetección, 53, 59. https://doi.org/10.4995/raet.2019.10580

Araya-López, R. A., Lopatin, J., Fassnacht, F. E., & Hernández, H. J. (2018). Monitoring Andean high altitude wetlands in central Chile with seasonal optical data: A comparison between Worldview-2 and Sentinel-2 imagery. ISPRS Journal Of Photogrammetry And Remote Sensing, 145, 213-224. https://doi.org/10.1016/j.isprsjprs.2018.04.001

Ashok, A., Rani, H. P., & Jayakumar, K. (2021). Monitoring of dynamic wetland changes using NDVI and NDWI based landsat imagery. Remote Sensing Applications Society And Environment, 23, 100547. https://doi.org/10.1016/j.rsase.2021.100547

Barducci, A., Guzzi, D., Marcoionni, P., & Pippi, I. (2009). Aerospace wetland monitoring by hyperspectral imaging sensors: A case study in the coastal zone of San Rossore Natural Park. Journal Of Environmental Management, 90(7), 2278-2286. https://doi.org/10.1016/j.jenvman.2007.06.033

Bende-Michl, U., Verburg, K., & Cresswell, H. P. (2013). High-frequency nutrient monitoring to infer seasonal patterns in catchment source availability, mobilisation and delivery. Environmental Monitoring and Assessment, 185(11), 9191–9219. https://doi.org/10.1007/s10661-013-3246-8

Bieroza, M. Z., Heathwaite, A. L., Bechmann, M., Kyllmar, K., & Jordan, P. (2018). The concentration-discharge slope as a tool for water qualitymanagement. Science of the Total Environment, 630, 738–749. https://doi.org/10.1016/j.scitotenv.2018.02.256

Blin, N., Hausner, M., Leray, S., Lowry, C., & Suárez, F. (2022). Potential impacts of climate change on an aquifer in the arid Altiplano, northern Chile: The case of the protected wetlands of the Salar del Huasco basin. Journal Of Hydrology Regional Studies, 39, 100996. https://doi.org/10.1016/j.ejrh.2022.100996

Bogena, H.R.; Montzka, C.; Huisman, J.A.; Graf, A.; Schmidt, M.; Stockinger, M.; Von Hebel, C.; Hendricks-Franssen, H.J.; Van Der Kruk, J.; Tappe, W.; et al. The TERENO-Rur Hydrological Observatory: A Multiscale Multi-Compartment Research Platform for the Advancement of Hydrological Science. Vadose Zone Journal 2018, 17, 1–22, doi:10.2136/vzj2018.03.0055.

Bol, R., Gruau, G., Mellander, P.-E., Dupas, R., Bechmann, M., Skarbøvik, E., et al. (2018). Challenges of reducing phosphorus based water eutrophication in the agricultural landscapes of northwest Europe. Frontiers in Marine Science, 5(August), 1–16. https://doi.org/10.3389/fmars.2018.00276

Cairoli, M., Souza, F., Stroomberg, G., Postma, G., Buydens, L., & Jansen, J. (2024). BAHYS—A Bayesian Modeling Framework for Long-Term Concentration-Discharge Hysteresis: A Case Study on Chloride. Water Resources Research, 60(6). https://doi.org/10.1029/2023wr035427

Chávez, R. O., Christie, D. A., Olea, M., & Anderson, T. G. (2019). A Multiscale Productivity Assessment of High Andean Peatlands across the Chilean Altiplano Using 31 Years of Landsat Imagery. Remote Sensing, 11(24), 2955. https://doi.org/10.3390/rs11242955

Chávez, R. O., Meseguer-Ruiz, O., Olea, M., Calderón-Seguel, M., Yager, K., Meneses, R. I., Lastra, J. A., Núñez-Hidalgo, I., Sarricolea, P., Serrano-Notivoli, R., & Prieto, M. (2022). Andean peatlands at risk? Spatiotemporal patterns of extreme NDVI anomalies, water extraction and drought severity in a large-scale mining area of Atacama, northern Chile. International Journal Of Applied Earth Observation And Geoinformation, 116, 103138. https://doi.org/10.1016/j.jag.2022.103138

Convención de Ramsar y EHAA. Estrategia Regional para la Conservación y Uso Sostenible de Humedales Altoandinos; Gobiernos de Ecuador y Chile, CONDESAN y TNC-Chile. Disponible en línea: https://humedaleschile.mma.gob.cl/ (acceso: 24 March 2024).

Cordero, R.R.; Feron, S.; Damiani, A.; MacDonell, S.; Carrasco, J.; Pizarro, J.; Karas, C.; Jorquera, J.; Sepulveda, E.; Cabello, F.; et al. Rapid Decline in Extratropical Andean Snow Cover Driven by the Poleward Migration of the Southern Hemisphere Westerlies. Scientific Reports 2024, 14, doi:10.1038/s41598-024-78014-0.

De la Fuente, A., Meruane, C., & Suárez, F. (2020). Long-term spatiotemporal variability in high Andean wetlands in northern Chile. The Science Of The Total Environment, 756, 143830. https://doi.org/10.1016/j.scitotenv.2020.143830

Diamantini, E., Lutz, S. R., Mallucci, S., Majone, B., Merz, R., & Bellin, A. (2018). Driver detection of water quality trends in three large European river basins. Science of the Total Environment, 612, 49–62. https://doi.org/10.1016/j.scitotenv.2017.08.172

Evans, C.& Davies, T.D. Causes of Concentration/Discharge Hysteresis and Its Potential as a Tool for Analysis of Episode Hydrochemistry. Water Resources Research 1998, 34, 129–137, doi:10.1029/97wr01881.

Filippa, G., Cremonese, E., Galvagno, M., Isabellon, M., Bayle, A., Choler, P., Carlson, B. Z., Gabellani, S., Di Cella, U. M., & Migliavacca, M. (2019). Climatic Drivers of Greening Trends in the Alps. Remote Sensing, 11(21), 2527. https://doi.org/10.3390/rs11212527

Flores, M.; Núñez, J.; Oyarzún, J.; Freixas, G.; Maturana, H.; Oyarzún, R. Surface Water Quality in a Sulfide Mineral-rich Arid Zone in North-Central Chile: Learning from a Complex Past, Addressing an Uncertain Future. Hydrological Processes 2016, 31, 498–513, doi:10.1002/hyp.11086.

Garreaud, R.D.; Boisier, J.P.; Rondanelli, R.; Montecinos, A.; Sepúlveda, H.H.; Veloso-Aguila, D. The Central Chile Mega Drought (2010–2018): A Climate Dynamics Perspective. International Journal of Climatology 2019, 40, 421–439, doi:10.1002/joc.6219.

Godsey, S.E.; Kirchner, J.W.; Clow, D.W. Concentration–Discharge Relationships Reflect Chemostatic Characteristics of US Catchments. Hydrological Processes 2009, 23, 1844–1864, doi:10.1002/hyp.7315.

Goldrich-Middaugh, G.M.; Ma, L.; Engle, M.A.; Ricketts, J.W.; Soto-Montero, P.; Sullivan, P.L. Regional Drivers of Stream Chemical Behavior: Leveraging Lithology, Land Use, and Climate Gradients Across the Colorado River, Texas USA. Water Resources Research 2022, 58, doi:10.1029/2022wr032155.

Guo, M., Li, J., Sheng, C., Xu, J., & Wu, L. (2017). A Review of Wetland Remote Sensing. Sensors, 17(4), 777. https://doi.org/10.3390/s17040777

Hernández, V.; Arumí, J.L.; Boll, J.; Duhalde, D.; MacDonell, S.; Oyarzún, R. Streamflow–Concentration Relationships of Surface Water in the Choapa Basin: Historical Analysis and Projections under Climate Change. Hydrological Sciences Journal 2023, 68, 1250–1263, doi:10.1080/02626667.2023.2212167.

House, W.A.& Warwick, M.S. Hysteresis of the Solute Concentration/Discharge Relationship in Rivers during Storms. Water Research 1998, 32, 2279–2290, doi:10.1016/s0043-1354(97)00473-9.

Hribljan, J., Cooper, D., Sueltenfuss, J., Wolf, E., Heckman, K., Lilleskov, E., & Chimner, R. (2015). Carbon storage and long-term rate of accumulation in high-altitude Andean peatlands of Bolivia. Mires And Peat, 15(12), 1-14. https://www.fs.fed.us/nrs/pubs/jrnl/2015/nrs_2015_hribljan_001.pdf

Hunsaker, C.T.& Johnson, D.W. Concentration-discharge Relationships in Headwater Streams of the Sierra Nevada, California. Water Resources Research 2017, 53, 7869–7884, doi:10.1002/2016wr019693.

Immerzeel, W.W.; Lutz, A.F.; Andrade, M.; Bahl, A.; Biemans, H.; Bolch, T; Hyde, S.; Brumby, S.; Davies, B.J.; Elmore, A.C.; et al. Importance and Vulnerability of the World's Water Towers. Nature 2019, 577, 364–369, doi:10.1038/s41586-019-1822-y.

Jombo, S., & Adelabu, S. (2023). Evaluating Landsat-8, Landsat-9 and Sentinel-2 imageries in land use and land cover (LULC) classification in a heterogeneous urban area. GeoJournal, 88(S1), 377-399. https://doi.org/10.1007/s10708-023-10982-8

Ju, Y., & Bohrer, G. (2022). Classification of Wetland Vegetation Based on NDVI Time Series from the HLS Dataset. Remote Sensing, 14(9), 2107. https://doi.org/10.3390/rs14092107

Kaltenecker, M.G.; Mitchell, C.P.J.; Howell, E.T.; Arhonditsis, G. Long-Term Trends in Water Quality and C-Q Relationships Reveal Complex Interactions between Changing Land Uses and Climate. Journal Of Hydrology 2024, 132511, doi:10.1016/j.jhydrol.2024.132511.

Klein, M. Anti Clockwise Hysteresis in Suspended Sediment Concentration during Individual Storms. CATENA 1984, 11, 251-257, doi:10.1016/s0341-8162(84)80024-7.

Knapp, J.L.A.; Von Freyberg, J.; Studer, B.; Kiewiet, L.; Kirchner, J.W. Concentration–Discharge Relationships Vary among Hydrological Events, Reflecting Differences in Event Characteristics. Hydrology And Earth System Sciences 2020, 24, 2561-2576, doi:10.5194/hess-24-2561-2020.

Knapp, J. L. A., & Musolff, A. (2024). Concentration-Discharge relationships revisited: overused but underutilised? Hydrological Processes, 38(11). https://doi.org/10.1002/hyp.15328

Krueger, T.; Quinton, J.N.; Freer, J.; Macleod, C.J.A.; Bilotta, G.S.; Brazier, R.E.; Butler, P.; Haygarth, P.M. Uncertainties in Data and Models to Describe Event Dynamics of Agricultural Sediment and Phosphorus Transfer. Journal of Environmental Quality 2009, 38, 1137–1148, doi:10.2134/jeq2008.0179.

Lagomasino, D., Price, R. M., Whitman, D., Campbell, P. K., & Melesse, A. (2014). Estimating major ion and nutrient concentrations in mangrove estuaries in Everglades National Park using leaf and satellite reflectance. Remote Sensing Of Environment, 154, 202-218. https://doi.org/10.1016/j.rse.2014.08.022

Li, Y., Hou, Z., Zhang, L., Qu, Y., Zhou, G., Lin, J., Li, J., & Huang, K. (2023). Long-term spatio-temporal changes of wetlands in Tibetan Plateau and their response to climate change. International Journal Of Applied Earth Observation And Geoinformation, 121, 103351. https://doi.org/10.1016/j.jag.2023.103351

Lintern, A., Webb, J. A., Ryu, D., Liu, S., Waters, D., Leahy, P., Bende-Michl, U., & Western, A. W. (2018). What Are the Key Catchment Characteristics Affecting Spatial Differences in Riverine Water Quality? Water Resources Research, 54(10), 7252-7272. https://doi.org/10.1029/2017wr022172

Liu, S. (2019). Predicting water quality in the Great Barrier Reef Catchments: Learning from long-term water quality monitoring data. Retrieved

from http://hdl.handle.net/11343/235555

Liu, S., Dupas, R., Guo, D., Lintern, A., Minaudo, C., Bende-Michl, U., Zhang, K., & Duvert, C. (2022). Controls on Spatial Variability in Mean Concentrations and Export Patterns of River Chemistry Across the Australian Continent. Water Resources Research, 58(12). https://doi.org/10.1029/2022wr032365

Liu, X., Zhou, Z., & Ding, Y. (2021). Vegetation coverage change and erosion types impacts on the water chemistry in western China. The Science Of The Total Environment, 772, 145543. https://doi.org/10.1016/j.scitotenv.2021.145543

Lloyd, C.E.M.; Freer, J.E.; Johnes, P.J.; Collins, A.L. Using Hysteresis Analysis of High-Resolution Water Quality Monitoring Data, Including Uncertainty, to Infer Controls on Nutrient and Sediment Transfer in Catchments. The Science of the Total Environment 2015, 543, 388–404, doi:10.1016/j.scitotenv.2015.11.028.

Luo, N., Yu, R., & Wen, B. (2024). Characteristics of Changes in Typical Mountain Wetlands in the Middle and High Latitudes of China over the Past 30 Years. Land, 13(8), 1124. https://doi.org/10.3390/land13081124

Macchioli-Grande, M.; Soto-Maass, A.; Pfeiffer, M.; Covarrubias, J.I.; Peña-Echeverría, A.; Perez-Fodich, A. Solute Generation and Transport in Semiarid Mountain Catchments of the Central Chilean Andes. Earth Systems and Environment 2025, doi:10.1007/s41748-025-00642-x.

Markovich, K.H.; Manning, A.H.; Condon, L.E.; McIntosh, J.C. Mountain-Block Recharge: A Review of Current Understanding. Water Resources Research 2019, 55, 8278–8304, doi:10.1029/2019wr025676.

Mashala, M. J., Dube, T., Mudereri, B. T., Ayisi, K. K., & Ramudzuli, M. R. (2023). A Systematic Review on Advancements in Remote Sensing for Assessing and Monitoring Land Use and Land Cover Changes Impacts on Surface Water Resources in Semi-Arid Tropical Environments. Remote Sensing, 15(16), 3926. https://doi.org/10.3390/rs15163926

Mitsch, W.J.; Bernal, B.; Hernandez, M.E. (2015) Ecosystem Services of Wetlands. Int. J. Biodivers. Sci. Ecosyst. Serv. Manag., 11, 1–4.

Moatar, F.; Floury, M.; Gold, A.J.; Meybeck, M.; Renard, B.; Ferréol, M.; Chandesris, A.; Minaudo, C.; Addy, K.; Piffady, J.; et al. Stream Solutes and Particulates Export Regimes: A New Framework to Optimize Their Monitoring. Frontiers in Ecology and Evolution 2020, 7, doi:10.3389/fevo.2019.00516.

Monteiro, A. T., Arenas-Castro, S., Punalekar, S. M., Cunha, M., Mendes, I., Giamberini, M., Da Costa, E. M., Fava, F., & Lucas, R. (2024). Remote sensing of vegetation and soil moisture content in Atlantic humid mountains with Sentinel-1 and 2 satellite sensor data. Ecological Indicators, 163, 112123. https://doi.org/10.1016/j.ecolind.2024.112123

Muñoz, A.A.; Klock-Barría, K.; Alvarez-Garreton, C.; Aguilera-Betti, I.; González-Reyes, A.; Lastra, J.A.; Chávez, R.O.; Barría, P.; Christie, D.; Rojas-Badilla, M.; et al. Water Crisis in Petorca Basin, Chile: The Combined Effects of a Mega-Drought and Water Management. Water 2020, 12, 648, doi:10.3390/w12030648.

Musolff, A.; Schmidt, C.; Selle, B.; Fleckenstein, J.H. Catchment Controls on Solute Export. Advances in Water Resources 2015, 86, 133–146, doi:10.1016/j.advwatres.2015.09.026.

Nainggolan, D., Hasler, B., Andersen, H. E., Gyldenkærne, S., & Termansen, M. (2018). Water quality management and climate change mitigation:Cost-effectiveness of joint implementation in the Baltic Sea region. Ecological Economics, 144, 12–26. https://doi.org/10.1016/j. ecolecon.2017.07.026

Nauditt, A.; Birkel, C.; Soulsby, C.; Ribbe, L. Conceptual Modelling to Assess the Influence of Hydro-Climatic Variability on Runoff Processes in Data Scarce Semi-Arid Andean Catchments. Hydrological Sciences Journal 2016, 62, 515–532, doi:10.1080/02626667.2016.1240870.

Obuchowicz, C., Poussin, C., & Giuliani, G. (2023). Change in observed long-term greening across Switzerland – evidence from a three decades NDVI time-series and its relationship with climate and land cover factors. Big Earth Data, 8(1), 1-32. https://doi.org/10.1080/20964471.2023.2268322

Pan, F., Xie, J., Lin, J., Zhao, T., Ji, Y., Hu, Q., Pan, X., Wang, C., & Xi, X. (2018). Evaluation of Climate Change Impacts on Wetland Vegetation in the Dunhuang Yangguan National Nature Reserve in Northwest China Using Landsat Derived NDVI. Remote Sensing, 10(5), 735. https://doi.org/10.3390/rs10050735

Peña-Guerrero, M. D., Nauditt, A., Muñoz-Robles, C., Ribbe, L., & Meza, F. (2020). Drought impact on water quality and potential implications for agricultural podruction in the Maipo River Basin, Central Chile. Hydrological Sciences Journal, 65(6), 1005-1021. https://doi.org/10.1080/02626667.2020.1711911

Pepin, N.; Bradley, R.S.; Diaz, H.F.; Baraer, M.; Caceres, E.B.; Forsythe, N.; Fowler, H.; Greenwood, G.; Hashmi, M.Z.; Liu, X.D.; et al. Elevation-Dependent Warming in Mountain Regions of the World. Nature Climate Change 2015, 5, 424–430, doi:10.1038/nclimate2563.

Pérez, C.A., Hedin, L.O., Armesto, J.J., 1998. Nitrogen mineralization in two unpolluted old-glowhforests of Contrsting biodiversity and Dynamics. Ecosystems 1, 1-12

Pohle, I.; Baggaley, N.; Palarea-Albaladejo, J.; Stutter, M.; Glendell, M. A Framework for Assessing Concentration-Discharge Catchment Behavior from Low-Frequency Water Quality Data. Water Resources Research 2021, 57, doi:10.1029/2021wr029692.

Pörtner, H.-O., DC Roberts, H. Adams, I. Adelekan, C. Adler, R. Adrian, P. Aldunce, E. Ali, ... (2022). Resumen técnico. En: Cambio climático 2022: impactos, adaptación y vulnerabilidad. Cambridge University Press. doi: 10.1017/9781009325844.002.

Ramsar Convention Secretariat. (2013). Manual de la Convención de Ramsar (6th ed.). Ramsar Convention Secretariat. Recuperado el 11 de marzo de 2024, de https://www.ramsar.org/sites/default/files/documents/library/manual6-2013-sp.pdf

Rapinel, S., Panhelleux, L., Gayet, G., Vanacker, R., Lemercier, B., Laroche, B., Chambaud, F., Guelmami, A., & Hubert-Moy, L. (2023). National wetland mapping using remote-sensing-derived environmental variables, archive field data, and artificial intelligence. Heliyon, 9(2), e13482. https://doi.org/10.1016/j.heliyon.2023.e13482

Salimi, S., Almuktar, S. A., & Scholz, M. (2021). Impact of climate change on wetland ecosystems: A critical review of experimental wetlands. Journal Of Environmental Management, 286, 112160. https://doi.org/10.1016/j.jenvman.2021.112160

Salmon, C.D.; Walter, M.T.; Hedin, L.O.; Brown, M.G. Hydrological Controls on Chemical Export from an Undisturbed Old-Growth Chilean Forest. Journal of Hydrology 2001, 253, 69–80, doi:10.1016/s0022-1694(01)00447-4.

Shaw, T.E.; Ulloa, G.; Farías-Barahona, D.; Fernandez, R.; Lattus, J.M.; McPhee, J. Glacier Albedo Reduction and Drought Effects in the Extratropical Andes, 1986–2020. Journal of Glaciology 2020, 67, 158–169, doi:10.1017/jog.2020.102.

Speir, S.L.; Rose, L.A.; Blaszczak, J.R.; Kincaid, D.W.; Fazekas, H.M.; Webster, A.J.; Wolford, M.A.; Shogren, A.J.; Wymore, A.S. Catchment Concentration–Discharge Relationships across Temporal Scales: A Review. Wiley Interdisciplinary Reviews Water 2023, 11, doi:10.1002/wat2.1702.

Squeo, F. A., Warner, B. G., Aravena, R., & Espinoza, D. (2006). Bofedales: high altitude peatlands of the central Andes. Revista Chilena de Historia Natural, 79(2). https://doi.org/10.4067/s0716-078x2006000200010

Ugalde, F.& Sepúlveda, S.A. Susceptibility Assessment for Glacier Hazards in the Volcán Catchment (33.82°S/70.00°W), Central Andes of Chile. Journal of South American Earth Sciences 2025, 105581, doi:10.1016/j.jsames.2025.105581.

U.S. Environmental Protection Agency. (2024). Why are wetlands important? Recuperado el 9 de noviembre de 2024, de https://www.epa.gov/wetlands/why-are-wetlands-important

U.S. Geological Survey. (2024). Why are wetlands important? Recuperado el 11 de marzo de 2024, de https://www.usgs.gov/faqs/why-are-wetlands-important

Uribe-Álvarez, M. C., Prieto, M., & Meseguer-Ruiz, O. (2021). Bofedal response to climate variability, local management, and water extraction: A case study of Chucuyo, Northern Chile. Journal Of Mountain Science, 19(1), 241-252. https://doi.org/10.1007/s11629-021-6974-1

Valois, R., Schaffer, N., Figueroa, R., Maldonado, A., Yáñez, E., Hevia, A., Carrizo, G. Y., & MacDonell, S. (2020). Characterizing the Water Storage Capacity and Hydrological Role of Mountain Peatlands in the Arid Andes of North-Central Chile. Water, 12(4), 1071. https://doi.org/10.3390/w12041071

Vaughan, M.C.H.; Bowden, W.B.; Shanley, J.B.; Vermilyea, A.; Sleeper, R.; Gold, A.J.; Pradhanang, S.M.; Inamdar, S.P.; Levia, D.F.; Andres, A.S.; et al. High-frequency Dissolved Organic Carbon and Nitrate Measurements Reveal Differences in Storm Hysteresis and Loading in Relation to Land Cover and Seasonality. Water Resources Research 2017, 53, 5345–5363, doi:10.1002/2017wr020491.

Vieira, F. R., & Christofaro, C. (2024). Contributions of the vegetation index (NDVI) in water quality prediction models in a semi-arid tropical watershed. Journal Of Arid Environments, 220, 105122. https://doi.org/10.1016/j.jaridenv.2024.105122

Vicuña, S.; Garreaud, R.D.; McPhee, J. Climate Change Impacts on the Hydrology of a Snowmelt Driven Basin in Semiarid Chile. Climatic Change 2010, 105, 469–488, doi:10.1007/s10584-010-9888-4.

Vivanco, E. Humedales y Turberas en Chile. Disponible en línea: https://obtienearchivo.bcn.cl/ (acceso: 24 March 2024).

Viviroli, D.; Dürr, H.H.; Messerli, B.; Meybeck, M.; Weingartner, R. Mountains of the World, Water Towers for Humanity: Typology, Mapping, and Global Significance. Water Resources Research 2007, 43, doi:10.1029/2006wr005653

Winter, C.; Lutz, S.R.; Musolff, A.; Kumar, R.; Weber, M.; Fleckenstein, J.H. Disentangling the Impact of Catchment Heterogeneity on Nitrate Export Dynamics from Event to Long-Term Time Scales. Water Resources Research 2020, 57, doi:10.1029/2020wr027992.

Yager, K., Prieto, M., & Meneses, R. I. (2021). Reframing Pastoral Practices of Bofedal Management to Increase the Resilience of Andean Water Towers. Mountain Research And Development, 41(4). https://doi.org/10.1659/mrd-journal-d-21-00011.1

Zhang, H., Guo, J., Li, X., Liu, Y., & Wang, T. (2023). Spatiotemporal Variation in and Responses of the NDVI to Climate in Western Ordos and Eastern Alxa. Sustainability, 15(5), 4375. https://doi.org/10.3390/su15054375

Zhang, Y., Gao, J., Liu, L., Wang, Z., Ding, M., & Yang, X. (2013). NDVI-based vegetation changes and their responses to climate change from 1982 to 2011: A case study in the Koshi River Basin in the middle Himalayas. Global And Planetary Change, 108, 139-148. https://doi.org/10.1016/j.gloplacha.2013.06.012

Zhi, W.; Li, L.; Dong, W.; Brown, W.; Kaye, J.; Steefel, C.; Williams, K.H. Distinct Source Water Chemistry Shapes Contrasting Concentration-Discharge Patterns. Water Resources Research 2019, 55, 4233-4251, doi:10.1029/2018wr024257.

Zhou, Y., Xu, J. F., Yin, W., Ai, L., Fang, N. F., Tan, W. F., et al. (2017). Hydrological and environmental controls of the stream nitrate concentration and flux in a small agricultural watershed. Journal of Hydrology, 545, 355–366. https://doi.org/10.1016/j.jhydrol.2016.12.015

Nota. Para el desarrollo de este trabajo, se utilizó la herramienta de inteligencia artificial generativa ChatGPT exclusivamente como apoyo en el proceso de redacción y para mejorar la claridad y coherencia del texto. Todas las decisiones conceptuales, metodológicas, analíticas y de interpretación de resultados fueron tomadas íntegramente por los autores, empleándose dichas herramientas únicamente con fines lingüísticos y editoriales. La exactitud, pertinencia y validez de todo el contenido generado por el sistema fueron verificadas manualmente.